Aus der Abteilung für Strahlenzytogenetik
Leiter: Prof. Dr. rer. nat. Horst Zitzelsberger
und der Abteilung für Analytische Pathologie
Helmholtz Zentrum München

MALDI imaging mass spectrometry in clinical proteomics research of gastric cancer tissues

Dissertation
zum Erwerb des Doktorgrades der Naturwissenschaften
an der Medizinischen Fakultät der
Ludwig-Maximilians-Universität zu München

vorgelegt von
Benjamin Balluff
aus Freiburg im Breisgau
2012

Gedruckt mit Genehmigung der Medizinischen Fakultät

der Ludwig-Maximilians-Universität München

Betreuerin bzw. Betreuer:	Prof. Dr. rer. nat. Horst Zitzelsberger
Zweitgutachter:	Prof. Dr. rer. nat. Axel Imhof
Dekan:	Prof. Dr. med. Dr. h.c. Maximilian Reiser, FACR, FRCR
Tag der mündlichen Prüfung:	25. Februar 2013

Content

1 Introduction

Cancer is a group of diseases which is defined as the change from normal cells inside the body to a malignant neoplasm [1]. Malignant neoplastic cells show uncontrolled growth, invasion of adjacent tissues, and metastatic potential. Jointly, they lead to the destruction of healthy organs, and finally to the death of the organism. The change from a normal cell to a cancer cell is the result of genetic factors in interaction with external factors which are mainly the exposure of the organism to chemical, physical or biological carcinogens, such as asbestos, ultraviolet and ionizing radiation, or chronic infections from viruses and bacteria [1]. In addition, the risk for developing cancer increases with age and an unhealthy lifestyle [2].

Cancer is still one of the biggest scourges of mankind as it is the second leading cause of disease related deaths worldwide (around 13% of all deaths), just exceeded by cardiovascular diseases [2]. The International Agency for Research on Cancer reported 12.7 million new cancer cases and 7.6 million cancer deaths in 2008 worldwide [3]. And the World Health Organization (WHO) expects the cancer burden to almost double by 2030, due to the growth and aging of world population and the increasing western lifestyle in developing countries [2]. The aging effect can already be observed in Germany, where the Robert Koch Institute reports more than 400,000 new incidences for 2006 (about 57% more than in the early 1980s) with a growing fraction of elderly and a shrinking fraction of young people [4]. However, the mortality in Germany decreased by more than 20% in the same time frame. This is mainly due to increased early detection rates and better treatment of cancers, especially of prostate and breast cancer, the two most common cancer types in Germany for men and women, respectively.

The example of Germany shows that mortality in cancer patients can be reduced dramatically if cases are detected early and treated appropriately. Early detection and monitoring markers such as the prostate-specific-antigen (PSA) for prostate cancer or new treatment strategies like the monoclonal antibody trastuzumab for treatment of breast cancers demonstrates the usefulness of molecular markers and the importance of acquiring more knowledge about cancer and its molecular mechanisms.

Among all cancer related deaths, gastric cancer is of high clinical importance as it takes the third rank, worldwide [2]. The reason for this high lethality – the 5-year survival rate is below 30% – is that most patients are diagnosed at an advanced stage, where treatment options are limited [2]. Thus, new early stage detection techniques, treatment options and knowledge about the molecular mechanisms of gastric cancer are needed to improve the outcome for gastric cancer patients.

In this context, the aim of this thesis was to investigate gastric cancer at a molecular level using MALDI imaging mass spectrometry. MALDI imaging mass spectrometry, short MALDI imaging, is a novel technology which assesses the spatial distributions of proteins and other molecules in tissue sections [5]. The conservation of the natural context of the tissue sections (morphology) combined with mass spectrometry allows an untargeted analysis of the molecular content of tissues resulting in cell-type specific molecular patterns.

MALDI imaging has demonstrated its versatility for analyzing morphological complex tissues in several research areas like plant tissues [6], complex cell cultures [7], animal surfaces [8], or human biological systems, like the human ocular lens [9]. However, the application of MALDI imaging has been focused since its beginning on biomedical questions with the focus on cancer research. There, MALDI imaging has been applied in numerous clinical and preclinical studies to a variety of tumor types, amongst others brain, breast, lung, ovarian, prostate, and gastrointestinal cancers [10, 11].

In this thesis, tissue sections from human gastric cancer samples were analyzed to discover diagnostic and prognostic protein patterns for gastric cancer which might enable the determination of more effective therapies.

1.1 Gastric cancer

1.1.1 Epidemiology

In 2008 gastric cancer was the fourth most common cancer-related malignancy in the world which led to the death of about 738,000 people taking the third rank in cancer related deaths (Figure 1-1) [2]. The ratio between men and women is about 2:1 [12]. In addition, there is a strong international imbalance with about 72% of the new cases happening in developing countries with highest rates in countries from East Asia and South America [2]. Explanations for these differences may be due to different cultural alimentation habits, with high consumption of salty foods and low consumption of fresh fruit and vegetables being associated with increased risk for stomach cancer [13, 14]. In contrast, there has been a steady decline in stomach cancer rates in the last decades in developed countries such as North America and Europe [2]. Similarly, in Germany the incidence and mortality rate have decreased in the last 30 years, too, making up nowadays about 3–4% of all cancer diseases and about 5% of all cancer related deaths [4].

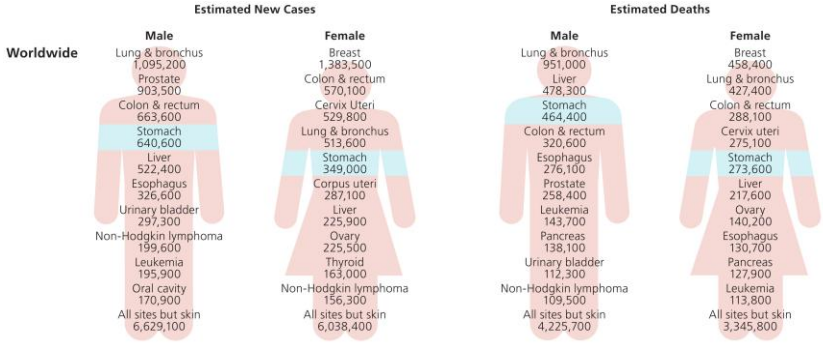

Figure 1-1 Estimated new cancer cases and deaths worldwide for the year 2008 in leading cancer sites. Gastric cancer was the fourth most common cancer malignancy in the world which led to the death of about 738,000 people taking the third rank in cancer related deaths. Modified from [2].

Despite this decline, gastric cancer is still of high clinical relevance as the five-year survival rate of patients in western countries remains very low with most rates below 30%; in the US the rate is 26%, in Europe about 25%, and in Germany around 30% [2, 4]. This is mainly due to the late detection of already advanced cancers — if the cancer is diagnosed at an early stage the survival rate may increase to over 60% — and the

lack of effective therapy options [2]. Unfortunately, less than 25% of stomach cancers are diagnosed at an early stage in the US and around 30% in the region of Munich and surroundings [15, 16]. The reason for the late detection of cancers is the absence of specific symptoms in the patients, the lack of sensitive serum markers and difficulties in detecting early stage cancers during diagnostic endoscopy; early stage cancers are often overlooked in a diagnostic endoscopy as they are very similar to a normal or inflamed stomach mucosa [17].

1.1.2 Stomach anatomy and histology

For understanding gastric cancer it is necessary to be familiar with the anatomy and histology of the healthy stomach.

The stomach is a muscular, hollow and J-shaped organ of the digestive system. It is located between the esophagus and the small intestine and can be divided into four regions: the cardia (food entry), the fundus, the body, and the pylorus (food exit) (Figure 1-2, A). The stomach is responsible for the mechanical and chemical disruption of ingested food before passing it for nutrient absorption to the intestine. The stomach wall is organized into four sections: the lumen-facing mucosa, the submucosa, the muscularis propria, and the serosa (Figure 1-2, B). The mucosa is separated from the underlying submucosa by a thin basal membrane. While the muscle layers of the muscularis propria contribute to the mixing and mechanical breakdown of the food, the chemical digestion is done by secretion of acids and proteolytic enzymes through the gastric mucosa [18].

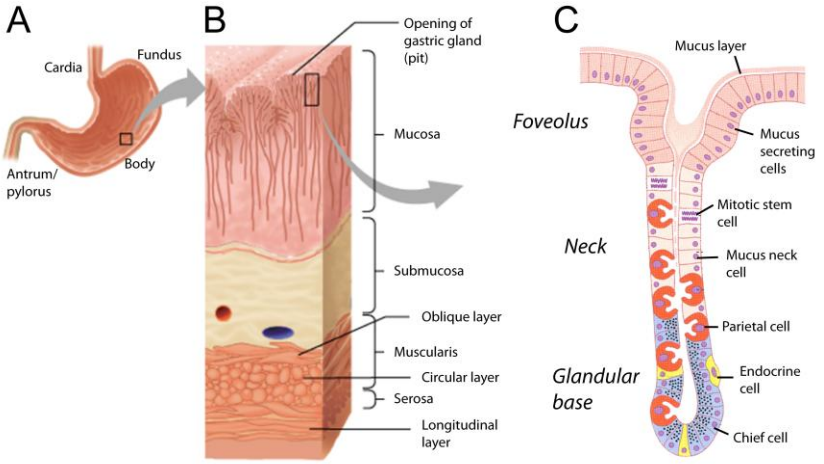

Figure 1-2 Stomach anatomy and mucosa histology. The stomach is divided into cardia, fundus, body, and antrum/pylorus (A). The stomach wall is structured into several layers: the epithelial mucosa, the submucosa, and the muscle layers muscularis and serosa (B). A magnification of the mucosa shows its cellular components according to which three layers can be distinguished: the surface epithelium, the mucosal neck, and the glandular base (C). Modified from [19, 20].

The mucosa can be divided roughly into three layers: the epithelial layer, the glandular neck, and the glandular base (Figure 1-2, C). The epithelial layer endues the inner surface of the stomach forming shallow depressions, so called gastric pits (foveolae gastricae). The foveolae are made up of epithelial cells which produce a carpet of mucus and undergo a continual replacement through division, in order to protect the mucosa against the aggressive contents (acids, enzymes) of the stomach. Each pit connects to several gastric glands that extend deep into the bottom of the mucosa. The layer between the gastric glands and the foveolae is called neck. The gastric gland is made up of different cell types [21]. The chief cells, most prominent in the base of the glands, secrete the proteolytic enzyme pepsin. The endocrine cells produce gastrins, serotonins and histamines, all of which stimulate and inhibit the production of the chief cells. The parietal cells are common in the neck of the glands and are responsible for production of hydrochloric acids which regulate the pH in the stomach. The regeneration of the mucosa is done by stem cells which are located at the top of the glandular neck. They renew the epithelial layer within 4–8 days and the glandular

base within 1–2 years [20]. The functional role of gastric stem cells in the pathogenesis of gastric tumors is not fully understood yet [21].

1.1.3 Histopathology and tumor classification

More than 90% of malignant tumors in the stomach are adenocarcinomas, i.e. cancers that originate from the glands of an epithelium (see epithelial mucosa in Figure 1-2) [1]. Less frequent tumors of the stomach include lymphomas (4%), carcinoids (3%), and gastrointestinal stromal tumors (2%) [1]. Gastric adenocarcinomas are biologically and genetically very heterogeneous which is reflected by their broad morphological diversity [22]. Therefore, classification systems based on histopathological features have been established by which the different types of adenocarcinomas can be distinguished. The most common classification schemes are those of the WHO and Laurén [23].

The WHO distinguishes five categories: tubular, papillary, mucinous, signet-ring cell, and mixed carcinomas. While tubular and papillary tumors differ in their shapes and architecture of tumor cell populations, mucinous tumors are defined as being made up of at least 50% of extracellular mucinous pools [22]. Signet-ring cell carcinomas consist mostly of malignant cells containing high levels of intracytoplasmic mucin which pushes their nuclei against the cell membranes creating a classical signet ring cell appearance [23]. Mixed carcinomas display a mixture of tubular, papillary, and signet-ring cells.

Another widely accepted classification system is the Laurén classification [15]. According to Laurén, lesions are classified as intestinal, diffuse, or mixed-type tumors [24]. The intestinal-type gastric carcinoma is histologically moderately to well-differentiated showing well defined glandular structures. Tumor cells are large, and nuclei are polymorphic and anisochromatic (Figure 1-3, A) [12]. In contrast, diffuse-type adenocarcinomas are histologically undifferentiated. They proliferate non-cohesively (diffuse) without gland formation (Figure 1-3, B) [25]. The diffuse-type resembles the mucinous and signet-ring cell tumor types of the WHO [23]. In general, the Laurén classification has proven useful in clinical management of patients (surgical therapy) and in evaluating the natural history of gastric carcinoma, especially with regard to its association with environmental factors, incidence trends and its carcinogenesis [23].

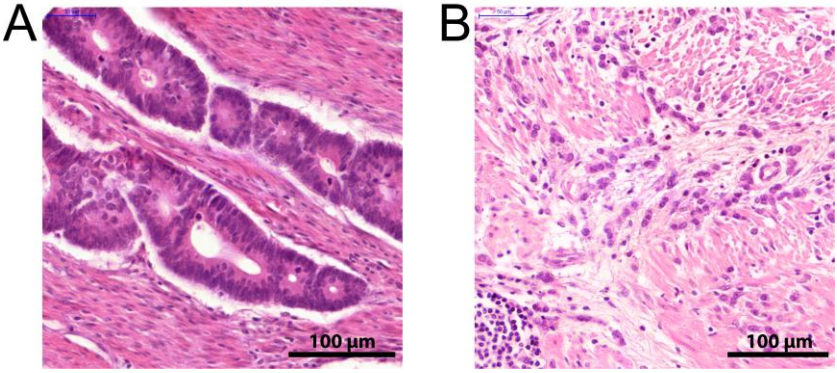

Figure 1-3 Main histological gastric cancer subtypes according to Laurén. The intestinal-type gastric carcinoma is histologically moderately differentiated showing polypus-like expansive growth (A). Diffuse-type carcinoma is undifferentiated showing diffuse infiltrative growth (B).

Mixed-type carcinomas contain tumor populations of both intestinal and diffuse-type.

Carcinomas of the above mentioned categories which are confined to the mucosa or submucosa are called early stage gastric cancers.

1.1.4 Etiology and carcinogenesis

The main two tumor types according to Laurén (diffuse and intestinal) differ in both their etiology as well as their carcinogenesis [26].

The development of intestinal-type gastric cancer has been associated with certain dietary factors like high intake of salty and smoke-preserved foods, and low intake of fruit and vegetables [15, 22]. Additional risk factors include smoking and a previous partial gastrectomy [15].

Major risk factor, however, is the infection with the bacterium *Helicobacter pylori* (*H. pylori*) which may provoke a chronic gastritis in the stomach [1]. The gastritis develops as a result of the combined influence of enzymes and toxins secreted by the bacterium and the release of noxious chemicals by the recruited neutrophils [1]. In this context, cancer risk increases with inflammatory intensity which depends on the aggressiveness of the *H. pylori* strain and on genetic factors in the host, e.g. polymorphisms in cytokine genes which may increase sensitivity to inflammation [25].

It has been proposed that the intestinal-type cancer develops, after initial chronic gastritis, through a sequence (Correa sequence) of precursor lesions (atrophic gastritis, intestinal metaplasia, and dysplasia) toward cancer (Figure 1-4) [12]. Histologically, chronic gastritis is characterized by a diffuse infiltration of the gastric mucosa by white blood cells with a good preservation of mucosal glands [27]. Loss of glands (atrophy) and their replacement by fibrous tissue is the next step toward neoplasia, and is called atrophic gastritis [27]. Next, at the stage of intestinal metaplasia, glands and the foveolar epithelium are replaced by metaplastic cells that resemble the morphology of the small intestinal or colonic mucosa [27]. Importantly, up to this point cells show normal cytological appearance [27]. Subsequent dysplasia features atypical changes in nuclear morphology and tissue architecture. Usually, cells of the dysplastic epithelium are enlarged, hyperchromatic, irregular in shape, and devoid of polarity [27]. The tissue architecture shows irregular structures, frequently forming adenomas with irregular lumens [27]. If a dysplasia breaks through the basal membrane into the submucosa, it is considered a carcinoma [22].

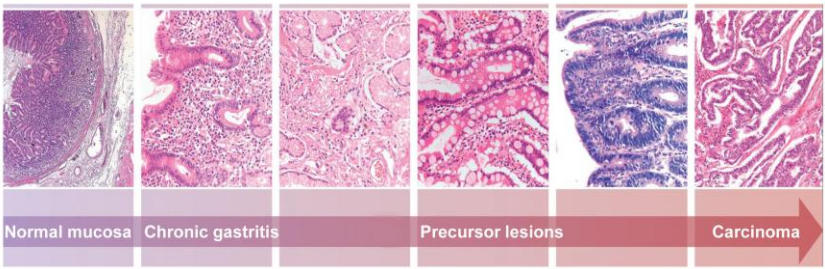

Figure 1-4 Correa sequence of precursor gastric cancer lesions. The sequence shows the proposed development of intestinal-type gastric cancer through a series of sequential precursor lesions which are histologically depicted from left to right: normal mucosa, chronic gastritis, mucosal atrophy, intestinal metaplasia, dysplasia, and finally intestinal-type carcinoma. Modified from [12].

In contrast, the carcinogenic pathway for diffuse-type gastric cancer is believed to develop through a shorter, still unidentified sequence of events from gastric epithelial cells [25].

Crucial for the development and progression of cancer is the accumulation of genetic defects. Genetic changes that happen during cancer development have been reported (Figure 1-5) [25]. Chronic infection might trigger the expression of important proteins

such as CDX2. This is a transcription factor that is important for the early differentiation and maintenance of intestinal epithelial cells which was found to be associated with the formation of intestinal metaplasia [28]. Further alterations for development of intestinal-type gastric cancer include loss or mutations in APC [29] and KRAS [30], and hypermethylation of promoter regions of mismatch repair proteins such as MLH1 [31]. Loss of TP53 could be found in both Laurén types [25]. Dysfunction of E-cadherin, an epithelial cell adhesion protein, is present in 50% of diffuse-type carcinomas [32]. Inherited mutations in the E-cadherin gene CDH1 are responsible for 1–3% of gastric cancers, called hereditary diffuse-type gastric cancer [12].

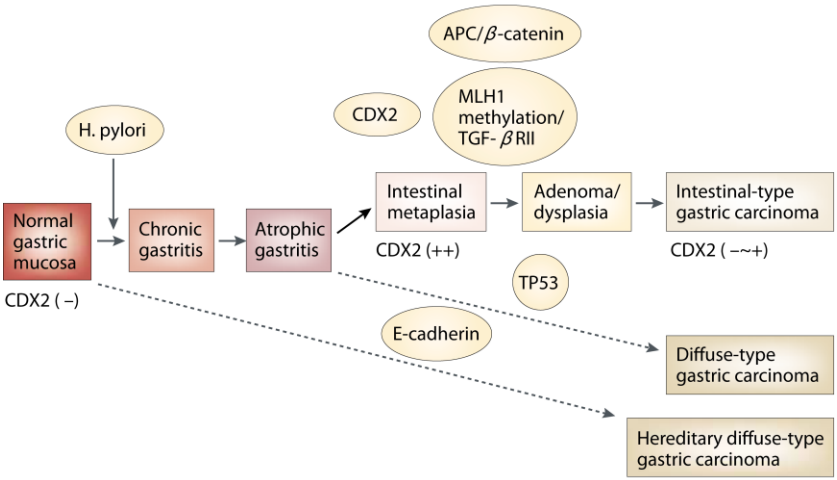

Figure 1-5 Models of the gastric carcinogenic pathway. Different sequences of events for developing intestinal or diffuse type gastric carcinoma have been proposed by Yuasa [25]. While defects in E-cadherin function are specifically associated with diffuse-type gastric cancer, non-hereditary carcinomas usually involve *Helicobacter pylori* infection. Subsequent inflammatory response and regeneration processes, together with genetic aberrations, may finally induce the carcinogenic sequence. Taken from [25].

Other molecular or genetic events drive the further behavior of the tumor. For instance, amplification of the HER2 gene which is frequent in about 7–34% of gastric cancers was found to be correlated with a poorer prognosis and liver metastases [33, 34]. On the contrary, loss or mutation of the PTEN gene was found in 20–30% of patients associated with metastatic gastric cancer [31].

1.1.5 Diagnosis and staging

Symptoms and diagnosis

In early stage gastric cancer symptoms are vague and therefore unrecognizable by the patient for several months or years [15]. Symptoms of advanced gastric cancer show pain in the abdominal region, stool bleeding, dysphagia, and vomiting. Systemic symptoms like aversion to meat and weight loss indicate disseminated disease. Thus, 80–90% of patients with symptoms presenting themselves to the physician have advanced cancer [23]. In some cases, the physician can detect the palpable advanced cancer (transmural tumor extension or enlarged lymph nodes) by body examination [15]. Serum based tumor markers like CEA, CA125, CA19-9, and CA72-4 have shown not to be reliable for diagnosis or staging [15]. Endoscopy of the upper gastrointestinal tract in combination with histological evaluation of biopsies is regarded the most sensitive and specific diagnostic method for detection of the tumor [23].

Staging

After detection, correct staging of the tumor is the most important requisite for an optimal therapy of the patient. The most widely used staging system for most tumor entities is the tumor-node-metastasis (TNM) classification system that is maintained by the Union for International Cancer Control (UICC), which is in its seventh edition [35]. The T category describes the extent of the primary tumor, N the status of regional lymph node metastasis, and M the absence or presence of distant metastasis. The degree of disease extent for each class is indicated by a tailing number, where a higher number correlates with an advanced disease stage. For practical purposes, TNM combinations can be condensed into stage groups which differ in their prognosis and appropriate treatment. In the TNM system, classification rules have been established for carcinomas of the stomach (Table 1-1).

Table 1-1 TNM classification system for gastric cancer

TNM categories		*Stage*	*T*	*N*	*M*
Extension of the primary tumor (T)		IA	T1	N0	M0
Tis	Carcinoma *in situ*: intraepithelial tumor, high grade dysplasia	IB	T1	N1	M0
T1a	Tumor invades lamina propria or muscularis mucosae		T2	N0	M0
T1b	Tumor invades submucosa	IIA	T1	N2	M0
T2	Tumor invades muscularis propria		T2	N1	M0
T3	Tumor invades subserosa		T3	N0	M0
T4a	Tumor perforates serosa	IIB	T1	N3	M0
T4b	Tumor invades adjacent structures		T2	N2	M0
Metastasis of regional lymph nodes (N)			T3	N1	M0
NO	No regional lymph node metastasis		T4a	N0	M0
NX	Less than 16 investigated lymph nodes	IIIA	T2	N3	M0
N1	1–2 regional lymph nodes affected		T3	N2	M0
N2	3–6 regional lymph nodes affected		T4a	N1	M0
N3a	7–15 regional lymph nodes affected	IIIB	T3	N3	M0
N3b	16 or more regional lymph nodes affected		T4a	N2	M0
Distant metastases (M)			T4b	N0/N1	M0
M0	No distant metastasis	IIIC	T4a	N3	M0
M1	Distant metastasis present		T4a	N2/N3	M0
		IV	any	any	M1

For practical assessment of TNM categories before surgery, different methods are employed. The depth of infiltration of the tumor (T category) can be best evaluated by endoscopic ultrasound [15]. This procedure may be also employed to determine near lymph node involvement (N category) [15]. More distant affected lymph nodes may be detected by X-ray computed tomography (CT) [12]. CT and other imaging modalities like abdominal sonography or positron emission tomography (PET) can be used to identify distant metastasis in the body (M category) [15].

Other histopathological categories have been introduced which require a tissue sample either from a surgery or bioptic analysis. A staging based on a pathological classification of a tissue sample is considered the most reliable classification and is indicated by a leading ‘p’ in the TNM nomenclature, e.g. pT1N1.

The grading category (G) classifies the carcinomas according to their grade of differentiation into the classes G1 to G4, where a higher number indicates a less differentiated tissue with regard to the healthy glandular structure. The differentiation

of a tumor is also reflected in the Laurén system, where diffuse type tumors represent poor differentiated carcinomas.

The absence or presence of residual tumor after surgery is described by the symbol R. R0 indicates full resection of tumor, R1 and R2 microscopic and macroscopic residual tumor, respectively [35]. Resection status strongly influences prognosis and thus further procedures after initial treatment [12, 36].

The TNM staging and its supplemental categories are the most important factors for an adaptation of the therapy to the individual situation of the patient. However, prognosis varies widely among patients of the same stage [37]. Thus, the complete applied therapy has to consider also other parameters such as the histopathological classification of the tumor, like Laurén subtypes, or molecular factors such as HER2 expression status, in order to apply optimal treatment for each patient.

1.1.6 Therapy

Surgery

Surgical therapy is the main pillar of gastric cancer treatment. The aim of this therapy is always the complete removal of primary tumor and affected lymph nodes, as incomplete resections, i.e. residual tumor at the resection margins (R1 or R2), worsen prognosis for the patients dramatically [15]. The appropriate surgical treatment depends on the previously determined tumor stage. Early stage gastric cancers (stage Ia) are mainly removed by endoscopic or laparoscopic surgery dependent on tumor differentiation and size [12]. In locally advanced cancers (stages Ib–IIIa) the chance of lymph node metastasis is already high. Thus, besides full resection (R0) of the tumor by full or partial gastrectomy, extended lymph node excision is recommended [15]. As mentioned before, the degree of resection is also determined by the histological type of tumor; a diffuse type cancer needs a more radical resection than intestinal type [15]. Patients suffering from advanced cancers (stages IIIb–IV) have infiltration of neighbor organs and/or distant metastasis which may not be surgically removed. In these cases, radio-chemotherapeutic approaches or treatment with biological agents like antibodies become important.

Neoadjuvant and adjuvant therapy

It seems likely that surgical therapy for local tumor control can – at least in developed countries – only be marginally improved [12]. Therefore, the effect of additional treatments by different cytostatic drugs (chemotherapy) in combination with radiotherapy is under strong investigation. Preoperative therapy actions are called 'neoadjuvant', and postoperative actions 'adjuvant'. It has to be mentioned at this point that existing guidelines for treatment of gastric cancer differ. In consequence, the following description will embrace, and not differentially explain, current treatment strategies for gastric cancer.

The rationale behind neoadjuvant therapies is three-fold: (i) it increases the probability for the application of the appropriate therapy (compliance) [15], (ii) the treatment is expected to downsize the tumor, thus facilitating a full surgical resection (R0) [12, 15], and (iii) this systemic preoperative therapy is the earliest way to delay systemic tumor spread [15]. The effect of neoadjuvant chemotherapy has been investigated in several studies which reported a beneficial effect for patients undergoing multimodal therapy [38, 39]. Consequently, this treatment option has been implemented in several national gastric cancer treatment guidelines [15, 36]. Initial studies on preoperative exposure of patients to radiation only or in combination with chemotherapy have shown promising results which have to be confirmed in larger patient cohorts [15].

Adjuvant approaches also include chemo- or radiotherapy. Present consent in guidelines is the application of combined chemoradiotherapy in a postoperative setting for locally advanced tumors and/or incomplete tumor resection [12, 36, 40]. Chemotherapy only is mostly considered when tumor is at an unresectable stage [37].

However, not all patients respond to chemotherapeutic pre- or postoperative treatment [15]. Thus, it would be useful to predict which patient will benefit from such a treatment and which not, as identified non-responders would not suffer from delayed surgical actions and chemotherapeutic side effects. One way that is believed to address this problem is the employment of molecular biomarkers [41]. One part of the thesis is dealing with the determination of such molecular markers, which is described in the results chapter 2.4.

Novel approaches

Despite all the above mentioned treatment options and strategies, the five-year survival rate of patients in western countries remains mostly below 30% [2]. Thus,

novel therapeutic agents, mostly in combination with established chemotherapeutic regimens, are being investigated in several clinical trials for advanced gastric cancers. Amongst them are also biological agents like the anti-EGFR antibody panitumumab (ClinicalTrials.gov Identifier: NCT00824785) or the EGFR inhibitor cetuximab (ClinicalTrials.gov Identifier: NCT00678535). Others include the tyrosine kinase inhibitor lapatinib (ClinicalTrials.gov Identifier: NCT00486954), the multi-targeted receptor tyrosine kinase inhibitor sunitinib [42], and the therapy with histone deacetylase inhibitors such as vorinostat (ClinicalTrials.gov Identifier: NCT01045538).

HER2 targeted therapy

The fact that patients can benefit from an additional treatment by biological agents, like antibodies, has been proven recently by the results of the ToGA Phase III trial [33]. This study investigated the effect of safety and efficacy of trastuzumab (trade name 'Herceptin', Hoffman-La Roche, Basel, Switzerland) in combination with regular chemotherapy in patients with HER2-positive, advanced gastric cancer [33]. Previous studies have identified HER2 overexpression to be associated with a poor outcome of patients with gastric cancer [43, 44]. HER2 overexpression is found in about 20% of gastric cancer patients with a significant bias toward intestinal type [37, 45]. Trastuzumab is a monoclonal antibody specifically targeting HER2 (also known as ERBB2), a human epidermal growth factor receptor. The therapeutic effect by trastuzumab is not fully understood yet, but it is believed to inhibit proliferation by blocking signaling pathways (Figure 1-6) [37].

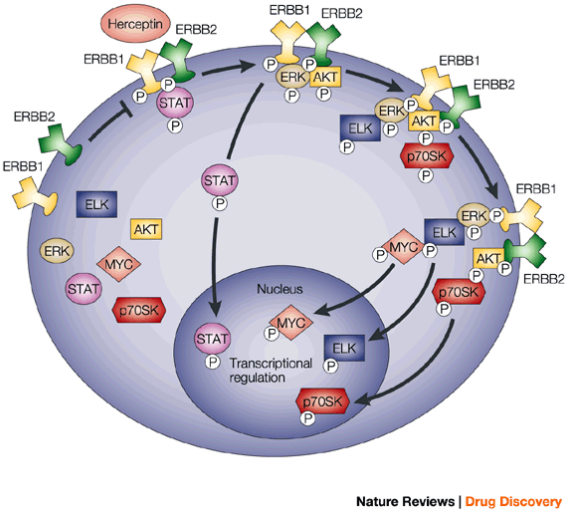

Figure 1-6 Protein signaling pathway involved in trastuzumab response. Trastuzumab (trade name 'Herceptin') is an antibody that recognizes HER2 and inhibits proliferation by blocking the down-stream signaling pathways. Taken from [46].

The ToGA trial provided evidence of a significant higher median survival for patients assigned to the trastuzumab treated arm (13.8 vs. 11.1 months; hazard ratio 0.74; 95% confidence interval: 0.60-0.91; $p<0.0046$) (Figure 1-7) [33].

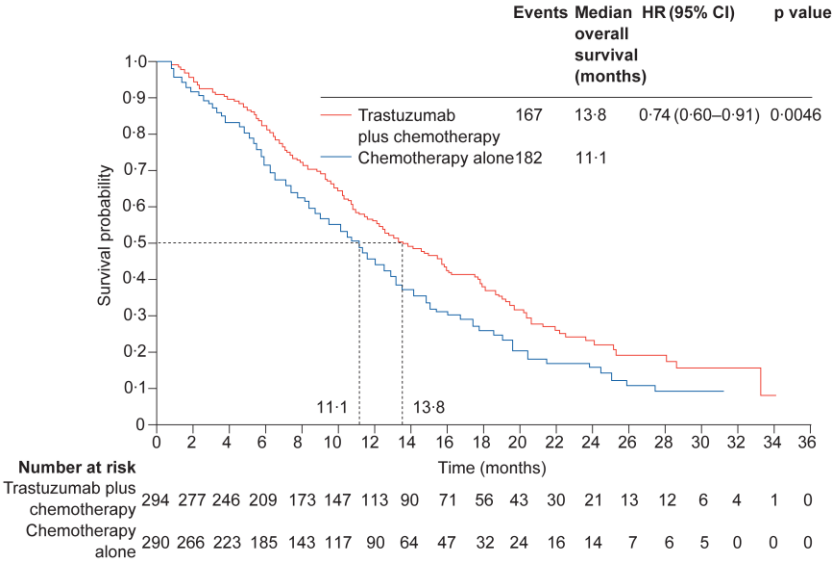

Figure 1-7 Overall survival benefit of trastuzumab treated patients with HER2-positive advanced gastric or gastro-esophageal junction cancer. Median overall survival (13.8 months) in those assigned to trastuzumab plus chemotherapy was significantly higher (hazard ratio 0.74; p=0.0046) than compared with those assigned to chemotherapy alone (11.1 months). Taken from [33].

In breast cancer, treatment with antibodies has been established as a standard option for HER2-positive patients. Likewise, new guidelines for gastric cancer treatment now recommend routine evaluation of HER2 status in gastric cancer specimens [36, 47].

HER2 testing

It is important that trastuzumab can only be used when the cancer has been shown to overexpress HER2. Currently, two testing methods are approved by the U.S. Food and Drug Administration for HER2 expression testing in cancer tissues in a clinical setting: immunohistochemical analysis (IHC) and fluorescence *in situ* hybridization (FISH). A modified breast cancer HER2 scoring system has been proposed for gastric cancer [48]. The differences are due to a different membrane staining pattern, a more frequent heterogeneity of HER2 positivity in gastric cancer and a less stringent correlation between HER2 amplification and protein overexpression [49]. According to this scoring system, a patient was only considered HER2-positive with a score of IHC3+ and/or a FISH-positive result, which is defined as HER2/centromer 17 ratio >2.2 or an

average HER2 gene copy number greater than six [48].However, both HER2 testing procedures, IHC and FISH, suffer from several disadvantages [50-52].

A mass spectrometry based approach may complement the two standard techniques because it offers multiplexing capability, i.e. the simultaneous measurement of several parameters at the same time. This is especially interesting in breast cancer where HER2, estrogen and progesterone receptor status are currently determined sequentially. Proof of an accurate HER2-status determination was provided by a study on basis of proteomic expression profiles obtained by MALDI imaging mass spectrometry [53]. In this work, the combination of seven mass signals was able to accurately define HER2-positive from HER2-negative breast cancer tissues, highlighting the potential of other analytical methods for tissue diagnostics (Figure 1-8) [53].

The example of HER2 shows that molecular prognostic factors can also act as novel therapeutic targets for either chemotherapeutics or biological agents like antibodies [37]. Thus, the aim should be to identify novel molecular markers with clinical relevance.

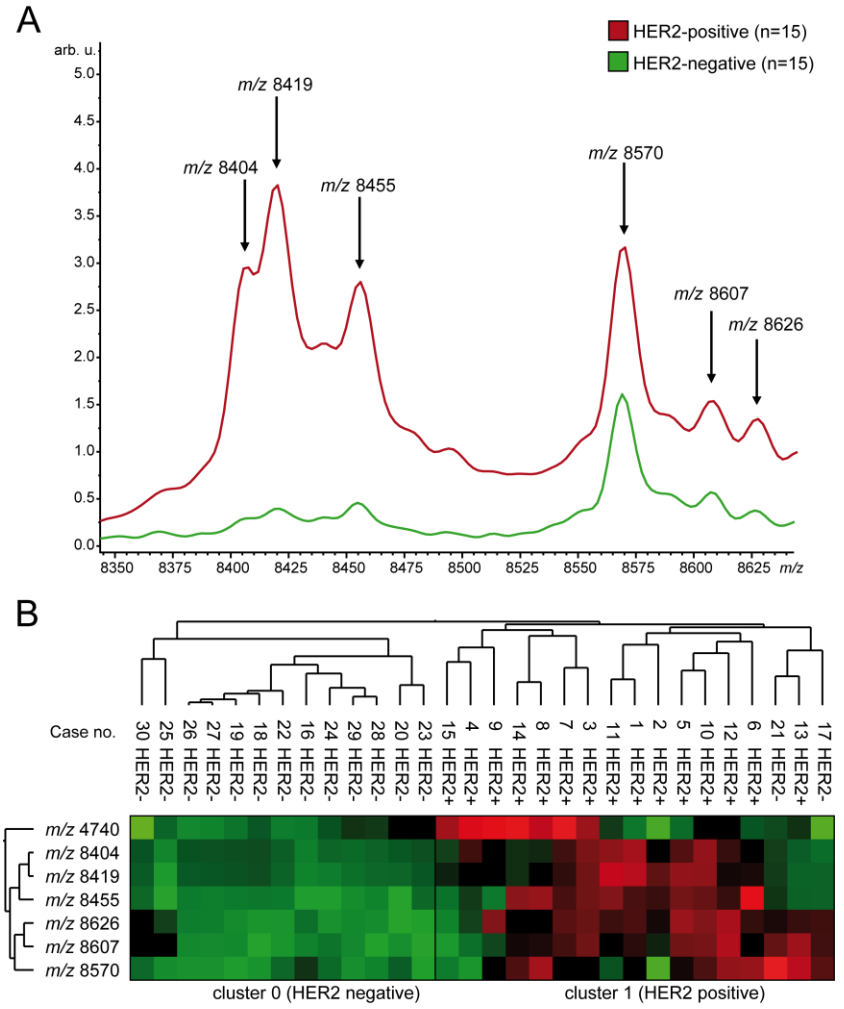

Figure 1-8 HER2 status correlated protein pattern in breast cancer. MALDI imaging was used to analyze 30 HER2 predefined breast cancer specimens which led to the discovery of a 7-signal protein pattern (top) which strongly correlated with the HER2 status of patients, as the hierarchical clustering on the 30 patients showed only two false positives (bottom, 93% accuracy). Taken from [53].

1.2 Proteomics for biomarker discovery

1.2.1 Biomarkers

The morphology based TNM staging system remains useful, but there is a variety in outcomes for patients with cancers of the same type or stage [54]. New factors like individual molecular markers or patterns may therefore subdivide traditional tumor classes into subsets that behave differently from each other [54]. Such biomarkers may aid in risk assessment, diagnosis of cancer, or monitor recurrence [55]. With regard to therapy they may act as prognostic indicator of disease progression or predict therapy response; thus, help establishing a personalized therapy for each patient. The different applications of biomarkers in stages of clinical evolution of cancer are depicted in Figure 1-9 [54]. In addition, these markers and their respective pathways may be starting points for further investigations which may lead to new therapeutic agents.

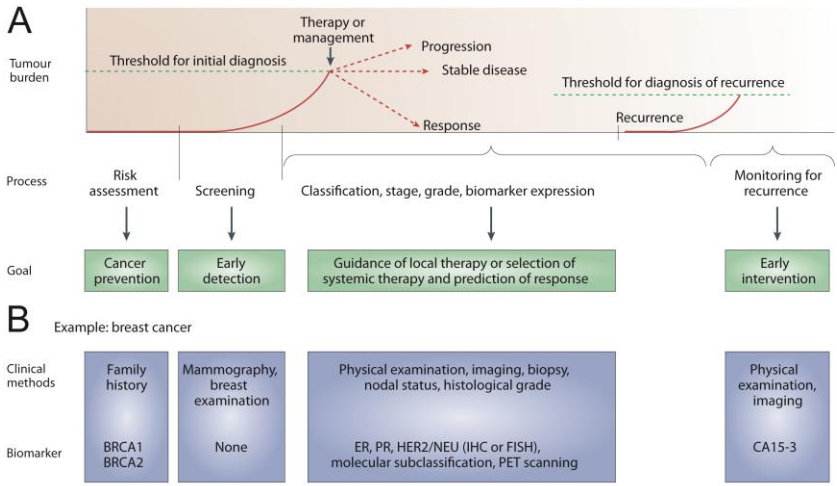

Figure 1-9 Use of biomarkers in stages of clinical evolution of cancer (A). Before diagnosis, markers might be used for risk assessment and screening. At diagnosis, markers can assist with staging, grading, and selection of initial therapy. Later, they can be used to monitor therapy, select additional therapy, or monitor for recurrent disease. As example, used clinical methods and biomarkers for breast cancer are listed in (B). Taken from [54].

Grouping of biomarkers

Regarding clinical application, most biomarkers fall into one of the following categories:

- **Diagnostic** markers: are used to detect cancer in a person and may thus also be used as monitoring marker after therapy or as screening marker
- **Prognostic** markers: are used to predict the course of disease and thus influence the aggressiveness of therapy
- **Predictive** markers: are used to predict whether a patient will respond to an applied therapy (mostly chemotherapy or targeted therapy)

In addition, biomarkers can be grouped also according to their biochemical molecule class. To account for the molecular complexity of tumors, markers have been searched on all molecular levels including:

- DNA-based markers: single nucleotide polymorphisms (SNPs), chromosomal aberrations, DNA copy numbers, microsatellite instability, and differential promoter-region methylation
- RNA-based markers: differential expression of mRNAs or regulatory RNAs like microRNAs
- Protein-based markers: differential expression of proteins or their post-translational modifications, such as proteolytic processing, acetylation, phosphorylation, or glycosylation, all of which are important processes in determining protein function
- Other molecular classes such as lipids, saccharides, or hormones
- Signatures: represent patterns of the above listed molecular entities (mostly RNA or protein expression profiles)

Requirements for biomarkers

The ideal features of a tumor marker or signature depend on the clinical question. However, in general an ideal biomarker should meet the following requirements: (i) high sensitivity and specificity for determination of clinical conclusion e.g. diagnosis; (ii) a cheap, rapid, and reproducible measurement; (iii) easy (best: non-invasive) access to the site of marker assessment such as plasma, serum or other body fluids [56].

It is a general agreement that combinations of multiple biomarkers may increase sensitivity and specificity, especially if positive and negative biomarkers are included into the signature [56]. In addition, a combination of these molecular species may not only increase general accuracy, but would remain more robust at a statistically significant level, as it has been reported that individual markers may vary for a variety of reasons [57]. Signatures are mostly combined to a classifier by statistical methods like decision trees, support vector machines, or clustering algorithms (for details see chapter 4.2.2 in statistical methods).

The proteome as biomarker source

In my studies presented here, I focused on the analysis of proteins as markers. The rationale is that proteins execute and control the vast majority of biological processes and thus reflect both the intrinsic genetic information of the cell as well as the influence of its environment [58]. The variety of proteins expressed in humans surpasses the number of protein-encoding genes by an order of magnitude (not considering their modifications) [58]. Furthermore, it has been realized that studying biological systems solely by mRNA expression is not sufficient as there is no absolute correlation between mRNA and corresponding protein levels [59]. In consequence, one of the best ways complex biological system are reflected is by proteins where the differences between various states of a biological system are reflected in the different amounts, activities, localizations and interactions of proteins [60]. All proteins present, including their modifications, in an organism or biological system at a certain state (disease, stress, normal circumstances), is called 'proteome'.

1.2.2 Sources of protein biomarkers

In an organism, protein markers can be produced either by the tumor itself or by other cells in response to the presence of the cancer, like inflammatory cells [41]. The markers are, therefore, expected to be present at highest concentration at the site of tumor or near reactive tissue, but may be also found in smaller concentrations in biological fluids, human excrements or secretions like plasma, serum, urine, stool, saliva, pancreatic juice etc. However, the most common sources used for biomarker discovery are blood and tumor tissues [55]. Other used sources for biomarker discovery may be cancer cell lines or animal models which are discussed more in detail by Kulasingam *et al*. [55].

Blood derived fluids

The main advantage of using blood derived fluids is that it can be obtained easily through a minimal invasive procedure, it is abundantly available, and that some blood components reflect several pathological states [55]. However, the protein concentrations in plasma differ in more than ten orders of magnitude (22 proteins make up 99% of the plasma proteome), making untargeted protein analyses very difficult [55, 61]. In addition, untargeted protein analyses on fluids have shown in the past that the proteins which were detected were often not tumor specific or even not reproducible, which may be due to active proteases, lipids, and other compounds which may depend on sample preparation variations [55, 56, 62, 63].

Tissues

Tumor tissues are more difficult to obtain as they must be removed invasively during surgery or during biopsy removal. However, they are considered a promising source for marker discovery. The rationale is that tissue samples contain higher concentrations of candidate proteins originating from tumor tissue that could subsequently be measured by targeted, and thus more sensitive, approaches in the bloodstream [55, 64]. Of importance, one has to consider that tissue may be extremely heterogeneous both in its cellular and molecular composition. Thus, a differentiated analysis of tissues can only be performed by technologies that take this complexity into account.

1.2.3 Proteomics for tissue analysis

In general, methods for the analysis of tissues can be divided into two groups: on the one hand lysate-based methods where structural information of the tissue is lost and on the other hand *in situ* methods that conserve the morphology, i.e. the tissue structure.

Classical *in situ* methods for studying proteins like the immunohistochemistry enable to study the spatial distribution of molecules within in tissue sections. However, they are not suitable for screening of biomarkers, as they require the labeling of the target molecules in advance by specifically binding dyes or antibodies in combination with chromophores or fluorophores [65]. In addition, only a few features can be labeled at the same time.

In contrast, lysate-based methods can analyze the molecular content of tissue without previous knowledge in a multiplex approach and are therefore technically very suitable for screening purposes, i.e. for *de novo* biomarker discovery. However, the unlabeled analysis of the proteome puts high demands on the analytical techniques as the human proteome is very complex. It is predicted to contain up to 1 million proteins resulting from the over 300 known post-translational modifications that can occur in different combinations with the different splice variants during expression [66]. In addition the proteins have a wide dynamic range in abundances (10^{10}, as shown for the plasma proteome) [61].

The technology for the large-scale study of the proteome is called 'proteomics' in analogy with large-scale genomics or transcriptomics initiatives. In proteomics, several lysate-based techniques have been established for the large-scale study of proteins with regard to their expression, structure, and function (Figure 1-10) [60].

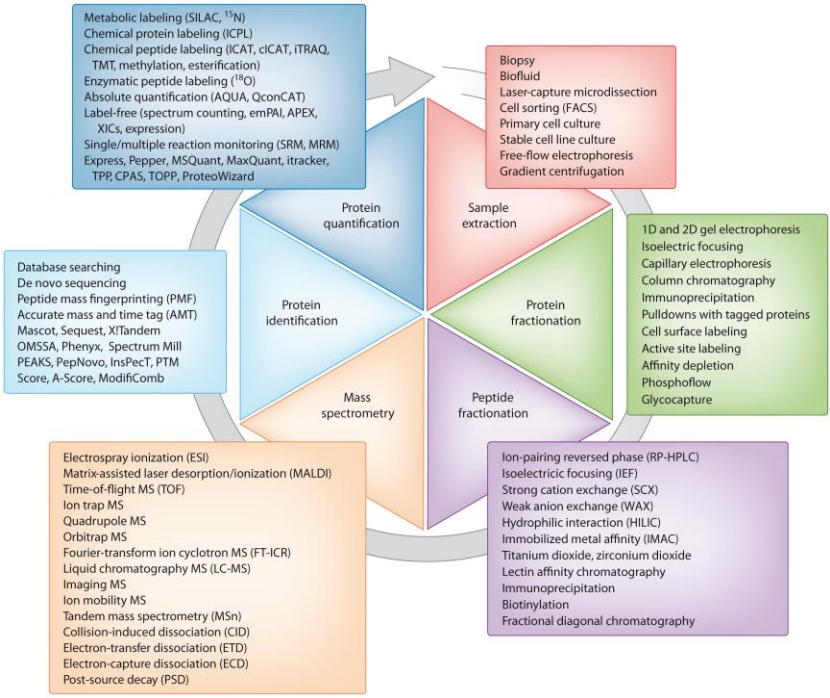

Figure 1-10 Technologies for proteomics. The figure shows the proteomic workflow from sample extraction to protein quantification. For each step in the workflow, a variety of techniques exist that are used for the large-scale study of proteins, termed proteomics. Taken from [60].

Especially mass spectrometry has become a key technology in proteomics as it offers an unlabeled high-throughput analysis of the molecular content of samples, ranging from small molecules over macromolecules, such as proteins, to modifications of proteins. Other techniques, such as the two-dimensional gel electrophoresis and the protein microarrays, fail to achieve the depth of informative proteome analysis as seen with mass spectrometry [67].

Nevertheless, in lysate-based analyses of tissues the localization of the analytes remains unknown. This makes interpretation of the results difficult, as the results may be blurred by the morphological complexity of the tissue.

In order to reduce this morphological complexity while maintaining cellular specificity of molecular analysis, laser capture microdissection (LCM) can be performed to isolate cells and tissue components of interest prior to analysis [64]. However, LCM is a highly tedious process while yielding low number of cells [55]. Consequently, the final amount of material puts even more sensitivity demands on analytical approaches [63].

One novel technology that overcomes this process is imaging mass spectrometry. Imaging mass spectrometry is an *in situ* technique with the advantages of lysate-based approaches. It offers mass spectrometry based analyses of the molecular content of tissue sections while preserving their morphological integrity. One of the most commonly employed imaging mass spectrometry techniques is MALDI imaging mass spectrometry, as it allows to measure large and small molecules at a reasonable spatial resolution with a simple technological set-up (in comparison to other imaging mass spectrometry technologies).

1.2.4 MALDI imaging mass spectrometry for tissue analysis

MALDI imaging is a mass spectrometry based approach which allows investigating the spatial distribution of proteins, lipids, drugs and other molecules in their morphological context of tissue sections (Figure 1-11). Conversely, it allows allocating molecular profiles to histomorphological entities, such as tumor areas etc. For this, MALDI mass spectra are acquired as pixels across a tissue section. A more detailed technological description of its principle, its workflow, advantages and limitations, can be found in the technical appendix of this thesis (chapter 4.1).

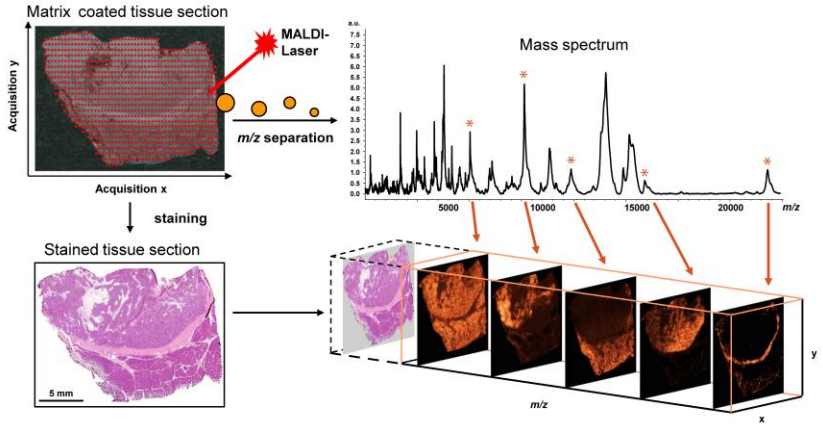

Figure 1-11 Technical principle of MALDI imaging mass spectrometry. A tissue section is coated with matrix before multiple MALDI experiments are performed in a predefined raster across the tissue section. After measurement, the intact section can be stained and digitally scanned for co-registration to the spatially resolved mass spectrometric data. This allows visualizing the distribution of masses within their morphological context of the analyzed tissue section. Abbreviations used: *m/z*, mass-to-charge-ration; MALDI, matrix-assisted laser desorption/ionization. Taken from [68].

Initially, two important studies gave evidence for the usefulness of direct MALDI tissue analysis to obtain meaningful protein signatures with clinical relevance from disease tissues. The first study, published in The Lancet, was able to distinguish different lung cancer histological entities, regional and distant metastasis, and finally survival of non-small-cell lung cancer patients by protein signatures [69]. Similarly, Schwartz and coworkers identified protein patterns that correlated with tumor histology and patient survival using a data set of 108 glioma patients [70]. Subsequently, MALDI imaging has been applied in numerous clinical and preclinical studies to a variety of tumor types, amongst others brain, breast, lung, ovarian, prostate, and gastrointestinal cancers [10]. These studies investigated tumor protein profiles obtained from tissues by MALDI imaging for correlation with clinical endpoints, like disease stage, survival, tumor recurrence, or therapy response [11, 71-74].

The spatially resolved data obtained by MALDI imaging also facilitates to investigate intra-sample molecular details such as tumor-normal interface zones or tumor heterogeneity in combination with the histomorphological information [75, 76].

With regard to the topic of this thesis, a summary of proteomic studies in diseases of the human lower and upper gastrointestinal system is presented in Table 1-2. Although the studies conducted are so far low in sample number, they illustrate the potential of histology-based analyses by MALDI imaging to provide novel biomarkers or patterns for a variety of different clinical purposes.

Table 1-2 Proteomics studies in gastrointestinal diseases using MALDI imaging mass spectrometry. Taken from [77]

Disease	Publication	Protein	Mass [Da]	Clinical purpose	Validation
Barrett's cancer	Elsner et al. [78]	61-protein signature	-	Carcinogenesis	-
		COX7A2	6720	Carcinogenesis /Prognosis	IHC
		S100-A10	11185	"	IHC
		28-protein signature	-	Marker for regional lymph node metastasis	-
		TAGLN2	22262	Marker for regional lymph node metastasis/Prognosis	IHC
Stomach cancer	Kim et al. [79]	73-protein signature	-	Tumor detection	-
		DEFA1	3439	"	-
		DEFA2	3368	"	-
		S100-A8	10840	"	-
		S100-A9	13158/12694	"	-
		17-protein signature	-	Early vs. advanced stage	-
	Balluff et al. [80]	7-protein signature	-	Prognosis in intestinal type gastric cancer	-
		DEFA1	3445	"	IHC
		CRIP1	8406	"	IHC
		S100-A6	10098	"	IHC
Liver cancer	Le Faouder et al. [81]	13-protein signature	-	Tumor marker	-
		Ubiquitin	8565	"	IHC, PCR
Liver autoimmune diseases	Bowlus et al. [82]	10-protein signature	-	Distinction of autoimmune hepatitis and primary sclerosing cholangitis	-
Pancreatic cancer	Djidja et al. [83]	Grp78	72288	Tumor marker	IHC
Colon colitides	M'Koma et al. [84]	5-protein signature	-	Distinction of ulcerative colitis and Crohn's colitis	-
Colon cancer	Meding et al. [85]	50-118 protein signature	-	Classification of cancer of unknown primary (liver metastasis from primary colon cancer)	-
	Meding et al. [86]	FXYD3	9264	Marker for regional lymph node metastasis	IHC
		S100-A11	11646	"	IHC

Some of the studies performed in gastric cancer will be explained more in detail in the following subsection.

Applications in gastric cancer

The potential of MALDI imaging for diagnostic purposes to detect gastric cancer has been investigated on endoscopic biopsies. Kim *et al.* used histology-directed MALDI profiling to analyze 63 gastric cancer and 43 healthy endoscopic biopsies. They found a protein profile which classified samples cancerous or healthy samples in the validation set with high predictive values: sensitivity and specificity were 93.8% and 95.5%,

respectively [79]. Signals overexpressed in tumors were identified as α-defensin-1, α-defensin-2, calgranulin A, and calgranulin B. Furthermore, a second protein profile could distinguish pathologic AJCC (American Joint Committee on Cancer) stage Ia from more advanced stage patients (Ib or higher). This may be potentially useful in identifying as patients with stage Ia that may be eligible for endoscopic treatments instead of surgical therapy [36].

This study shows that useful molecular profiles can be obtained by MALDI analyses from even smallest amounts of unprocessed fresh frozen tissue samples like biopsies for assisting in the diagnosis of cancers.

Human gastric cancer tissues are known to be very heterogeneous [87]. This may be due to the intrinsic heterogeneity of solid tumors based on e.g. distinct grades of differentiation, local differences in metabolic activity, the local inflammatory response. [88].

MALDI imaging may allow assessing this complexity. This has been shown in a first study by Deininger *et al*. on ten sections of gastric cancer patients which were subjected to MALDI imaging analyses. The *in situ* proteome expression profiles were analyzed by hierarchical clustering and were found in good correlation with the histological structure of the samples (Figure 1-12). But more interestingly, this examination revealed also histologically invisible distinct tumor areas. This shows that MALDI imaging may detect phenotypic differences in tissues, such as tumor subclones, that are invisible by conventional morphology based methods [88].

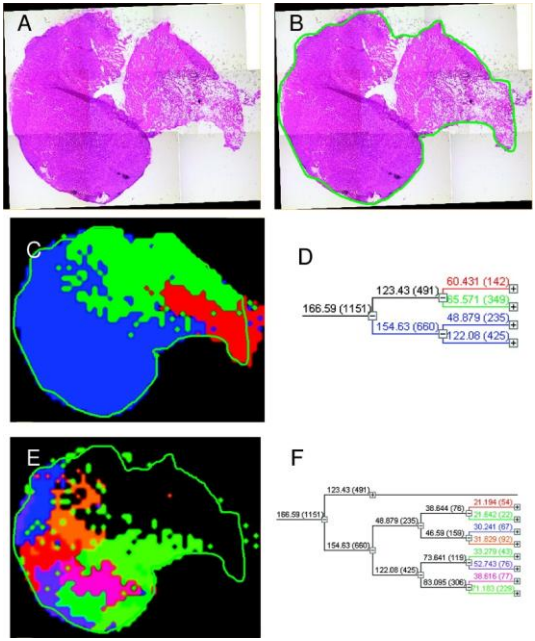

Figure 1-12 MALDI imaging for the detection of tumor heterogeneities beyond histology. The application of a hierarchical clustering to single spectra of a stomach tumor sample measured by MALDI imaging is shown. In (D) the top three branches of the clustering show the solid tumor in blue, as visualized in (C); pixels are colored according to the color of the dendrogram nodes. Expansion of the tumor branches of the clustering tree lead to a more detailed clustering of the spectra in the solid tumor (F), revealing phenotypic differences beyond histology (E), for example, tumor subclones. Taken from [88].

The applicability of MALDI imaging to FFPE tissue microarrays, which might enable high-throughput analyses, has been shown in a very small study (n=12). Formalin-fixed paraffin-embedded tissue microarrays comprising nine gastric cancer and three normal stomach tissue cores have been analyzed by Morita *et al.* After tryptic digest, they found 14 signals to distinguish gastric cancer samples of different differentiation grades and 54 signals to separate healthy from cancer tissues [89]. Tandem mass spectrometry identified one of the signals as histone H4, which was remarkably strongly expressed in poorly differentiated cancer tissues [89].

1.3 Aims of thesis

The overall aim of my thesis was to discover novel biomarkers in different gastrointestinal cancers (colon, gastric, and Barrett's cancer) with the focus on gastric cancer.

Biomarkers might enrich the possibilities to aid in early detection, prediction of therapy response, prognosis or potential to metastasize in patients with cancer. Molecular biomarkers can be searched on a genetic, transcriptomic, proteomic, or epigenetic level (DNA methylation, histone modifications) in tissues or body fluids.

With the intention to search for biomarkers on a protein and epigenetic level in tissue samples of patients, I set up own studies in gastric cancer and participated in studies of colon and Barrett's cancer.

In gastric cancer, matrix-assisted laser desorption/ionization (MALDI) imaging mass spectrometry ("MALDI imaging") was used for the morphologically differentiated analysis of tissues in order to acquire cell type specific (such as from tumor cell populations, inflammatory cells, etc.) protein expression patterns that can be correlated with clinical endpoints of the patients.

A major challenge faced by clinicians treating patients with gastric cancer is how to best assess patient outcome and predict the clinical course of the disease in order to apply the most appropriate treatment regimen. Thus, in one study, the tumor protein profiles obtained by MALDI imaging were used to discover novel protein biomarkers in human gastric cancer tissues that indicate the overall survival of patients. In another study, tumor protein profiles were used for generating a classifier that determines HER2 status in gastric cancer patients. The HER2 expression status is important for therapy selection with regard to the administration of Herceptin. This study was based on our previous results where HER2-status could be reliably predicted in breast cancer patients [53].

Importantly, the selection of samples from a tissue collection is crucial for the success of a research study. In both studies this selection has been performed carefully. This includes histological evaluation and matching for clinical parameters (as good as possible) except the one that is investigated, while maintaining the number of samples in the study cohort high in order to guarantee sufficient statistical power.

In the study of prognostic markers, 63 frozen tissue samples were left after matching for the tumor progression status (T=2) and histological filtering to intestinal-type gastric cancers. This can be regarded a high sample number, as follow-up clinical information (survival data) must be available for patient samples, which is often limited in frozen research samples. A similar situation was given in the HER2 classification study, where HER2 status was only available for few samples. The reason is that at the time of my study, the HER2 status was not routinely evaluated in gastric cancer patients.

Finally, one important aim was to test the results on an independent patient set in order to confirm their validity and reproducibility [90]. For validation of the proposed markers, immunohistochemistry was performed on large patient cohorts using tissue microarrays (TMA) [64]. Also here, the selection of samples was performed carefully.

In collaborative research, I also aimed to find clinically relevant markers in colon and Barrett's cancer. While MALDI imaging was applied in both cancer types to find markers for the potential of the tumor to metastasize, epigenetic analyses were performed in colon cancer samples only. In the latter, DNA methylation of candidate genes was tested for the ability to predict therapy response prediction or to detect the presence of tumor precursors.

2 Published results

2.1 Summary of presented publications

In the presented publications, matrix-assisted laser desorption/ionization (MALDI) imaging mass spectrometry was used for the proteomic analysis of gastric cancer tissue samples, with the aim of

- Identifying proteins that predict disease outcome of patients with intestinal-type gastric cancer after surgical resection
- Generating a proteomic classifier that determines HER2-status in order to aid in therapy decision with regard to trastuzumab (Herceptin) administration.

In the first study, a seven-protein signature was found to be associated with an unfavorable overall survival independent of major clinical covariates after analyzing 63 intestinal-type primary resected gastric cancer samples by MALDI imaging. Of these seven proteins, three could be identified as CRIP1, HNP-1, and S100-A6, and validated immunohistochemically on tissue microarrays of an independent validation cohort (n=118). While HNP-1 and S100-A6 were found to further subdivide early (UICC-I) and late stage (UICC-II-III) patients into different prognostic groups, CRIP1, a protein previously unknown in gastric cancer, was confirmed as a novel and independent prognostic factor for all patients in the validation cohort. The protein pattern described here serves as a new independent indicator of patient survival complementing the previously known clinical parameters in terms of prognostic relevance.

In the second study, we hypothesized that MALDI imaging mass spectrometry may be useful for generating a classifier that may determine HER2-status in gastric cancer. This assumption was based on our previous results where HER2-status could be reliably predicted in breast cancer patients [53]. Here, 59 gastric cryo tissue samples were analyzed by MALDI imaging and the obtained proteomic profiles were used to create HER2 prediction models using different classification algorithms. Astonishingly, the breast cancer proteomic classifier from our previous study was able to correctly predict HER2-status in gastric cancers with a sensitivity of 65% and a specificity of 92%. In order to create a universal classifier for HER2-status, breast and non-breast cancer samples were combined, which increased sensitivity to 78%; specificity was 88%. This study provides evidence that HER2-status can be identified on a proteomic level across

different cancer types suggesting that HER2 overexpression may constitute a widely spread molecular event independent of the tumor entity.

2.2 Zusammenfassung der veröffentlichten Arbeiten

Im Rahmen dieser Doktorarbeit wurden zwei Arbeiten publiziert, in denen die bildgebende Massenspektrometrie als zentrale Methode zur proteomischen Analyse von Magenkarzinomgeweben eingesetzt wurde. Dabei wurden folgende Ziele verfolgt:

- Identifizierung prognostischer Proteinmarker für Patienten mit intestinalem Magenkarzinom
- Generierung eines proteomischen Klassifikators zur Bestimmung des HER2-Status zur Entscheidungshilfe für eine Behandlung mit Trastuzumab (Herzeptin)

In der ersten Studie wurde eine Signatur bestehend aus sieben Proteinsignalen gefunden, deren Überexpression unabhängig von anderen klinischen Parametern ein schlechtes Gesamtüberleben der Patienten indizieren. Hierzu wurden 63 Gewebeproben von Patienten mit Magenkarzinom intestinalen Typs mittels MALDI Imaging analysiert. Drei der sieben Proteinsignale konnten als CRIP1, HNP-1 und S100-A6 identifiziert werden. Diese wurden anschließend an einem unabhängigen Patientenkollektiv (n=118) immunhistochemisch anhand von Tissue Microarrays validiert. Dabei zeigte sich, dass die beiden Proteine HNP-1 und S100-A6 bestehende klinische Gruppen nach ihrem Risiko weiter aufstratifizieren konnten; HNP-1 Magenkarzinompatienten im frühen Stadium (UICC I) und S100-A6 Patienten im fortgeschrittenen Stadium (UICC II-III). Darüber hinaus konnte CRIP1 als unabhängiger prognostischer Faktor für alle Patienten des Validierungskollektives bestätigt werden. Perspektivisch könnte die hier beschriebene Proteinsignatur vorhandene klinische Parameter als neuer und unabhängiger Indikator für das Überleben von Magenkrebspatienten ergänzen.

In der zweiten Studie wurden Proteinexpressionsmuster benutzt, um den HER2-Status in Magenkrebsgeweben vorauszusagen; denn seit kurzem ist der epidermale Wachstumsfaktor-Rezeptor HER2 eine wichtige tumorbiologische Zielstruktur bei der Behandlung von Magenkrebspatienten mit dem therapeutischen Antikörper Trastuzumab. In einer vorherigen Studie konnten wir die Machbarkeit der HER2-Status-Bestimmung durch MALDI Imaging erfolgreich anhand von Brustkrebsproben demonstrieren [53]. Unter der Annahme, dass der HER2-Überexpression – unabhängig vom Tumortyp – charakteristische molekulare Veränderungen zugrunde

liegen, wurde untersucht, ob eine Bestimmung des HER2-Status in Magenkrebspatienten mit Hilfe von Proteinexpressionsmustern aus Brustkrebspatienten erfolgen kann. Hierzu wurden, zusätzlich zu den bereits vorhandenen 48 Brustkrebsgeweben, 59 Magenkrebsfälle mittels MALDI Imaging analysiert und verschiedene HER2-Klassifikationsmodelle erstellt und verglichen. Der HER2-Status in Magenkrebsfällen konnte mit einem Mammakarzinom-spezifischen Profil mit einer Sensitivität von 65% und einer Spezifität von 92% bestimmt werden. Zusätzlich wurden die Expressionsprofile aller vorhandenen Tumorarten zusammengeführt, um einen universellen HER2-Klassifikator zu erstellen. Dies führte zu einer verbesserten Vorhersagequalität (Sensitivität: 78%, Spezifität: 88%). Dass sich der HER2-Status über verschiedene Tumorentitäten hinweg auf proteomischer Ebene bestimmen lässt, legt nahe, dass die Überexpression von HER2 ein unabhängiges molekulares Ereignis darstellt, ungeachtet der Herkunft des Tumors. Zudem unterstreichen die Ergebnisse das diagnostische Potential der bildgebenden Massenspektrometrie zur schnellen und zuverlässigen Bestimmung von tumorbiologischen Zielstrukturen, wie HER2.

2.3 MALDI imaging identifies prognostic seven-protein signature of novel tissue markers in intestinal-type gastric cancer

Balluff B, Rauser S, Meding S, Elsner M, Schöne C, Feuchtinger A, Schuhmacher C, Novotny A, Jütting U, Maccarrone G, Sarioglu H, Ueffing M, Braselmann H, Zitzelsberger H, Schmid RM, Höfler H, Ebert MP, and Walch A.

Am J Pathol. 2011 Dec;179(6):2720-9.

2.3.1 Journal description and standing

The American Journal of Pathology (ISI abbreviation: *Am J Pathol*) publishes papers on the cellular and molecular biology of diseases. Focus is given on work that advances basic and translational knowledge of the pathogenesis, classification, diagnosis, and mechanisms of diseases, with preference for studies which consider morphology.

The American Journal of Pathology is indexed by Thomson Reuters in the category Pathology. With an impact factor of 5.224 and a 5-year impact factor of 5.971 in the 2010 Journal Citations Reports it takes rank four of 76 journals within its category.

2.3.2 Abstract

Proteomics-based approaches allow us to investigate the biology of cancer beyond genomic initiatives. We used histology-based matrix-assisted laser desorption/ionization (MALDI) imaging mass spectrometry to identify proteins that predict disease outcome in gastric cancer after surgical resection.

A total of 181 intestinal-type primary resected gastric cancer tissues from two independent patient cohorts were analyzed. Protein profiles of the discovery cohort (n=63) were directly obtained from tumor tissue sections by MALDI imaging. A seven-protein signature was found to be associated with an unfavorable overall survival independent of major clinical covariates (HR=4.03; 95% CI: 1.69 - 9.61; P=0.002). The prognostic significance of three individual proteins identified (CRIP1, HNP-1, and S100-

A6) was validated immunohistochemically on tissue microarrays of an independent validation cohort (n=118). While HNP-1 and S100-A6 were found to further subdivide early (UICC-I) and late stage (UICC-II-III) patients into different prognostic groups (P=0.024, P=0.013), CRIP1, a protein previously unknown in gastric cancer, was confirmed as a novel and independent prognostic factor for all patients in the validation cohort (HR=1.57; 95% CI: 1.01-2.44; P=0.044).

The protein pattern described here serves as a new independent indicator of patient survival complementing the previously known clinical parameters in terms of prognostic relevance. These results show that this tissue-based proteomic approach may provide clinically relevant information that might be beneficial in improving risk stratification for gastric cancer patients.

2.3.3 Introduction

Although the incidence of gastric cancer has declined worldwide over the past 30 years, especially in Western countries, it remains the second leading cause of cancer-related death and accounts for 9.7% of cancer deaths globally [3, 91]. Despite complex treatment regimens and further understanding of its biology and possible causes, surgery is the only potentially curative treatment for gastric cancer [92]. Patients with stage I disease have a good prognosis, whereas those with stage IV disease show a poor prognosis. Interestingly, the prognosis varies widely in patients with stage II or III disease for as of yet undetermined biologic reasons [93].

The clinical and biological behavior of individual gastric cancer patients cannot be understood through the analysis of individual or small numbers of genes, so cDNA microarray analysis has been used with some success to simultaneously investigate thousands of RNA expression levels and attempt to identify patterns associated with biological characteristics [94-96]. However, mRNA expression is often poorly correlated with levels of protein expression, and such analyses cannot detect important post-translational modifications of proteins such as proteolytic processing, phosphorylation, or glycosylation, all of which are important processes in determining protein function [97]. Accordingly, comprehensive analysis of protein expression patterns might improve our ability to understand the molecular complexities of tumor tissues.

Matrix-assisted laser desorption/ionization (MALDI) imaging mass spectrometry, or MALDI imaging, is a powerful tool for investigating protein patterns through the direct (*in situ*) analysis of tissue sections [5]. Similarly to immunohistochemistry, MALDI imaging has advantages over other assay methods (i.e., those requiring homogenization) because it is morphology driven [98]. This characteristic allows to directly evaluate tumor cells, to determine correlations with other morphologic features, and to assay smaller patient tumor tissue specimens, such as surgical or endoscopic biopsy specimens [79]. These features make it an interesting tool for tissue analysis and molecular histology [99]. In addition, MALDI imaging can determine the distribution of hundreds of compounds in a single measurement without any need for labeling [100]. The great potential of a highly sensitive and molecularly specific technology such as MALDI imaging to the field of oncology is currently being realized. Until now, this technique has been successfully applied to various types of cancer tissues, including human non-small cell lung cancer, gliomas, and ovarian, prostate, and breast cancer [69, 70, 72, 101-103]. Analysis of the resulting complex mass spectrometry data sets using modern biocomputational tools has resulted in the identification of both disease state, response prediction, and patient prognosis-specific protein patterns [69-71].

To explore the possibility of using tissue-based proteomic analysis as a predictor of outcome in resected gastric cancer, we used MALDI imaging for direct tissue analysis of protein expression to identify proteins that predict disease outcome in patients with intestinal gastric cancer.

2.3.4 Material and methods

Study Population and Tissues

All tissues investigated in this study were obtained from patients (n=181) who underwent gastrectomy between 1991 and 2005 at the Surgery Department at the Technische Universität München. Histological classification was performed according to the WHO and the TNM classification systems designed by the International Union Against Cancer (UICC) [23, 104]. All tumors analyzed in this study were intestinal type tumors according to Lauren's classification system [24]. Follow-up data were available for all patients, and the overall survival was calculated from the date of surgical resection to the date of death or last follow-up. This study was approved by the Institutional Review Board and the Ethics Committee of the Faculty of Medicine of the

Technische Universität München with informed consent from all subjects and patients. The clinicopathological data of all patients are listed in Table 2-1.

Table 2-1 Correlation of spectral features and their respective identified proteins with clinicopathological parameters for the patient series

	Discovery cohort (n=63)								*Validation cohort (n=118)*			
		MALDI imaging *m/z* signals								Immunohistochemistry antigens		
	No. of patients	3445 (HNP-1)	6278	8406 (CRIP1)	8453	10098 (S100-A6)	11353	11613	No. of patients	HNP-1 (*m/z* 3445)	CRIP1 (*m/z* 8406)	S100-A6 (*m/z* 10098)
Sex *		0.257	0.348	0.953	0.383	**0.002**	0.579	0.951		0.448	0.092	0.259
Male	46								89			
Female	17								29			
Age †		0.114	0.220	0.159	0.564	**0.039**	0.290	0.947		**0.009**	0.152	0.678
Primary tumor †		—	—	—	—	—	—	—		0.248	0.375	0.224
pT1	0								15			
pT2	63								54			
pT3	0								44			
pT4	0								5			
Regional lymph nodes †		0.730	0.572	0.059	0.396	0.081	0.400	0.305		**0.016**	0.964	**0.023**
pN0	18								36			
pN1	24								35			
pN2	16								35			
pN3	5								9			
pNx	0								3			
Distant metastasis ‡		0.976	0.321	0.089	0.687	**0.005**	**0.036**	0.616		0.517	0.779	**0.038**
M0	54								87			
M1	9								31			
Resection status ‡		0.675	0.238	0.055	0.129	**0.011**	0.448	0.150		0.196	0.624	0.361
R0	53								81			
R1	9								26			
Rx	1								11			
Grading †		0.389	0.685	0.720	0.389	0.227	**0.033**	0.104		0.168	0.388	**0.018**
G1	0								1			
G2	16								36			
G3	47								81			
Overall survival §		0.075	**0.009**	**0.018**	**0.022**	**0.013**	**0.012**	**0.026**		0.086 ¶	**0.016**	0.077 **

Bold print values indicate that the P value is < 0.05.

* P value calculated by *t*-test.

† P value calculated by Spearman's rank correlation.

‡ P value calculated by Mann-Whitney *U* test.

§ P value calculated by univariate Cox proportional hazard regression.

¶ Union Internationale Contre le Cancer (UICC) stage I.

** UICC stages II and III.

Discovery cohort

Fresh-frozen tissue samples were obtained from 63 primary resected gastric carcinoma patients that were matched to UICC-T status (T=2). Patients were on average 66.5 years old (range: 33–85), and their median overall survival time was 33.1 months (range: 0–53.4). The tissues were snap-frozen and stored in liquid nitrogen. This discovery cohort was used for tissue-based proteomic analysis by MALDI imaging.

Validation cohort

The patient cohort of the validation set was comprised of 118 tumor samples and was provided in triplicate in formalin-fixed paraffin-embedded tissue microarrays from the Institute of Pathology of the Technische Universität München. The clinicopathological data of this independent sample set are also included in Table 2-1. The patients' median overall survival time was 54.7 months (range: 0–135.5), and their mean age was 66.4 years (range: 41–80). The validation of the proteins was performed in this independent patient cohort by immunohistochemical analyses.

MALDI imaging for the discovery of survival-related proteins

Frozen tissue sections from the discovery cohort were cut on a cryostat (CM1950, Leica Microsystems, Wetzlar, Germany) at a 12 µm thickness onto indium-tin-oxide coated glass slides (Bruker Daltonics, Bremen, Germany). After brief washing in both 70% and 100% ethanol pro analysis solutions, slides were coated with sinapinic acid matrix solution (Sigma-Aldrich, Taufkirchen, Germany) at 10 mg/ml in water/acetonitrile 40:60 (v/v) with 0.2% trifluoroacetic acid pro analysis (TFA) by an automated spraying device (ImagePrep, Bruker Daltonics).

For mass spectrometric measurements, tumor areas were defined using the FlexControl 3.0 and FlexImaging 2.1 software packages (both Bruker Daltonics). Spectra were acquired using the Ultraflex III MALDI-TOF/TOF (Bruker Daltonics) in positive linear mode, whereas ions were detected in a mass range of *m/z* 2,500–25,000 with a lateral resolution of 70 µm. A ready-made protein standard was employed for spectra calibration (Bruker Daltonics).

Following the MALDI experiments, the glass slides were incubated in 70% ethanol to elute the matrix and then stained with hematoxylin and eosin. Finally, the stained slides were scanned with a digital slide scanning system (Mirax Desk, Carl Zeiss MicroImaging, Göttingen, Germany) and co-registered to the MALDI imaging results to align mass spectrometric data with the histological features of the very same sections.

Tumor specific spectra were selected using the FlexImaging software (Bruker Daltonics). Eighty spectra per case were picked randomly and were imported into the ClinProTools 2.2 software (Bruker Daltonics), upon which the data underwent normalization, recalibration (both to enable comparability of measurements), and peak picking. After processing, the data were exported for further statistical analyses.

Protein identification

Ten cryosectioned slices (25 µm each) of three different tissue specimens underwent protein extraction with aqueous 0.1% TFA and ultrasonication. The extracted proteins were separated on an mRP-C18 column (Agilent Technologies, Santa Clara, CA, USA), and the fractionated aliquots were collected in a 96-well-plate. The HPLC fractions were manually spotted onto a PAC target (Bruker Daltonics) and analyzed by MALDI-MS (Ultraflex I, Bruker Daltonics) in order to locate fractions containing the *m/z* species of interest. Fractions of interest underwent tryptic digestion, and the resulting peptides were separated on a nano-RP-HPLC column (PepMap, LC Packings, Sunnyvale, CA, USA), which was connected to a linear quadrupole ion trap mass spectrometer (LTQ Orbitrap XL, Thermo Scientific, Waltham, MA, USA) equipped with a nano-ESI ion source. All obtained MS/MS spectra were searched in the NCBInr human sequence database using Mascot (v2.2.06, Matrix Science, London, UK). The final evaluation of the protein/peptide identification results was done using the Scaffold 3 software framework (Proteome Software, Portland, OR, USA).

Validation of proteins by immunohistochemistry

Immunohistochemical staining of the 3 µm tissue microarray sections was carried out using an automated stainer (Discovery XT) and a DAB Map kit (both, Ventana Medical Systems, Tucson, AZ, USA). The dilutions used for primary antibodies against HNP-1 (BMA Biomedicals, Augst, Switzerland), CRIP1 (AbD Serotec, Oxford, UK), and S100-A6 (Thermo Scientific) were 1:400, 1:100, and 1:100, respectively.

The analysis of the immunohistochemical staining was conducted with an image analysis platform (Definiens Enterprise Image Intelligence Suite, Definiens AG, Munich, Germany). For this purpose, all stained slides were scanned at 20X objective magnification by a digital slide scanner (Mirax Desk, Carl Zeiss MicroImaging), and the images were imported into the image analysis software. Specific rule sets were then defined to detect and quantify the immunohistochemical staining intensities of semantic classes. While the quantified parameter for CRIP1 and S100-A6 staining was the brown intensity of the tumor cells, the area of the peptide expressing granulocytes was the quantified parameter for HNP-1.

Statistical Analysis

Correlations between the investigated parameters and clinicopathological features were determined as outlined in Table 2-1.

M/z species associated with overall survival, obtained by MALDI imaging, were identified by corrected multiple testing using the Significance Analysis of Microarrays (SAM) package with a maximum false discovery rate of 0.1 [105]. To investigate the predictive power of the combined MALDI imaging signals, all patients were clustered into two groups by hierarchical clustering. The dendrogram was calculated using the Ward linkage method based on a weighted Euclidean distance. Each weight corresponded to the reciprocal of the respective *m/z* species' univariate *P* value. The correct classification rate of this protein pattern to one of the groups was tested by establishing a classification model based on a support vector machine, running with standard parameters (kernel=radial, cost=1) and a 10-fold cross-validation.

Multivariate analyses for the assessment of clinical parameter influences were done by Cox regression with p-values calculated by the Wald test. Kaplan-Meier curves were calculated by defining favorable and unfavorable prognostic groups using an intensity-based threshold score, which maximized overall survival differences between both respective groups while minimizing imbalances in group sizes. Differences between the curves were assessed using the log-rank test.

All statistical analyses were performed within the R statistical environment (R Foundation for Statistical Computing, Vienna, Austria), in which *P* values <0.05 were considered statistically significant and values between 0.05 and 0.1 were considered trends.

2.3.5 Results

MALDI imaging reveals seven survival-associated proteins

To detect protein signals associated with overall survival in gastric cancer, we acquired the cancer protein profiles of 63 patients utilizing MALDI imaging mass spectrometry in the discovery cohort. This strategy allowed the histology-directed acquisition of cancer cell-specific protein spectra from the measured tissue samples. On average, we could resolve between 150 and 200 peaks per case within the mass range of *m/z* 2,500 to 25,000 and a mass accuracy of +/-3 *m/z*. For example, a representative tumor peak (*m/z* species) and the morphological features of an individual patient's tissue sample are shown in Figure 2-1.

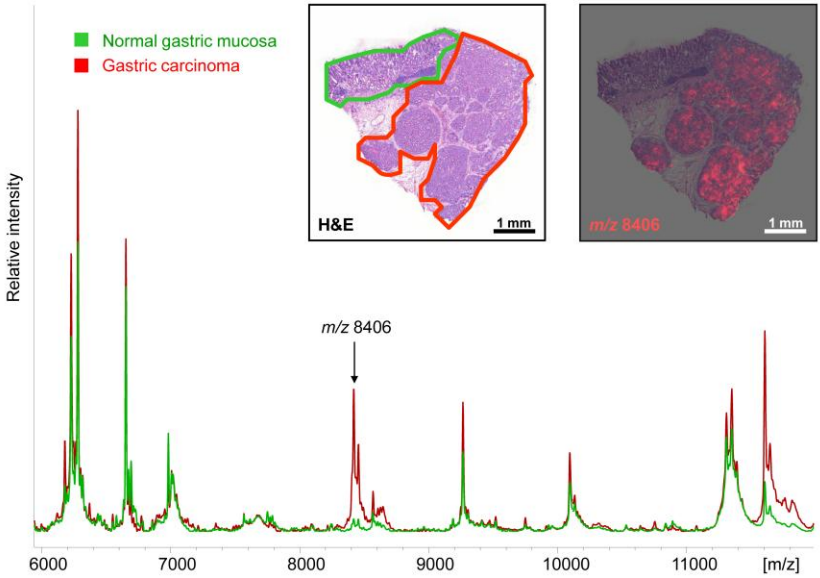

Figure 2-1 MALDI imaging reveals cell type-specific profiles, as shown in this comparison of gastric carcinoma (red) and normal gastric mucosa (green) from an individual patient's tissue. In this study, one example of differentially expressed masses (*m/z* 8406), exclusively present in cancer cells (right insert, red visualization), was found to correlate significantly with the patients' overall survival.

After setting the false discovery threshold to 0.1 and excluding correlated features, we found seven *m/z* species at an average of *m/z* 3445, *m/z* 6278, *m/z* 8406, *m/z* 8453, *m/z* 10098, *m/z* 11353, and *m/z* 11613, which were associated with patient survival (see Supplemental Figure 2-1). Correlations to clinicopathological parameters are listed in Table 2-1.

The influence of each *m/z* species on survival was then studied in more detail. Univariate Cox regression showed that, with the exception of *m/z* 3445 (P=0.075) which indicates a prognostic trend, all signals exhibit a strong non-favorable effect on survival. *M/z* 6278 (P=0.009) has the highest prognostic value, followed by *m/z* 11353 (P=0.012), *m/z* 10098 (P=0.013), *m/z* 8406 (P=0.018), *m/z* 8453 (P=0.022), and *m/z* 11613 (P=0.026) (Table 2-1). Setting intensity thresholds for each single *m/z* signal resulted in poor and good prognosis groups which all differed significantly in terms of overall survival (all P<0.05). A selection of Kaplan-Meier graphs for the long-and short-

term survivor groups are depicted in Figure 2-2, A and B, and Figure 2-3, A (for all Kaplan-Meier graphs see Supplemental Figure 2-2).

Multivariate Cox regression models of each respective *m/z* species, with nodal and resection status as well as distant metastasis status as covariables, showed that *m/z* 6278, *m/z* 8453, *m/z* 10098, and *m/z* 11613 are independent prognostic factors (all $P<0.05$), whereas *m/z* values of 3445 ($P=0.063$) and 8406 ($P=0.07$) showed slight dependencies (Table 2-2). In contrast, *m/z* 11353 does not exert an independent influence on survival ($P=0.16$).

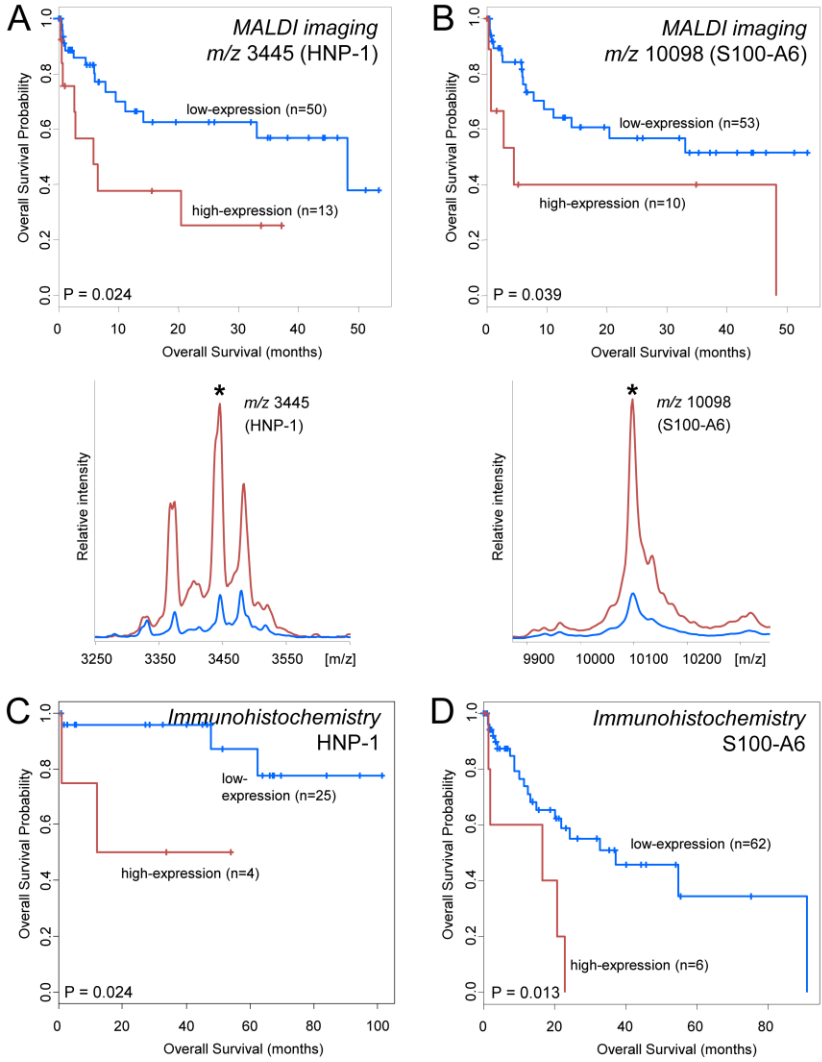

Figure 2-2 *M/z* 3445 and 10098, as measured by MALDI imaging and identified as HNP-1 and S100-A6 correlate with the survival of patients (A, B). Kaplan-Meier analyses in the immunohistochemical validation confirmed their prognostic value, although this effect was only observed in UICC-stage I patients (C, n=29) for HNP-1 and in UICC-stages II-III for S100-A6 (D, n=68).

Table 2-2 Multivariate survival analyses

Covariable	*Hazard ratio*	*95% Confidence interval*	*P value*
MALDI imaging			
m/z 3445 (HNP-1)	1.032	0.998 - 1.070	0.063
Nodal status	2.304	1.382 - 3.840	**0.001**
Distant metastasis	0.724	0.163 - 3.220	0.670
Resection status	1.398	0.273 - 7.160	0.690
m/z 6278	1.332	1.088 - 1.630	**0.006**
Nodal status	2.869	1.661 - 4.960	**0.000**
Distant metastasis	0.661	0.165 - 2.640	0.560
Resection status	0.531	0.092 - 3.080	0.480
m/z 8406 (CRIP1)	1.458	0.970 - 2.190	0.070
Nodal status	2.477	1.459 - 4.210	**0.001**
Distant metastasis	0.521	0.109 - 2.490	0.410
Resection status	0.772	0.116 - 5.160	0.790
m/z 8453	3.626	1.275 - 10.31	**0.016**
Nodal status	2.579	1.527 - 4.360	**0.000**
Distant metastasis	0.760	0.185 - 3.130	0.700
Resection status	0.643	0.121 - 3.420	0.600
m/z 10098 (S100-A6)	1.219	1.012 - 1.470	**0.037**
Nodal status	2.522	1.469 - 4.330	**0.001**
Distant metastasis	0.407	0.078 - 2.130	0.290
Resection status	1.042	0.171 - 6.350	0.960
m/z 11353	1.177	0.939 - 1.480	0.160
Nodal status	2.091	1.231 - 3.550	**0.006**
Distant metastasis	0.585	0.138 - 2.480	0.470
Resection status	1.668	0.326 - 8.530	0.540
m/z 11613	1.694	1.082 - 2.650	**0.021**
Nodal status	2.570	1.529 - 4.320	**0.000**
Distant metastasis	0.584	0.121 - 2.820	0.500
Resection status	0.867	0.137 - 5.470	0.880
Seven-protein signature	4.031	1.691 - 9.610	**0.002**
Nodal status	2.501	1.521 - 4.110	**0.000**
Distant metastasis	0.725	0.183 - 2.870	0.650
Resection status	1.165	0.260 - 5.220	0.840
Immunohistochemistry			
CRIP1 (*m/z* 8406)	1.570	1.012 - 2.440	**0.044**
Primary tumor	1.660	0.939 - 2.950	0.081
Nodal status	1.670	1.045 - 2.670	**0.032**
Distant metastasis	1.090	0.437 - 2.720	0.860
Resection status	1.030	0.363 - 2.950	0.950
S100-A6 (*m/z* 10098) *	3.800	1.130 - 12.81	**0.031**
Primary tumor	1.720	0.611 - 4.860	0.300
Nodal status	2.190	0.865 - 5.570	**0.098**
Distant metastasis	1.120	0.310 - 4.050	0.860
Resection status	1.670	0.355 - 7.830	0.520

Data are calculated by Cox proportional hazard regression. Bold print indicates that the *P* value is < 0.05.
*Union Internationale Contre le Cancer (UICC) stages II and III only.

Identification of three survival-related protein markers: HNP-1, CRIP1, and S100-A6

Protein identification of *m/z* 3445 was performed by tissue extraction and fractionation followed by bottom-up tandem mass spectrometry. Human neutrophil

peptide-1 (HNP-1) was identified with a Mascot Score of 109. Protein scores above 56 indicate identity or extensive homology (P<0.05) (see Supplemental Figure 2-3). Additionally, this mass has already been reported as HNP-1 in several other studies [71].

Signal *m/z* 8406 (+/-3 *m/z*) has previously been identified by our group as Cysteine-rich intestinal protein 1 (CRIP1) [53]. Similarly, the signal at *m/z* 10098 corresponds to the calcium binding protein, S100-A6, as previously shown by Schwartz *et al*. [70]

The other four molecular species have remained unidentified and require further elucidation efforts.

Validation on an independent patient cohort by immunohistochemistry confirms the prognostic relevance of the identified protein markers

Based on the results of the discovery study, we validated the predictive power of the identified proteins CRIP1, S100-A6, and HNP-1 using an independent test cohort comprised of 118 patients.

Although univariate analysis indicated a significant correlation of CRIP1 (P=0.016) on patient survival for all UICC stages, slight associations were found for HNP-1 and S100-A6 for certain subgroups. S100-A6 slightly reflected the survival in UICC stages II-III (P=0.077) and HNP-1 slightly the survival in UICC stage I patients (P=0.086). These findings are in line with the Kaplan-Meier analyses, as shown in Figure 2-2. Next, the global prognostic value of CRIP1 was further investigated in a multivariate analysis. CRIP1 was found to be the strongest variable, besides nodal status (P=0.032), to indicate the outcome of patients (P=0.044), therefore confirming its high predictive power (Table 2-2). This finding is also shown in the Kaplan-Meier analyses together with immunohistochemical examples of low and high expression of CRIP1 in Figure 2-3. Similarly, S100-A6 has a significant independent effect on the survival of stage II and III patients (P=0.031).

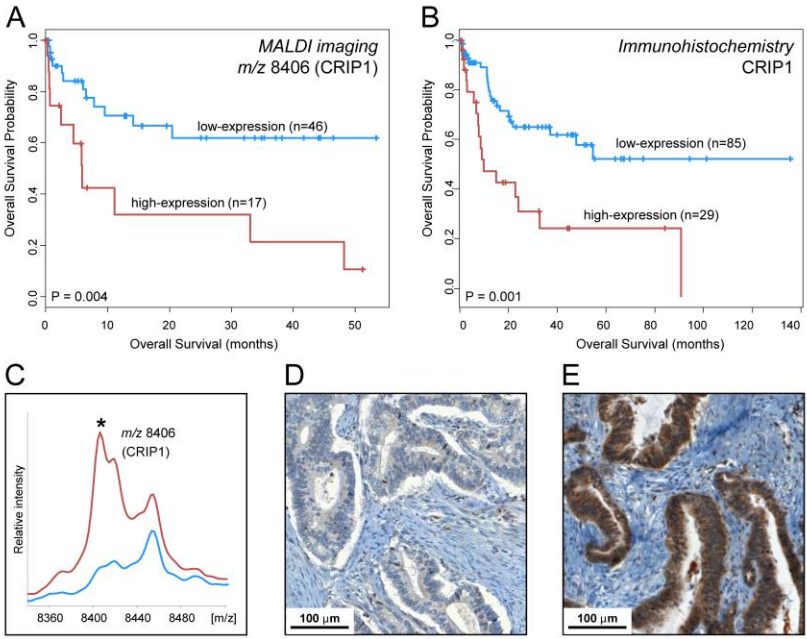

Figure 2-3 CRIP1, a previously unknown protein in gastric cancer, was found by MALDI imaging as a novel prognostic factor in the discovery cohort (A, C). Immunohistochemical validation confirmed this by showing a strong relationship between the high expression of CRIP1 (E) and poor survival (B) and vice versa (B, D), as calculated by Kaplan-Meier analysis (n=114).

Seven-protein signature predicts the outcome of patients independently of clinical parameters

To improve prognostic ability further, all seven markers were combined to establish a survival prediction model. Therefore, unsupervised clustering was applied to discriminate patients into two groups according to their seven-protein signature (Figure 2-4, A). The difference in patient outcome between both groups was assessed by univariate Kaplan-Meier analysis (P=0.002) (Figure 2-4, B) and multivariate Cox regression (P=0.002) (Table 2-2). This analysis indicated the strong predictive value of the signature independent of nodal or distant metastasis and resection status.

The discriminatory power of this pattern (Figure 2-4, C) between the two tumor subgroups was assessed by cross-validation of a classification model (support vector machine), which achieved a classification accuracy of 98% (95% CI: 91% to 100%).

A combination of mass signals representing the three identified proteins was found sufficient to be a significant indicator for patient survival, and even independent from clinical parameters. However, the full signature adds significantly more prognostic information (see Supplemental Figure 2-4).

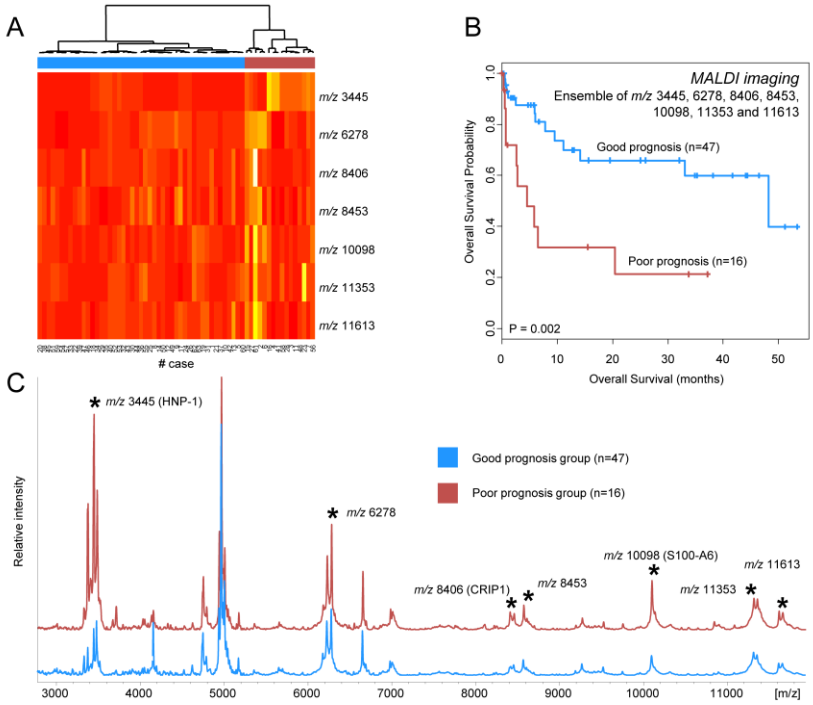

Figure 2-4 The prognostic power of a combined pattern was investigated by clustering all patients according to the seven protein signals (A, C). The main two branches of the tree were found to represent a good (blue) and a poor prognosis group (red) (B). Moreover, this pattern predicts patient outcome independently of major clinicopathological parameters (Table 2-2).

2.3.6 Discussion

Previous studies have defined prognostic subsets of gastric cancer based on gene or microRNA expression patterns [94-96, 106]. However, mRNA expression cannot always indicate which proteins are expressed or how their activity might be modulated after translation [107, 108]. Accordingly, analysis of the proteome in tumor

tissues might better reflect the underlying pathological state of cancers than gene expression patterns. A few tissue-based reports in gastric cancer have shown that proteomic patterns with surface-enhanced laser desorption/ionization-TOF can distinguish cancer patients from non-cancer patients [109, 110]. A very recent report in gastric cancer demonstrated that protein profiles obtained from endoscopic biopsy samples via MALDI imaging can distinguish pathologic early stage tumors from more advanced tumors [79]. However, none of the mentioned studies performed prognostic evaluations of the protein patterns. This study is the first to show that tissue-based proteomic profiling by MALDI imaging is able to identify protein patterns that predict patient survival in intestinal-type gastric cancer. Previously known and, more importantly, previously unknown protein biomarkers were identified, amongst them HNP-1, CRIP1, and S100-A6. Interestingly, both HNP-1 and CRIP1 have been described in the context of the immune system [111, 112]. It is known from clinical and experimental studies that the immune system is a significant determinant of epithelial tumorigenesis and further development [113].

Cysteine-rich intestinal protein 1 (CRIP1), a so far unknown protein in gastric cancer, was found in this study as an independent prognostic factor in the validation cohort (Table 2-2). Human CRIP1 belongs to the LIM family and is a tissue-specific developmentally regulated protein which is involved in protein–protein interactions during transcription [114-117]. CRIP1 has been suggested to play a role in the host defense system, too, and differential expression of CRIP1 can change cytokine patterns and the immune response [112]. In this context, an elevated level of CRIP1 in tumor cells may be sensible as it has been proposed that immune cells are actively recruited by tumors to exploit their pro-angiogenic and pro-metastatic effects. This is supported by gene expression analyses where mRNA of CRIP1 has been found to be overexpressed in various tumor types, including colorectal, pancreatic, prostate, breast, and cervical cancers [118-122]. However, this is the first study that describes CRIP1 to affect patient survival. No other significant correlations to major clinical parameters were found for CRIP1 in our study. Since the functional characterization of CRIP1 is currently inadequate, the precise role of CRIP1 in cancer cells is unclear and requires further investigation.

HNP-1 is an antimicrobial peptide that is expressed in human neutrophils of the innate immune system and found to be present in a variety of tumor types, including gastric and colon cancer [110, 111, 123]. The link between a chronic active inflammatory process, where neutrophils make up a significant portion of the inflammatory cell

infiltrate, and the onset of carcinoma has been convincingly demonstrated at the gastric and intestinal mucosal level [124]. It has been shown in cancers that a strong presence of infiltrating innate immune cells, such as neutrophils, correlates with increased angiogenesis and poor prognosis, whereas an abundance of infiltrating lymphocytes correlates with favorable prognosis [113]. This is reflected in several serum based studies that investigated the ratio between neutrophils and lymphocytes in different cancer types like in renal cell carcinoma or breast cancer [125, 126]. However, this study is the first to show the prognostic significance of HNP-1 in gastric cancer tissues. The results of this study underscore the assumptions that the immune system and associated proteins, represented here by HNP-1 and CRIP1, take a key role in tumor behavior and therefore clinical outcome for the patients.

In contrast, S100-A6, a calcium binding protein, has not been reported to be linked to the immune system. Amongst many versatile functions of S100-A6, it has been mainly described to be involved in cytoskeleton rearrangement since actin binding proteins, like annexins, have been identified as its target (see Supplemental Figure 2-5) [127]. In this context, interactions with tumor associated proteins like annexin A2 and p53 may indicate a role of S100-A6 in cancer progression and metastasis [128, 129]. And indeed, increased levels of S100-A6 have been found to be associated with metastasis or survival in colon and pancreatic cancer, respectively [130, 131]. Similarly, our study showed a significant correlation of S100-A6 expression with clinical parameters such as regional lymph node metastasis, distant metastasis, tumor cell differentiation, and prognosis. This is highly concordant with a recent study in gastric cancer demonstrating the association between S100-A6 expression and various clinicopathological features including clinical patient outcome [132]. Unfortunately, little is still known about the exact mechanism of S100-A6 with regard to an aggressive tumor phenotype. Nevertheless, our observations support the general findings that S100-A6 plays an important role in the progression and prognosis in gastric cancer patients.

The other four molecular species have remained unidentified so far and require further elucidation efforts. Since there is so far no universal strategy in MALDI imaging proteomics for identifying the molecular nature of a peak, each protein requires an individual identification approach and elaborate protocol adaptations [60, 133].

We shifted the emphasis of our study to the combination of these molecular species that are directly related to prognosis as it has been reported that individual markers may vary for a variety of reasons, but at a statistically significant level, a signature

would remain more robust [57]. The seven-protein signature described was found to be a new independent indicator of patient survival and may complement the previously known clinical parameters such as lymph node metastasis and stage in terms of prognostic relevance.

Importantly, the amount of tissue required for MALDI imaging is much smaller than any other available method using molecular profiling techniques such as array-based gene expression profiling. Thus, our study shows that protein profiles can be obtained from smallest amounts of unprocessed fresh frozen tissue samples, which are readily collectable in a clinical setting, to accurately predict prognosis. Since such small tissue samples can be used, it would be of great interest to analyze the protein expression patterns of tissue samples from small endoscopic biopsies or attempt to derive patterns associated with response to specific treatments and correlate these findings with the risk of progression to cancer. If these data are confirmed in larger numbers of patients, tissue-based proteomics profiling by MALDI imaging could have implications for the clinical management of patients with gastric cancer.

2.3.7 Supplementary material

Supplemental Figure 2-1

A

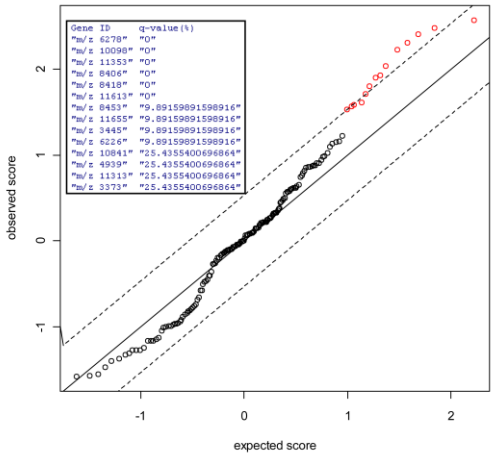

B

	m/z 6278	m/z 10098	m/z 11353	m/z 8406	m/z 8418	m/z 11613	m/z 8453	m/z 11655	m/z 3445	m/z 6226
m/z 6278	1.00	0.62	0.27	0.49	0.54	0.65	0.53	0.52	0.00	0.86
m/z 10098	0.62	1.00	0.54	0.63	0.56	0.69	0.28	0.75	0.02	0.27
m/z 11353	0.27	0.54	1.00	0.37	0.26	0.44	0.11	0.49	0.13	0.05
m/z 8406	0.49	0.63	0.37	1.00	0.89	0.69	0.50	0.66	-0.06	0.40
m/z 8418	0.54	0.56	0.26	0.89	1.00	0.66	0.60	0.59	-0.13	0.51
m/z 11613	0.65	0.69	0.44	0.69	0.66	1.00	0.54	0.85	-0.21	0.50
m/z 8453	0.53	0.28	0.11	0.50	0.60	0.54	1.00	0.45	-0.06	0.57
m/z 11655	0.52	0.75	0.49	0.66	0.59	0.85	0.45	1.00	-0.19	0.34
m/z 3445	0.00	0.02	0.13	-0.06	-0.13	-0.21	-0.06	-0.19	1.00	-0.07
m/z 6226	0.86	0.27	0.05	0.40	0.51	0.50	0.57	0.34	-0.07	1.00

Supplemental Figure 2-1 A: Significance Analysis of Microarrays (SAM) plot. Circles in plot represent individual *m/z* species. Dashed lines delimit the area of random effect. Red circles indicate that higher expression correlates with a higher risk. The inset lists the *m/z* species together with their individual q-values (indirectly related to the false discovery rate, which was set to a maximum of 10%). B: Correlation coefficients between *m/z* species. Correlation coefficients were calculated by Spearman's rank correlation. Values above 0.8 were considered highly correlated. Thus, the correlated signals with the lower q-values (*m/z* 6226, *m/z* 8418, and *m/z* 11,655) were excluded from further consideration.

Supplemental Figure 2-2

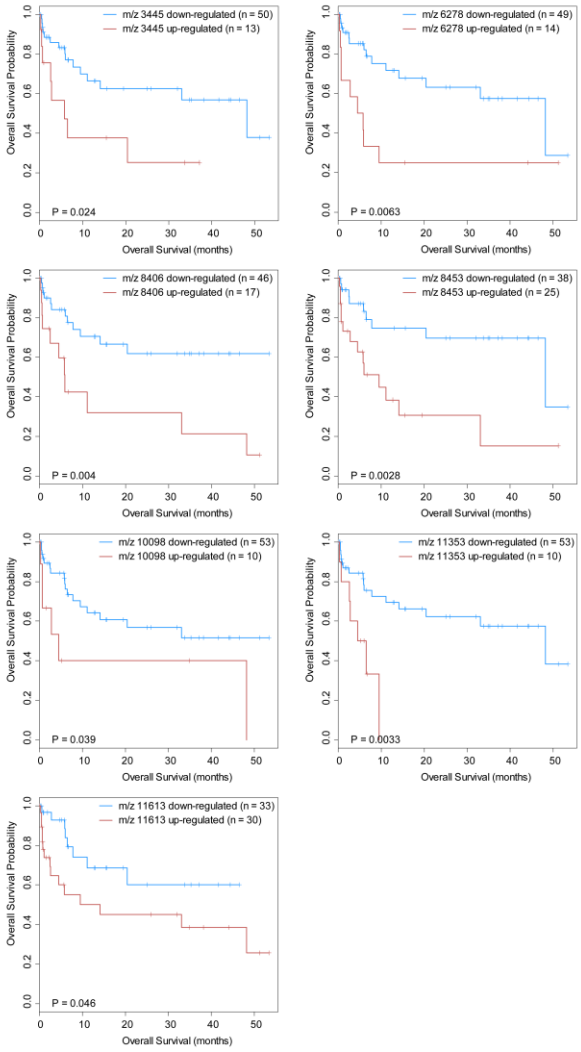

Supplemental Figure 2-2 Kaplan-Meier graphs for MALDI imaging *m/z* species 3445, 6278, 8406, 8453, 10098, 11353, and 11613.

Supplemental Figure 2-3

4758146 (100%), 10.201,0 Da

gi|30316322|sp|P59665.1|DEF1_HUMAN RecName: Full=Neutrophil defensin 1; AltName: Full=HNP-1; Short=HP-1; Short=HP1; AltName: Full=Defensin, alpha 1; Contains: RecName: Full=HP 1-56; Contains: RecName: Full=Neutrophil defensin 2

2 unique peptides, 2 unique spectra, 5 total spectra, 18/94 amino acids (19% coverage)

MRTLAILAAI LLVALQAQAE PLQARADEVA AAPEQIAADI PEVVVSLAWD ESLAPKHPGS
RKNMACYCRI PACIAGERRY GTCIYQGRLW AFCC

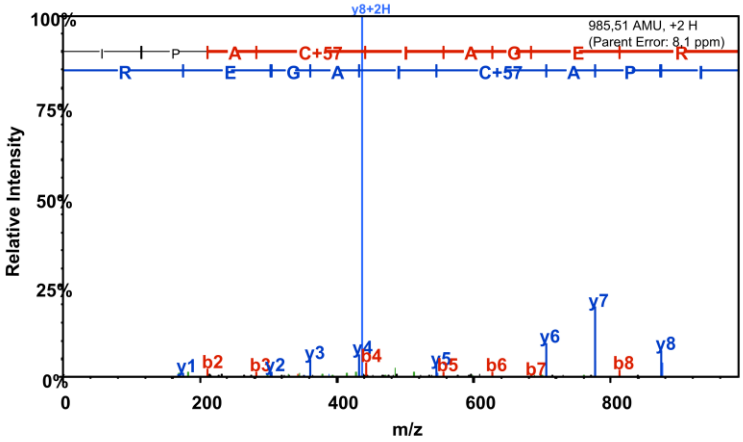

Supplemental Figure 2-3 Fragment spectra of HNP-1 identification. Neutrophil defensin 1 was identified with a Mascot score of 109 (P < 0.05). Neutrophil defensin 1 is cleaved into the peptides HNP-1 or HNP-2 (see Uniprot entry: P59665). HNP-2 differs from HNP-1 by the absence of one amino acid residue. Theoretical mass calculations from the resulting peptides identified *m/z* 3445 as HNP-1 and *m/z* 3373 as HNP-2.

Supplemental Figure 2-4

A

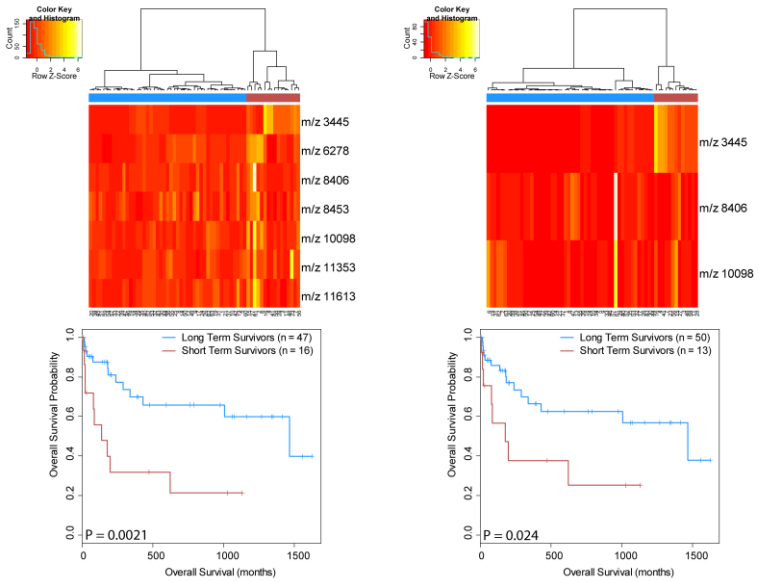

B

	Hazard ratio	Lower 95% CI	Upper 95% CI	*P* value
3-protein signature	3.172	1.28	7.86	**0.013**
Nodal status	2.394	1.457	3.93	**0.00057**
Distant metastasis	0.767	0.198	2.98	0.7
Resection status	1.352	0.312	5.85	0.69

	Hazard ratio	Lower 95% CI	Upper 95% CI	*P* value
3-protein signature	0.317	0.0635	1.59	0.16
7-protein signature	9.533	1.9819	45.85	**0.0049**

Supplemental Figure 2-4 Comparison of seven- and three-signal protein signature. Seven-signal (left) and three-signal (right) protein signatures obtained by MALDI imaging were compared with regard to their prognostic information. Therefore, patients were first clustered on basis of the respective signature (upper panels: see Materials and Methods in main manuscript) and the resulting groups were then compared by Kaplan-Meier analyses (lower panels) (A). Multivariate survival analyses by COX regression were performed in the MALDI imaging data set to assess the prognostic value of the three-signal protein signature in comparison with major clinical parameters (B, top) and with the seven-signal signature (B, bottom). Both analyses show that the three-protein signature is sufficient to be a significant indicator for patient survival, and even independent from clinical parameters. However, the full signature adds significant prognostic information.

Supplemental Figure 2-5

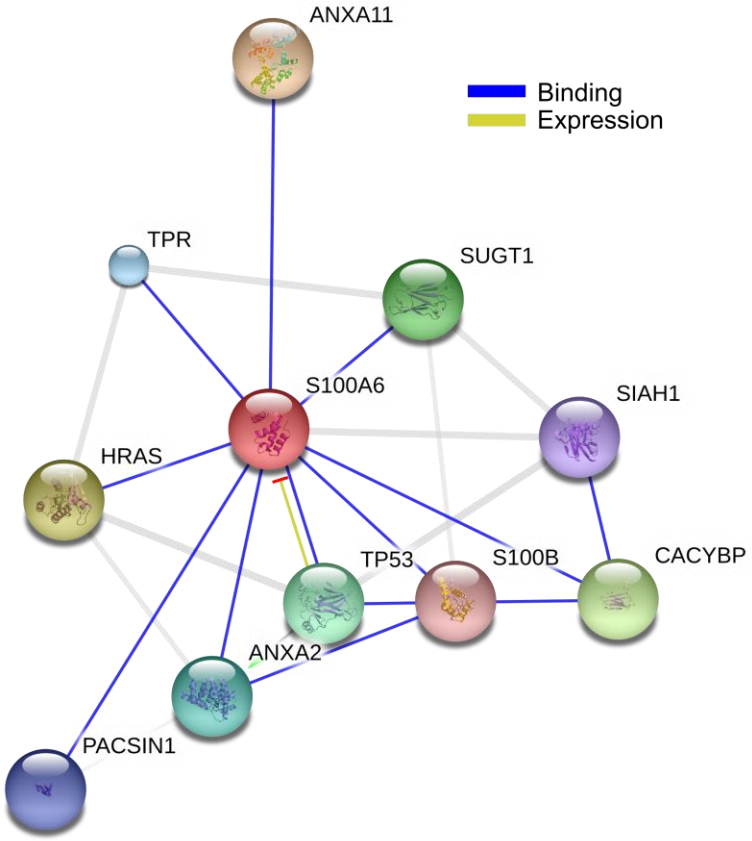

Supplemental Figure 2-5 Known and predicted interactions of S100-A6 (S100A6) with other proteins. This functional protein association network was obtained by searching the STRING online database (http://string-db.org) for the entry "S100A6," Interestingly, S100-A6 binds directly to proteins such as p53 (TP53) and annexin 2 (ANXA2), which have been extensively described in the context of cancer.

2.4 Classification of HER2/neu status in gastric cancer using a breast-cancer derived proteome classifier

Balluff B, Elsner M, Kowarsch A, Rauser S, Meding S, Schuhmacher C, Feith M, Herrmann K, Röcken C, Schmid RM, Höfler H, Walch A, and Ebert MP.

J Proteome Res. 2010 Dec 3;9(12):6317-22.

2.4.1 Journal description and standing

The Journal of Proteome Research (ISI abbreviation: *J Proteome Res*) publishes content encompassing all aspects of global protein analysis and function, emphasizing the synergy between physical and life sciences resulting in a multidisciplinary approach to the understanding of biological processes.

The journal is indexed by Thomson Reuters in the category Biochemical Research Methods. With an impact factor of 5.460 and a 5-year impact factor of 5.617 in the 2010 Journal Citations Reports it takes rank nine of 71 journals within its category. However, it ranks second in journals focusing on proteomics topics.

2.4.2 Abstract

HER2-testing in breast and gastric cancers is mandatory for the treatment with trastuzumab. We hypothesized that imaging mass spectrometry (IMS) of breast cancers may be useful for generating a classifier that may determine HER2-status in other cancer entities irrespective of primary tumor site.

A total of 107 breast (n=48) and gastric (n=59) cryo tissue samples were analyzed by IMS (HER2 was present in 29 cases). The obtained proteomic profiles were used to create HER2 prediction models using different classification algorithms.

A breast cancer proteome derived classifier, with HER2 present in 15 cases, correctly predicted HER2-status in gastric cancers with a sensitivity of 65% and a specificity of 92%. In order to create a universal classifier for HER2-status, breast and non-breast cancer samples were combined, which increased sensitivity to 78%, specificity was 88% respectively.

Our proof of principle study provides evidence that HER2-status can be identified on a proteomic level across different cancer types suggesting that HER2 overexpression may constitute a unique molecular event independent of the tumor site. Furthermore, these results indicate that IMS may be useful for the determination of potential drugable targets, as it offers a quicker, cheaper and more objective analysis than the standard HER2-testing procedures immunohistochemistry and fluorescence *in situ* hybridization.

2.4.3 Introduction

Overall prognosis in patients with advanced gastric cancer is poor [134]. Recently, Bang and coworkers reported the first results from a phase III trial which compared a systemic chemotherapy with cisplatin and capecitabine with and without trastuzumab in patients overexpressing human epidermal growth factor receptor 2 (HER2) in gastric cancers [33]. In this trial, patients with trastuzumab exhibited a significant improvement of progression free and overall survival. This is the first phase III trial demonstrating the efficacy of a targeted drug in a subgroup of gastric cancers exhibiting overexpression of the respective target [135].

In this context, the identification of drugable targets in this and other cancers is an important approach in order to develop new treatment strategies [136]. Inasmuch as numerous trials with all types of targeted drugs are now being conducted in almost all cancer types, identifying a strategy to find and rapidly confirm the presence of (multiple) targets in a cancer sample may facilitate the selection of the targeted drug that can be successfully administered.

Matrix-assisted laser desorption/ionization (MALDI) imaging mass spectrometry (IMS) allows the specific acquisition of proteomic profiles from histopathological interesting features like tumor cell populations through the direct analysis of thin tissue sections [137]. In recent years, IMS has been used to profile different cancers and has been shown to allow for the classification of different clinical features of cancers, such as

prognosis, lymph node metastasis and response prediction [69, 72, 99, 138-140]. Recently, we demonstrated that this modality can also be used to identify a proteomic signature that separates breast cancers based on HER2 status [53]. These findings underscored the potential of IMS in tissue diagnostics, especially since the two standard procedures for HER2 testing, based on immunohistochemistry (IHC) and fluorescence *in situ* hybridization (FISH), are either less accurate or time and cost expensive [50-52]. In contrast, IMS provides an objective classification compared to IHC, which suffers from observer variability, while consuming less money and time (several hours) compared to FISH (1–2 days). In addition, IMS allows, as a label-free and multiplexing approach, to determine several clinical parameters at once.

In an aim to facilitate the identification and rapid confirmation of potentially drugable targets in gastric cancer, we hypothesized that the previously identified breast-cancer derived proteomic algorithm may also be able to predict HER2 status in gastric or other cancers types.

2.4.4 Material and methods

Tissue specimens

Human tissue samples were collected, after obtaining informed consent from patients undergoing gastrectomy at the University Hospital of Berlin (gastric cancer test set) and the University Hospital of Munich (gastric cancer training set), Germany. Samples were snap-frozen during surgery and stored at -80° C until analysis. A total of 59 tissue samples, 45 from gastric cancer test set and 14 from gastric cancer training set, were analyzed.

HER2 status was determined in 2000 breast cancer patients. 48 samples of these patients were selected for this study according to the following criteria: breast cancer of type Invasive Ductal Carcinoma with clear HER2 status, availability of cryo material, and strong presence of tumor cell populations in the respective cryo tissue section. This set has been previously divided into a discovery (breast cancer training set) and a validation set (breast cancer test set), consisting of 30 and 18 cases, respectively [53].

An overview of all sample sets and the subsequent experimental workflow is depicted in Figure 2-5. Clinical and histological characteristics of all patients, including UICC staging, Laurén classification, estrogen/progesterone status, and HER2 status are

summarized in Table 2-3. This study was approved by the Ethics Committee of the Technische Universität München.

Table 2-3 Clinical and molecular characteristics of the patient series

Set characteristics	*Gastric Cancer*		*Breast Cancer*	
	Training set	Test set	Training set	Test set
Patients	14	45	30	18
Mean age (range)	64.9 (42–84)	67.9 (40–85)	60.1 (38–91)	61.4 (36–84)
HER2-IHC				
IHC 3+/2+	4/0	4/3	13/2	6/0
IHC 1+/0	1/9	12/26	2/13	6/6
HER2-FISH				
positive	4	n.a.	15	n.a.
negative	10	n.a.	15	n.a.
UICC stage - T				
pT1	0	1	12	1
pT2	11	21	16	11
pT3	3	18	1	1
pT4	0	5	1	0
pTx	0	0	0	5
UICC stage - N				
pN negative	3	4	17	6
pN positive	11	41	12	7
pNx	0	0	1	5
Laurén type (HER2+)				
intestinal	10 (4)	28 (4)	n.a.	n.a.
diffuse	4 (0)	11 (0)	n.a.	n.a.
mixed	0	6 (0)	n.a.	n.a.
ER / PR status				
ER +	n.a.	n.a.	14	5
ER -	n.a.	n.a.	16	13
PR +	n.a.	n.a.	9	13
PR -	n.a.	n.a.	21	5

Abbreviations: HER2 = human epidermal growth factor receptor 2; IHC = immunohistochemistry; FISH = fluorescence *in situ* hybridization; ER = estrogen receptor; PR = progesterone receptor; n.a. = not available

Assessment of HER2 status

HER2 status was evaluated in tumor tissue samples from 2000 breast cancers patients and 110 gastric cancer patients by both fluorescence *in situ* hybridization (FISH) and immunohistochemistry (IHC) on formalin-fixed, paraffin-embedded tissue blocks. Determination of HER2 status was performed according to the guidelines of the American Society of Clinical Oncology for HER2 testing for breast cancer, where a positive HER2 result is an IHC staining of 3+, a negative result is a staining of 0 or 1+. In case a staining was 2+, FISH was performed. A FISH ratio >2.2 (polysomy ratio) is considered HER2 positive; otherwise negative [141].

In case paraffin-embedded tissue blocks were not available HER2 status was assessed on the respective cryo tissues by IHC only (both test sets), according to the subsequent protocol. 10 µm thick sections were incubated with the primary antibody (anti-human c-erbB2 polyclonal antibody, Dako Denmark; dilution 1:300) at room temperature for one hour. The final immunohistochemical staining was carried out using an automated staining platform (Discovery XT, Ventana Medical Systems) according to the recommendations of the manufacturer. For cryo section staining, HER2 status was regarded positive with an IHC staining of 3+ (uniform membranous staining of >20% of tumor cells); conversely, HER2 status was regarded negative if IHC staining was classified as 0, 1+, or 2+, as reported by Bang *et al*. for gastric cancer patients not benefitting significantly from HER2 treatment [33].

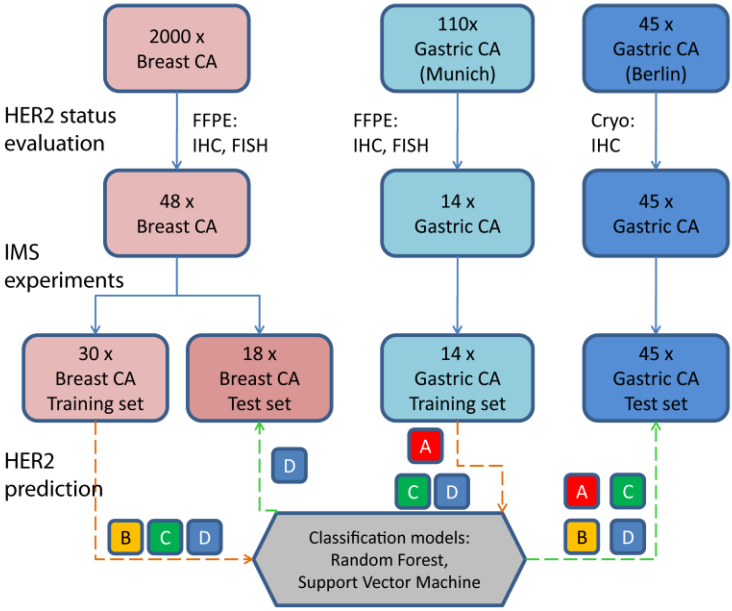

Figure 2-5 Experimental workflow. Three cancer (CA) collectives were evaluated for HER2 expression by IHC and/or FISH (top). Appropriate cryo tissues were subjected to IMS analysis (center). For HER2 status prediction, data were arranged in different set-ups, named A–D (Table 2-4), into either the training or test set, indicated by dashed lines in orange and green, respectively (bottom).

MALDI imaging mass spectrometry experiments and image processing

Tissue samples were cryosectioned (12 µm) onto conductive glass slides and prepared for measurement as outlined before [53]. Spectra were acquired using the Ultraflex III MALDI-TOF/TOF in positive linear mode (Bruker Daltonik), in a mass range of *m/z* 2,500–25,000 and a sampling rate of 0.1 GS/s. The lateral resolution for MALDI-IMS was set to 150 µm for the gastric cancer test set and the breast cancer training set. The second gastric cancer sample set and the breast cancer validation set were measured at 70 µm. 200 laser shots were accumulated per pixel at constant laser power. For calibration of spectra a ready-made protein standard was employed (Bruker Daltonik).

Following MALDI-IMS experiments, glass slides were washed for matrix removal in 70% ethanol, stained with hematoxylin and eosin, and scanned with a digital slide scanning system (Mirax Desk, Carl Zeiss MicroImaging). Finally, the tissue scans and MALDI-IMS results were superimposed to correlate mass spectrometric data with the histological features of the same section. This allowed for a direct, and therefore specific, on tissue selection of tumor related mass spectra.

Data processing and statistical analysis

Through all patients, spectra associated with tumor areas were selected using the FlexImaging 2.1 software (Bruker Daltonik). A total of 400 tumor spectra per patient were imported to the ClinProTools 2.2 software for data processing (Bruker Daltonik). This processing includes normalization according to the total ion count of each spectrum, peak identification, and alignment of spectra to correct for mass shifts between measurements.

For classification and statistical data exploration, the processed data were exported to the R statistical software (R Foundation for Statistical Computing). HER2 status prediction on cancer samples was implemented using two classification algorithms, namely either a Support Vector Machine (e1071 package) or a Random Forest (randomForest package). Both classification algorithms have proven their suitability for a variety of high-dimensional classification problems in biomedicine, amongst others also for proteomic data sets [53, 142-147]. In our study, we explored the ability of these classifiers to predict HER2 expression status using different training and test set combinations, as listed in Table 2-4. An *m/z* species was included into the prediction model if its area under curve (AUC) exceeded either 0.7 or 0.8, as calculated by receiver operating characteristic (ROC) analyses between HER2-positive and HER2-negative samples in the training set [148]. Moreover, training sets were chosen to

have close to equal parts of HER2 positive and negative samples in order to ensure sensitivity for infrequent HER2 positivity [149].

Due to computational limitations in spectra processing, 40 spectra were selected at random for each patient. As the Random Forest algorithm produces non-deterministic outcomes [150] and to reduce effects on our results due to random spectra selection, we repeated the spectra selection, processing, and classification ten times. Thus, the evaluation criteria sensitivity, specificity, accuracy, and their respective confidence intervals (CI) were averaged over all ten classification runs for each class prediction model.

Classification models were compared by calculating the Mann–Whitney *U* test (two-sided) on the three evaluation criteria across the ten runs. P-values <0.05 were considered statistically significant. These results are provided in detail as supplementary material.

2.4.5 Results

Imaging mass spectrometry for HER2 classification on human tissue samples

Breast cancer samples (training set n=30, test set n=18), and non-breast cancer samples (gastric adenocarcinomas; training set n=14, blinded test set n=45) underwent mass spectrometric analysis utilizing MALDI-IMS. The obtained mass spectra, labeled as either HER2-positive or HER2-negative by IHC and/or FISH, were used to arrange training and test set data (see Materials and Methods for a detailed description).

In the following, we report the prediction quality for HER2 status using two classification algorithms, namely a Support Vector Machine (SVM) and a Random Forest classifier, focusing on the results with an AUC threshold of 0.8 for the feature selection (for results with AUC=0.7 see Supplemental Table 2-1). The classification models were trained and tested in four different combinations, named A to D as listed in Table 2-4.

Table 2-4 Training set – test set line-ups

Setting	*Training set (HER2+/HER2-)*		*Test set (HER2+/HER2-)*	
A	Gastric Cancer	(4/10)	Gastric Cancer	(4/41)
B	Breast Cancer	(15/15)	Gastric Cancer	(4/41)
C	Gastric + Breast Cancer	(19/25)	Gastric Cancer	(4/41)
D	Gastric + Breast Cancer	(19/25)	Gastric + Breast Cancer	(10/53)

Sample sets as referred in Table 2-3 are combined to different training and test set scenarios (A–D). The numbers in parenthesis indicate the number of HER2-positive versus HER2-negative samples in the respective sets.

In a first attempt (Table 2-4, A), the classifiers should make use of the HER2 associated proteomic patterns from gastric cancer samples only to predict HER2 status in gastric cancer samples. We achieved a high accuracy for the SVM (91%; 95% confidence interval (CI-95%): ±0%), but both methods perform poorly as we obtained sensitivities of 0% (Table 2-5, A). This may be due to susceptibilities of the models to class distribution imbalances and the small number of samples in the training set.

Next, we investigated the classificatory capability when proteomic data originating from one cancer type is employed for prediction in another cancer type. Here, spectral data from breast cancer was used to predict the HER2 status in all gastric cancer samples (Table 2-4, B). The SVM based classifier was able to detect 65% of the HER2 positive patients (CI-95%: ±8%) while maintaining a high specificity of 92% (CI-95%: ±2%; Table 2-5, B).

Generation and testing of a universal HER2 classifier

In an effort to generate and evaluate a universal HER2 classifier, the next training set combined the profiles of different cancer types. Therefore, non-breast cancer samples were added to the previous training set. The classification performance was assessed twice; first on a test set consisting just gastric cancer samples (Table 2-4, C), and secondly on a mix of breast and gastric cancer samples (Table 2-4, D).

While there is no significant improvement in overall accuracy for the models in setting C, the Random Forest's sensitivity benefitted significantly from the addition of the gastric cancer samples in the training set (from 28% to 50%; CI-95%: ±7%; p=0.004;

Table 2-5, C; Supplemental Table 2-3). Similarly, the sensitivity of the Support Vector Machine slightly increased to 73% (CI-95%: ±5%).

Finally, in order to test the classifiers for universal classificatory power, also breast cancer patients were added to the test set (Table 2-4, D). Because of the high prevalence of breast cancer cases in the training set, all classifiers gain in sensitivity ($p<0.05$; Supplemental Table 2-3), even though with a little drawback in specificity ($p<0.05$; Supplemental Table 2-3). This finally results in sensitivities of 70% (CI-95%: ±3%) and 78% (CI-95%: ±3%) for the Random Forest and SVM with specificities of 87% (CI-95%: ±2%) and 88% (CI-95%: ±1%), respectively (Table 2-5, D).

Table 2-5 Classification results for training set – test set line-ups A–D

Setting		*Random Forest*			*Support Vector Machine*		
		Sensitivity	Specificity	Accuracy	Sensitivity	Specificity	Accuracy
A	Mean	0%	40%	37%	0%	100%	91%
	CI-95%	±0%	±4%	±4%	±0%	±0%	±0%
B	Mean	28%	95%	89%	65%	92%	90%
	CI-95%	±9%	±0%	±1%	±8%	±2%	±1%
C	Mean	50%	93%	89%	73%	91%	89%
	CI-95%	±7%	±2%	±2%	±5%	±1%	±1%
D	Mean	70%	87%	84%	78%	88%	87%
	CI-95%	±3%	±2%	±2%	±3%	±1%	±1%

Prediction performances of the two classification algorithms - Random Forest and Support Vector Machine - were evaluated according to their sensitivity, specificity, and accuracy within their 95% confidence intervals (CI) for each setting as described in Table 2-4.

2.4.6 Discussion

In breast cancers overexpression of HER2 is present in approximately 10%–34% of invasive breast cancers, and overexpression is known to be associated with a more aggressive biology of the tumor leading to a poor prognosis and response to chemotherapy [151]. Therefore, HER2 expression status is routinely evaluated for every patient with newly diagnosed primary breast cancer by two testing methods: immunohistochemical analysis and fluorescence *in situ* hybridization. Positively tested patients are eligible for treatment with trastuzumab, a monoclonal antibody directed to HER2, where breast cancer patients benefit from a higher survival rate [152, 153]. The efficacy of this therapy has led to investigate the role of HER2 expression in other cancer types, including gastric and gastroesophageal adenocarcinomas.

In gastric cancer about 20% of the patients also show overexpression of HER2, with an imbalance in occurrence which favors intestinal (~24%) versus diffuse type (~5%) tumors [37, 48]. Recent studies also indicate that HER2 may be of prognostic significance in gastric and esophageal cancers, where HER2 overexpression is associated with a poor survival [37]. Furthermore, anti-tumor activity of trastuzumab has been documented on gastric cancer cell lines [154-157] and xenograft models [158, 159]. On the basis of these results, clinical studies have started to explore the therapeutic effect of trastuzumab on HER2-positive gastric cancer patients. The extensive phase III ToGA trial provided the first evidence that targeting HER2 results in a demonstrable survival benefit for patients [33].

Thus, based on the relevance of determining the HER2 status in breast cancers and gastric cancers with regard to the selection of trastuzumab, we hypothesized that the HER2 status of a cancer may constitute a unique molecular feature that results from a range of specific molecular alterations that are independent of the site of the tumor and that might be reflected at the proteome level.

In order to test this hypothesis we used imaging mass spectrometry (IMS), which allows the development of proteome classifiers which can separate cancers of specific clinical and molecular characteristics [69, 72, 140]. IMS leads to the specific acquisition of proteomic profiles from histopathological interesting features like tumor cell populations through the direct analysis of thin tissue sections [137]. Because IMS combines the advantages of label-free mass spectrometry with histology, it has developed rapidly throughout the last years in profiling of diseased tissues [99, 138, 139]. Recently, we reported that IMS may generate a proteomic signature which correlates with HER2 expression and could be used to accurately define HER2-positive from HER2-negative breast cancer tissues [53]. In continuative, not-published experiments, we also proved the separability of gastric cancer according to HER2 status on cell lines (data not shown).

Based on these findings and the importance of rapid detection and confirmation of drugable targets in these cancers, we hypothesized that a breast cancer derived proteomic algorithm could also be used in gastric adenocarcinomas in order to predict HER2 status. Prediction of HER2 status by IMS is thereby based on the detection of masses which reflect molecular alterations that underlie HER2 overexpression.

We explored the quality of HER2 status prediction by two different classification algorithms on various training and test set combinations. In our first setting, classifiers

were trained on spectra derived from non-breast cancer in order to predict HER2 status in gastric cancer patients. However, in line with other studies [37, 48, 157], we observed a very low frequency of HER2-positive gastric cancers. This leads to the assumption that the training set may not be representative and balanced enough to become sensitive for HER2 positivity. In this scenario none of the classifiers achieved a good classification performance.

In an innovative approach we used the expression profiles of the fully balanced breast cancer set from Rauser *et al*. in order to predict HER2 status in non-breast cancers [53]. Interestingly, the classification models obtained sensitivities of 65% (SVM: AUC=0.8) and 50% (Random Forest: AUC=0.7) while keeping specificities over 90%. The reason for the increase might be two-fold. First, the capability of the two algorithms to generalize to situations not presented in the training sets (over-fitting robustness), in our case the classification of gastric cancer samples by a breast cancer trained model. Second, the emphasis of the training set on *m/z* species that better reflect HER2 status. This would support our main hypothesis. In the previous scenario the very same *m/z* species showed the same trend, but were overshadowed by signals that may be associated with some other unknown feature (Figure 2-6).

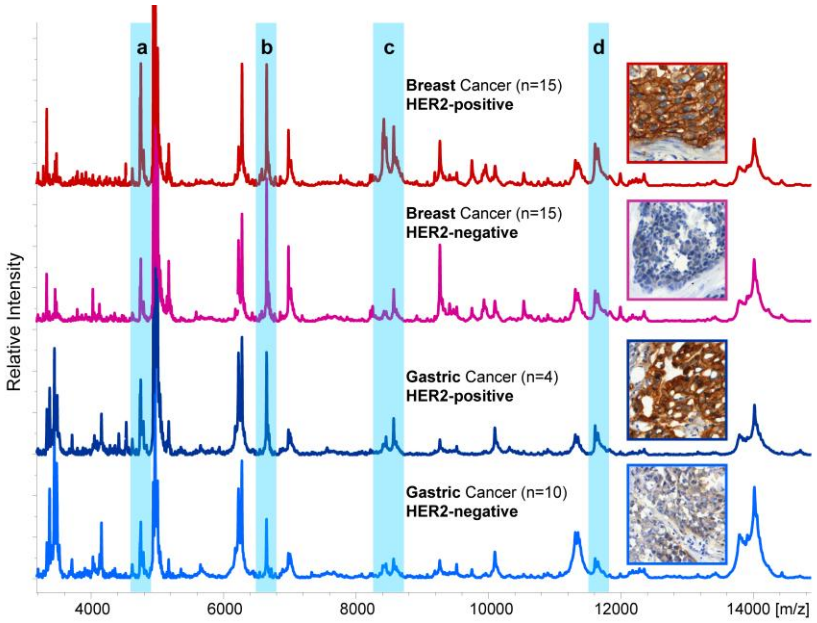

Figure 2-6 Proteomic profiles of breast and gastric cancer tissues. A classifier based solely on the low-number gastric cancer training set may be biased by signals that are not associated with HER2 status (e.g. signals: b, d). Employing the well-characterized breast cancer training set will strengthen those *m/z* species in the classification model that are known to be HER2 specific (signals: a, c).

As a next step, spectral data of breast and non-breast cancer were combined in an aim to construct a universal HER2 classifier. The performance of this classifier was tested both on a non-breast cancer set (setting C) as well as on a mixed cancer set (breast and gastric cancer in setting D).

The SVM showed a significantly higher accuracy in the last setting (D) than the Random Forest approach (p=0.025; Supplemental Table 2-1). This may be linked to the better fit of the SVM to the training data (p=0.003, see Supplemental Table 2-1). However, the Random Forest showed similar results at an AUC=0.7 (see Supplemental Table 2-1). Thus, together with other advantages, like little parameterization and internal feature selection, it is an attractive alternative to the SVM [160].

In both settings C and D, the two classifiers benefit from this addition by obtaining high sensitivity values of up to 70% and 78% (D). Together with high values for specificity (87% and 88%), both models offer an accurate classification of mixed cancer groups for HER2 expression status.

In summary, in our pre-clinical study we found that HER2 status of gastric cancer could be predicted accurately by protein patterns originated from breast cancer, yielding accuracies above 90% independent of the prediction method. Although these results must be validated in larger series and can only be regarded as proof of principle, our findings indicate that – based on a proteome based classifier – molecular characteristics of cancers can be identified that are independent of the site of the tumor and may, therefore, reflect unique molecular and genetic alterations that help to identify drugable targets across different cancer types.

2.4.7 Supplementary material

Supplemental Table 2-1

Supplemental Table 2-1 Comparison of classification performances between Random Forest (RF) and Support Vector Machine (SVM)

Minimum AUC – setting	*Performance values (mean)*						*Comparison: RF vs. SVM*		
	Random Forest (RF)			*Support Vector Machine (SVM)*			*P-values (Wilcoxon test)*		
	Sensitivity	*Specificity*	*Accuracy*	*Sensitivity*	*Specificity*	*Accuracy*	*Sensitivity*	*Specificity*	*Accuracy*
0.7 – A	0.0	42.7	38.9	0.0	100.0	91.1	-	0.000	0.000
B	50.0	95.1	91.1	77.5	40.0	43.3	0.020	0.010	0.000
C	47.5	89.8	86.0	72.5	40.7	43.6	0.000	0.000	0.000
D	69.0	86.0	83.3	86.0	44.7	51.3	0.000	0.000	0.000
0.8 – A	0.0	40.5	36.9	0.0	100.0	91.1	-	0.000	0.000
B	27.5	95.1	89.1	65.0	92.2	89.8	0.000	0.001	0.150
C	50.0	92.9	89.1	72.5	91.0	89.3	0.001	0.064	0.903
D	70.0	86.6	84.0	78.0	88.3	86.7	0.002	0.318	0.025

Supplemental Table 2-2

Supplemental Table 2-2 P-values (Wilcoxon *U* test) of statistical comparison of classification performances between 0.7 and 0.8 AUC thresholds

Setting	*Accuracy*		*Sensitivity*		*Specificity*	
	RF	*SVM*	*RF*	*SVM*	*RF*	*SVM*
A	0.394	-	-	-	0.381	-
B	0.027	0.001	0.004	0.046	0.676	0.035
C	0.180	0.000	0.648	1.000	0.209	0.000
D	0.606	0.000	0.648	0.010	0.753	0.000

Supplemental Table 2-3

Supplemental Table 2-3 P-values of statistical comparison (Wilcoxon *U* test) of classification performances between the settings A–D

Minimum AUC	*Settings*	*Accuracy*		*Sensitivity*		*Specificity*	
	to compare	*RF*	*SVM*	*RF*	*SVM*	*RF*	*SVM*
0.7	A vs. B	0.000	0.000	0.000	0.001	0.000	0.000
0.7	B vs. C	0.015	0.196	0.648	0.048	0.033	0.132
0.7	C vs. D	0.196	0.167	0.000	0.002	0.209	0.380
0.8	A vs. B	0.000	0.105	0.000	0.000	0.000	0.000
0.8	B vs. C	0.714	0.556	0.004	0.167	0.049	0.164
0.8	C vs. D	0.001	0.023	0.002	0.013	0.002	0.016

3 Conclusion and outlook

The aim of my thesis was to search for molecular markers associated with clinically relevant questions such as prognosis or therapy prediction in patients with gastrointestinal cancers. In the results presented in this thesis, I showed protein expression profiles and single markers identified by MALDI imaging that are correlated with the overall survival and the HER2 expression status of gastric cancer patients. These marker profiles enable a stratification of patients with regard to survival and trastuzumab therapy selection which allows a more individual adaption of the treatment strategy. In comparison to other MALDI imaging studies, both published studies involved a large number of patient samples (181 for the survival study and 107 for the HER2 study), thereby raising the confidence of the results.

In the first study (section 2.3), a seven-protein signature was found to be correlated with the overall survival of intestinal-type gastric cancer patients, independently of major clinical parameters. Identification and immunohistochemical validation of three proteins confirmed their prognostic value for the stratification of existing clinical patient groups which might benefit from a different treatment. Future experiments for the functional characterization of the three proteins in gastric cancer cell lines have to evaluate their role in gastric cancer and their potential of new therapeutic targets. The protein identification rate, however, shows that one bottleneck in MALDI imaging is still the protein identification. New approaches are being developed that employ other mass analyzer technologies than TOF, such as Fourier transform based analyzers, together with alternative sample preparation protocols to achieve higher identification rates of *m/z* species [161, 162].

Even though a protein can be identified, there is no guarantee that it can be measured and therefore validated by other techniques. This is especially true for combinatorial protein modifications that can easily be detected by mass spectrometry but hardly be discovered by other approaches [163]. Such modifications can harbor clinical relevant information, which has also been shown in the same study, where a peak belonging to a single acetylated histone H4 could also be correlated with a reduced survival of the 63 gastric cancer patients (data was not included in publication). This modification, which is frequent on histones, belongs to the epigenetic effects which regulate gene-expression through chromatin remodeling [164]. As a multitude of new epigenetic

drugs are being developed, one can imagine the application of MALDI imaging to directly measure both, the drug's distribution, as well as the effects on its target molecules ("pharmacoproteomics") [165].

In the second presented study (section 2.4), protein expression profiles from gastric and breast cancers were used for the classification of the HER2 status of tumors, which is important for therapy decision making. As the MALDI imaging approach is more specific and less sensitive than the standard HER2 testing procedures, one may speculate if the reported protein classifier may detect all responders compared to the standard HER2 testing procedures, which can result in false-positive rates of up to 20% [166]. However, this hypothesis has to be tested in subsequent studies with clinical response data available. Interestingly, the HER2 classifier appeared to be applicable across different adenocarcinoma types, including breast and gastric cancer, and even cancer of the gastro-esophageal junction (data not shown). This suggests that HER2 overexpression might be based on common molecular events irrespective of the tumor type and that data obtained by MALDI imaging can be combined and compared across different cancers and studies. A subsequent project from a colleague extended this idea and combined the data from six tumor types in order to determine the primary tumor of metastatic tumors [85].

It is of importance that the determination of HER2 status has been carried out on the mean spectra over cancer regions, i.e. the spatial distribution within data sets was not considered. However, this might be problematic in cases where HER2 positive cells constitute a minority and thus signals indicating HER2 positivity may be lost in the average spectrum [167]. To address this problem, a supervised, pixel-based classification of the HER2 status of breast cancers sections was carried out in consecutive experiments. This approach facilitated to identify samples with heterogeneous HER2 expression. This could be important because intratumoral heterogeneity has been identified as a major factor to influence prognosis and therapy response of patients [168, 169]. In this context, a high spatial resolution is required in order detect even smallest but relevant tissue cell populations.

An increased spatial resolution could also have extended my studies to diffuse-type gastric cancers. These were mostly excluded from my studies because diffuse-type gastric cancer is characterized by a non-adhesive growth leading to the wide-spread distribution of single cancer cells in a tissue which makes their measurement without single cell resolution difficult. Several groups have worked on sample preparation

procedures and instrumentation to achieve now measurements at cellular and even sub-cellular level [170, 171].

Another important practical obstacle in imaging mass spectrometry is still the quantification of the signals measured. Solving this issue could facilitate inter-laboratory comparability and reproducibility, opening possibilities for multicenter studies and, therefore, the clinical applicability of MALDI imaging. This has been recognized by the MALDI imaging community and is therefore in the focus of recent investigations [172]. Although both of my studies included an independent validation step, such harmonization would facilitate to test the general applicability of both protein signatures in larger multicenter cohorts, also prospectively. If my data are confirmed in larger numbers of patients, tissue-based proteomics profiling by MALDI imaging could have implications for the clinical management of patients with gastric cancer.

In that way, one could envision the translation of MALDI imaging into clinico-pathological routine. Especially in gastroenterology, which is significantly based on bioptic diagnostics, tissue samples from patients could be tested by MALDI imaging for the protein signatures found in my studies (Figure 3-1). This could assist the clinician in the clinical management of the patients with regard to therapy decision making and survival prediction – thus, making one more step towards a more personalized medicine.

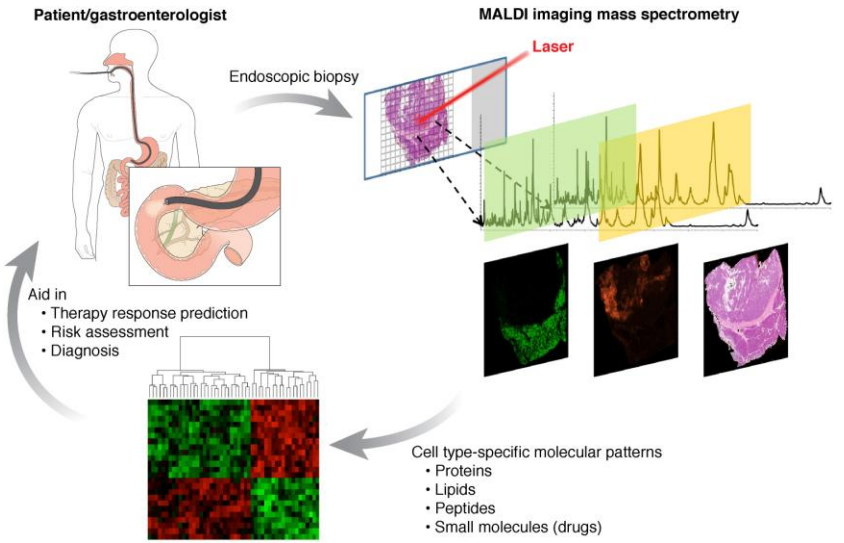

Figure 3-1 Visionary application of MALDI imaging in a clinical setting (gastroenterology). MALDI imaging is able to analyze even smallest tissue samples from patients, such as endoscopic biopsies, which are routinely collected in a gastroenterological setting. The subsequent MALDI imaging analysis is quick, histology-directed and allows extracting spatially resolved, cell type-specific molecular signatures from a wide variety of molecule classes. These patterns may, therefore, objectively support the clinician or pathologist in relevant questions such as in tissue diagnostics, therapy response prediction, or disease outcome prediction. Taken from [77].

4 Technical appendix

4.1 MALDI imaging mass spectrometry

In the following subsections the basics, the advantages and limitations of mass spectrometry will be briefly explained with regard to the relevant issues for MALDI imaging. Then, more details will be given on the principle, the workflow and the applications of MALDI imaging.

4.1.1 Mass spectrometry

Mass spectrometry refers to a methodology that ionizes sample molecules and separates the ions according to their mass-to-charge (*m/z*) ratio in high vacuum. The result, a mass spectrum, is a graphical plot of measured ion intensity versus its *m/z* value (example: Figure 4-3, B and C) [60].

Components of a mass spectrometer

A mass spectrometer device consists of three major parts: an ion source, where the analytes are ionized, a mass analyzer which separates the ions according to their *m/z* ratio, and a detector which records the ion current (Figure 4-1) [173].

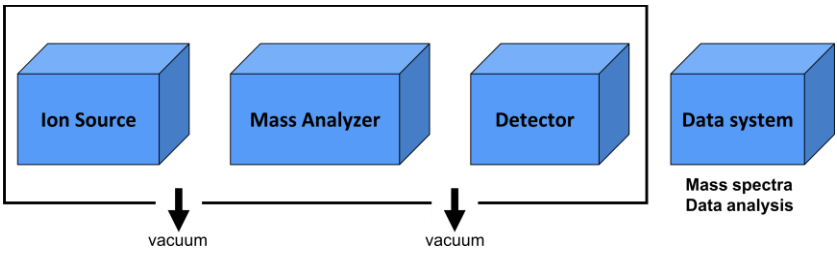

Figure 4-1 Principal components of a mass spectrometer. A mass spectrometer device consists of an ion source, where the analytes are ionized, a mass analyzer which separates the ions according to their *m/z* ratio, and a detector which records the ion current. The system must be under vacuum condition for the unhindered analysis of the analytes. A data analysis system for the interpretation of the recorded data is also a basic component.

There are several techniques for the ionization of an analyte. These can be grouped into four basic categories: electron, spray, desorption, and chemical ionization techniques [174]. Electron and chemical ionization are suitable for small, volatile compounds. In contrast, “soft” ionization techniques like the electrospray ionization (ESI) and matrix-assisted laser desorption ionization (MALDI) samples allow measuring large labile molecules such as proteins. While ESI ionizes molecules within liquid

samples, MALDI is applied for ionization of molecules embedded into a solid matrix [173]. Both methods have been crucial for the rapid advance in proteomics [60]. With regard to mass spectrometry as an imaging technique, the ionization must be done from a solid surface, leaving the desorption methods, such as MALDI, as the only choice [174].

Matrix-assisted laser desorption/ionization (MALDI)

Preparation for MALDI experiments requires the sample to be mixed with a low molecular weight organic molecule, called 'matrix'. This matrix has to show high energy absorption at the wavelength of the applied laser beam. In addition, each type of matrix favors the ionization/desorption of a different type of biomolecules (Table 4-1) [173]. The most common matrix compounds in proteomic experiments are 2,5-dihydroxybenzoic acid (DHB), α-cyano-4-hydroxycinnamic acid (CHCA), and sinapinic acid (SA) [175]. These compounds are usually dissolved in a 50%–70% acidified organic solvent solution which promotes analyte extraction [175].

Table 4-1 Common matrices. Taken from [173]

Analyte	*Matrix*
Peptides	2,5-Dihydroxybenzoic acid (DHB, gentisic acid)
	alpha-Cyano-4-hydroxycinnamic acid (CHCA)
	3-Hydroxypicolinic acid (3-HPA)
	2,4-Dinitrophenylhydrazine (2,4-DNPH)
Proteins	2,5-Dihydroxybenzoic acid (DHB, gentisic acid)
	alpha-Cyano-4-hydroxycinnamic acid (CHCA)
	3,5-Dimethoxy-4-hydroxycinnamic acid (SA, sinapinic acid)
Oligonucleotides	4,6-Trihydroxyacetophenone (THAP)
	3-Hydroxypicolinic acid (3-HPA)
Lipids	2,5-Dihydroxybenzoic acid (DHB, gentisic acid)
	2,6-Dihydroxyacetophenone (DHA)

After evaporation of the solvent, analyte molecules are embedded into the crystal grid of the matrix (Figure 4-2). Under high vacuum conditions, a pulsed laser beam is directed toward the co-crystal. Matrix molecules are excited by the laser energy which results in an explosion and transition of matrix and embedded sample analytes into the gas phase. During this process ionization of the analyte molecules (M) takes place which typically results in single protonation $(M+H)^+$ or deprotonation $(M-H)^-$; addition of a single sodium $(M+Na)^+$ or potassium atom $(M+K)^+$ is less frequent.

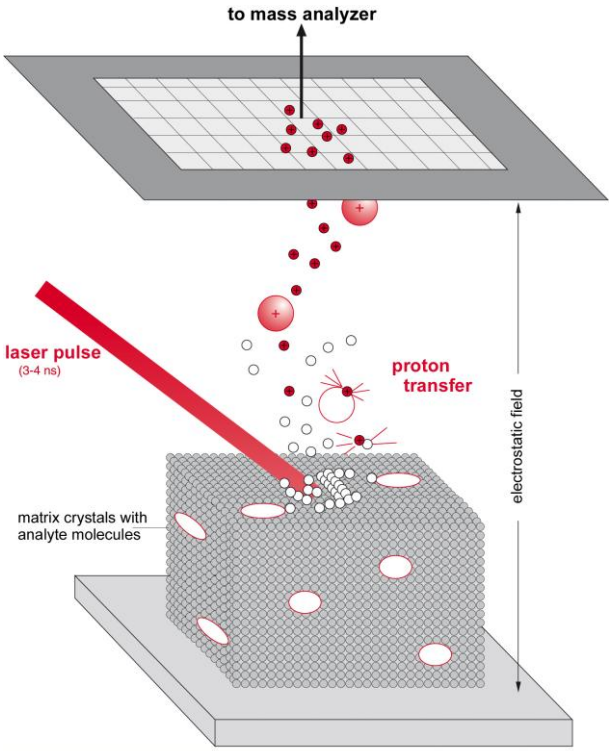

Figure 4-2 Principle of matrix-assisted laser desorption/ionization (MALDI). Analytes are co-crystallized with a light absorbing matrix. A short laser pulse irradiates the matrix surface. The matrix absorbs the energy which leads to a desorption process of both matrix and analyte molecules. During this process analytes are ionized by protonation which facilitates the acceleration of the produced ions by an electrostatic field towards the mass analyzer. Modified from [173].

MALDI is referred to as "soft" ionization method as most of the energy is absorbed by the matrix, leading to less fragmentation of the analyte components. This makes MALDI especially suitable for the ionization for larger biomolecules such as peptides or proteins which in turn makes it attractive for proteomics research.

Mass analyzers

Once the ions have been created they have to be separated in a second step by the mass analyzer. This can be done according to the needs of the scientist on the basis of

different physical principles. There are plenty of different mass analyzer techniques including quadrupole, ion trap, time-of-flight (TOF), Fourier-transform ion cyclotron resonance (FT-ICR), or Orbitrap mass analyzers. For a concise overview and comparison of these technologies please refer to the literature [67, 174]. Most commercial MALDI based mass spectrometers are combined with a time-of-flight (TOF) separator.

Time-of-flight mass analyzer

Briefly, in the time-of-flight (TOF) approach, the *m/z* value of a molecule is determined by measuring its flight time through a drift tube under high vacuum (Figure 4-3) [11].

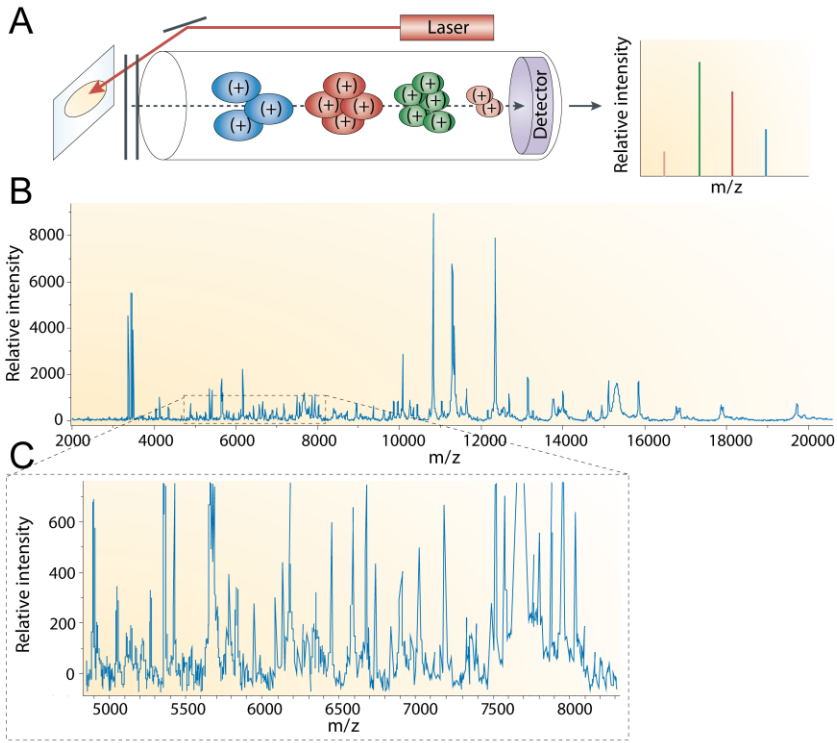

Figure 4-3 Time-of-flight (TOF) separation of MALDI ions. Following acceleration in the MALDI ion source, the ions can be separated according to their different times of flight trough a vacuum tube which depend on their mass and charge (*m/z*) (A). The intensities measured by the detector depend on the number of ions with the same *m/z*. A typical mass spectrum in the

mass range between *m/z* 2,000 and 20,000 is shown in (B), with a magnification of the mass range between *m/z* 5,000 and 8,000 (C). Taken from [11].

Directly after the molecules having been ionized they undergo, still in the ion source device, acceleration in an electrostatic field (Figure 4-2). At the end of the acceleration path, all molecules, even of different masses, have gained the same potential energy. This corresponds to the amount of kinetic energy that the molecules dispose to traverse the subsequent linear field-free drift region:

$$E_{pot} = z * e * U = E_{kin} = {}^{1}/_{2} * m * v^2$$

Formula 1 Energy for traversing TOF drift tube. Abbreviations: z, charge number of the particle; e, elementary charge; U, the electric potential for acceleration; m, mass of the particle; v, resulting velocity of the particle at the end of acceleration. Taken from [173].

The final velocity of a molecule through the flight tube is, thus, determined by its mass and charge. Obviously, heavier molecules will be slower than lighter molecules (Figure 4-3, A). Given a known length for the flight tube, the time to traverse the tube is:

$$t = L/\mathrm{v}$$

Formula 2 Time for traversing TOF drift tube. Abbreviations: t, time for traversing the TOF drift tube; L, length of drift tube; v, velocity of particle. Taken from [173].

By measuring the time from laser pulse till ion hit at the detector, the *m/z* ratio of a molecule can be calculated by combining the two previous equations:

$$\frac{m}{z} = \frac{(2 * e * U * t^2)}{L^2}$$

Formula 3 Calculation of mass to charge ratio. Abbreviations: *m/z*, mass to charge ratio; e, elementary charge; U, the electric potential for acceleration; t, time to traverse drift tube; L, length of the drift tube. Taken from [173].

An important property of a mass analyzer is the mass resolution. The resolution in mass spectrometry is the ability to distinguish two peaks with similar mass-to-charge ratios [173]. There are effects that reduce the resolution. Molecules of the same mass may have an initial kinetic energy spread which may be caused by differences in place and time of ionization or differences in amount and direction of initial velocities [176]. The introduction of a reflector may correct these differences, thus yielding higher mass resolutions [176].

The reflector is made of an electrostatic field that deflects the ion beam at the end of the flight tube toward a second detector (Figure 4-4). The depth of penetration into the electrostatic field depends on the kinetic energy of the ions; the more energy, the deeper the penetration and the longer the total way to reach the final detector. Thus, differences in initial energies of equal masses can be corrected by depth of penetration into the reflector. However, this is only true for lower *m/z* values. At higher *m/z* the reflector fails to achieve significant higher resolutions [176].

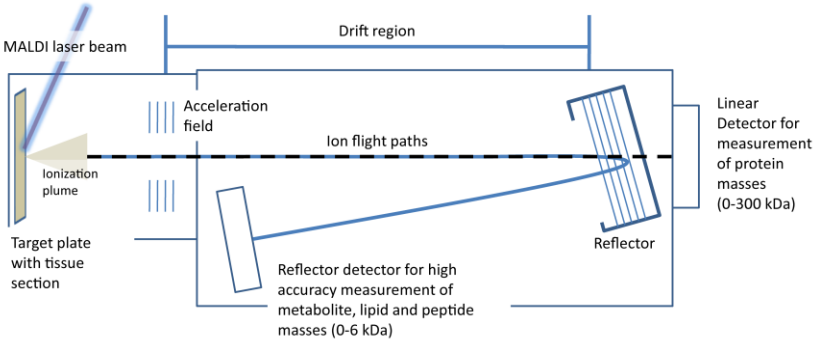

Figure 4-4 Principle of TOF based mass spectrometer with reflector. The reflector consists of an electrostatic field that deflects the ion beam at the end of the flight tube toward a second detector. The depth of penetration into the electrostatic field corrects differences in initial energies of equal masses, thus increases the resolution power of the mass spectrometer, however only for molecules up to 6kDa. For detection of higher molecular weight molecules the electrostatic field of the reflector is disabled and the linear detector is activated. Taken from [175].

Tandem mass spectrometry

The reflector is also used to separate fragments of molecules that occur in the area of the first drift region. This phenomenon is called post-source-decay (PSD). PSD ions cannot be separated by a linear TOF mass analyzer as they have the same kinetic energy but different masses. However, the analysis of the PSD fragments delivers useful information concerning the structure and identity of the original ion.

The measurement of PSD fragments of a specific parent ion may be realized by two consecutively arranged TOF mass analyzers (TOF/TOF, a.k.a. MS/MS, or tandem MS). The first TOF section acts as precursor *m/z* selector by deflecting other ions than of interest. The fragmented ions are then separated and detected by the second TOF [177]. Optionally, the precursor ion may be also artificially dissociated by collision gas

in an intermediate region, before being transmitted to the second TOF component [176].

Tandem MS has become one of the major tools for biomolecule analysis in the mass range *m/z* 500– 3,000 [176]. In proteomics, proteins are moved to the MS/MS mass range by performing a proteolytic digest, so that the resulting peptides of the proteins are actually analyzed.

Abilities of MALDI-TOF mass spectrometry for proteomics research

MALDI-TOF based mass spectrometry has become an indispensable tool in proteomics research. This is mainly due to its abilities listed below:

- Soft ionization by MALDI enables measurement of intact large biomolecules such as oligonucleotides, peptides, and proteins.
- Rapid, label-free and simultaneous (multiplexing) acquisition of hundreds to thousands of mass signals.
- Measurement of post-translational modifications (PTM) such as phosphorylation, acetylation and methylation, as PTMs alter the mass of a protein in a predictable fashion [60].
- High sensitivity (down to femtomoles) which allows even small amounts of sample volumes to be analyzed [67].
- Mass range, which reaches from small (100 Da) to large molecules (>300 kDa), allowing measurement of small molecules, metabolites, lipids, peptides and proteins [175].
- Determination of the identity or structure of molecules by analysis of their PSD fragments

Besides these powerful abilities, MALDI-TOF also suffers from several disadvantages:

- No direct knowledge of molecular identity, but “only” *m/z* values
- PSD-based identification best possible on pre-purified (by gel or liquid chromatography) small peptides (<4,000 Da) or digested proteins
- Mass resolution and accuracy drops with higher mass range

4.1.2 MALDI imaging mass spectrometry

MALDI imaging mass spectrometry has been developed in the late 1990s with the idea to extend the application of conventional MALDI-TOF experiments to tissue sections to incorporate histological information [137]. During an MALDI imaging experiment a mass spectrum is acquired for each measuring spot, a so called pixel, in a predefined raster across a sample tissue section, resulting in a two dimensional distribution map for each measured *m/z* value (Figure 1-11) [68]. Importantly, as the sample is not damaged during the measurements, the very same tissue section can be stained conventionally afterwards, digitally scanned, and directly co-registered to the mass spectrometric data. This allows studying the spatial distribution of mass signals, corresponding to proteins, within their histological context. Furthermore, protein signatures can be specifically allocated to certain cell-type, such as tumor cells, inflammatory cells, connective tissue, etc.

MALDI imaging was not the first mass spectrometry based imaging method. Secondary ion mass spectrometry (SIMS), introduced in the 1960s, uses an ion beam of high-energy particles to cause, upon impact onto a sample surface, the emission of secondary ions that are then analyzed in a mass analyzer. SIMS instruments achieve nanometer size pixels but are usually limited in their mass range to below 1,000 Da [178].

In contrast to SIMS, MALDI allows investigating higher molecular weight content of tissues, such as proteins, peptides, lipids in their histomorphological context, however at a lower lateral resolution with typical pixel sizes of 20 to 200 µm available on commercial systems [68].

Until now, MALDI imaging of tissues is mostly done on cryo-preserved tissues. Nevertheless, new protocols are in development which enable the application to formalin-fixed, paraffin-embedded (FFPE) or alcohol preserved tissues [179-182]. In the next paragraph, the workflow of a typical MALDI imaging experiment is described for the well-established analysis of frozen tissues, which has been used in this thesis to analyze proteins.

Sample preparation

The whole workflow is depicted schematically in Figure 4-5.

As first step, a native tissue section is placed by cryo-sectioning onto a pre-chilled and conductive glass slide. The conductive glass slide, typically realized by indium-tin-oxide

coating, facilitates mass spectrometry experiments and histological analysis to be done on the very same section. In our studies, slides were previously coated with poly-L-lysine for better tissue adherence. The samples are then briefly rinsed in an increasing alcohol solution series to remove salts and fixate the tissue.

As in any other MALDI experiment, samples have to be covered with a crystalline matrix before mass spectrometry can be performed. The analytes are extracted by the solvent in the matrix solution and incorporated into the matrix crystal structure after evaporation of the solvent. In direct tissue analysis by MALDI imaging, organic matrix solution is placed over the entire tissue section. The matrix deposition needs to be homogeneous and reproducible in order to guarantee comparability within and between measurements. The matrix can be applied either manually, by robotic spotting, nebulization, or sublimation, before laser shots are subsequently performed across the tissue sample. Systematic multi-measurement studies should use automated devices to guarantee the comparability of different measurements. An overview of different matrix application techniques can be found elsewhere [68, 175].

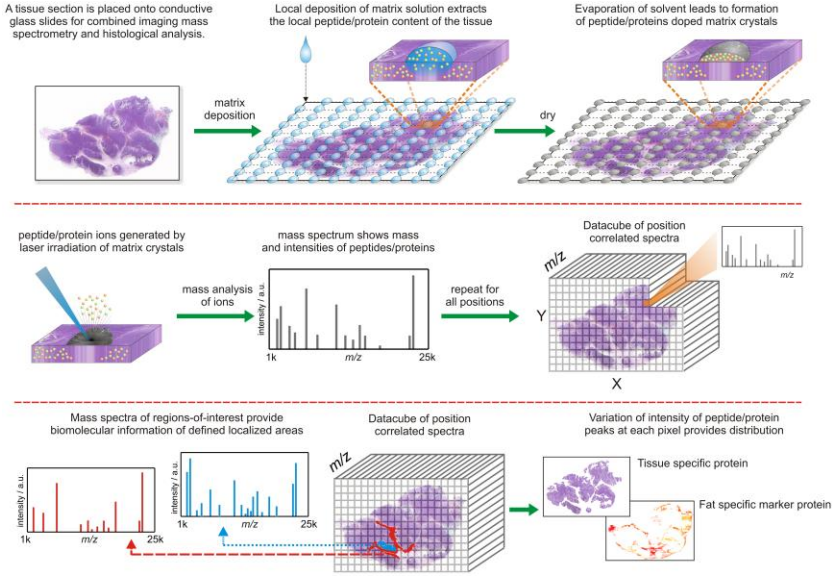

Figure 4-5 MALDI imaging mass spectrometry workflow. Before measurement a tissue section is cut and mounted onto a conductive glass slide and covered by a MALDI compatible matrix, which forms analyte-matrix co-crystals (top panel). MALDI mass spectrometry experiments are

repeated for all measurement spots on the tissue section (middle panel). The distance between the measurement spots defines the spatial resolution (=pixel size) of the resulting MALDI image. The intact tissue section can be stained and superimposed to the spatially resolved mass spectrometric data. This allows on the one hand visualizing mass signals for correlation with the underlying tissue morphology (lower panel, right). On the other hand, cell-type specific expression profiles can be obtained from regions of interest within the tissue (lower panel, left). Taken from [183].

Sample measurement

After introducing the sample slide into the mass spectrometer, measurement regions are defined, which are then analyzed within a user-defined lateral resolution which is typically between 20 µm and 200 µm on commercial instrumentation [184]. An even higher lateral resolution could be achieved by Chaurand *et al*. using a custom-built mass spectrometer. They were able to perform MALDI imaging measurements of phospholipids at a cellular level, reaching resolutions lower than 5 µm [170].

The lateral resolution, i.e. the distance between the measurement spot, is limited both by the laser focus size as well as the average size of the matrix crystals [185]. Automated spotting devices have the advantage to apply small droplets of matrix or enzymatic solutions in a precise, uniform and highly reproducible manner. However, the droplet size (≥150 µm) determines the maximum lateral resolution. Automated spray coaters, like the ImagePrep station (Bruker Daltonik, Bremen, Germany) achieve smaller droplet sizes (~20 µm), thus facilitating higher resolution measurements [175].

The sample may be analyzed in linear or reflector mode depending on the type of analytes and the corresponding *m/z* range which varies between the different matrices. Mass ranges for proteins are usually between 2,000 and 30,000 Da, for peptides between 600 and 4,000 Da, and for small molecules between 100 and 800 Da.

Co-registration of stained sample

One of the great advantages of MALDI imaging is that the tissue sample is not destroyed during the measurement. This allows for the precise correlation of mass spectrometric imaging data with the morphological features of the very same tissue section, as a consecutive section may differ in morphological details. For this, the matrix is eluted after the measurement by washing the sample with an alcohol solution before staining it with hematoxylin and eosin (H&E) [103]. The slide is then scanned with a digital slide-scanner and co-registered to the mass spectrometric data.

Data processing and analysis

After co-registration, the spatial distribution of all *m/z* values can be assessed within the histomorphological features of the tissue (Figure 1-11).

For clinical studies, the analysis pipeline is usually to extract the mass spectrometric data from histological interesting regions with designated states (e.g. healthy tissue, tumor tissue, or responder patient). Next, these data usually undergo normalization, recalibration (both to enable comparability between measurements), and peak picking. After processing, the peaks intensities (=mass signals representing molecules) of these spectra are tested for correlation with given biological or clinical endpoints. The spectra may also be clustered to investigate the molecular composition of a tissue sample without prior knowledge (more details can be found in the chapter 4.2 on statistical methods in MALDI imaging).

Protein identification

While MALDI imaging allows measuring hundreds of masses at once, it has the problem that only the molecular weight of molecules is reported without any name associated to them. This makes an additional protein identification step necessary. Protocols to identify the names corresponding to the masses are neither standardized nor universally applicable. These approaches can be grouped according to their site of measurement, on-tissue or extract based, and the application of digest, top-down versus bottom-up (Figure 4-6) [98].

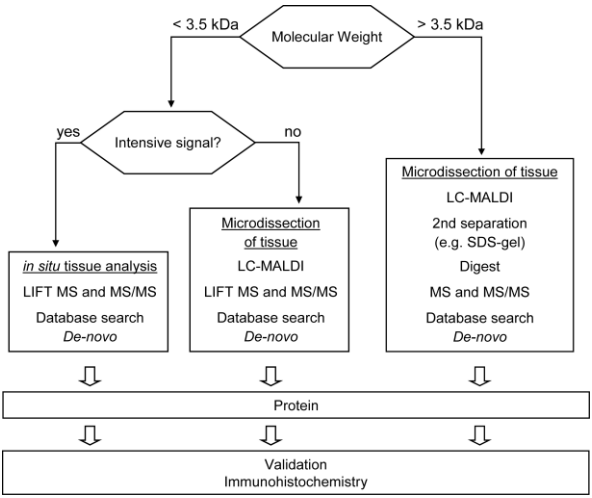

Figure 4-6 Workflow of protein identification. Depending on the molecular weight of the molecule of interest, either top-down or bottom-up identification has to be performed. For smaller molecules (<3.5kDa), a direct ionization and gas phase fragmentation (MS/MS) of the protein of interest inside the mass spectrometer can be performed (top-down), whereas the analysis of larger molecules involves protease digestion of the protein (bottom-up), usually within a mixture of other proteolytic fragments. Thus, additional separation steps by liquid chromatography (LC) or gel electrophoresis are necessary. Taken from [98].

In the top-down approach, no digestion is performed so that the full protein is fragmented and the resulting ions are used for identification. The advantage of the top-down approach is that the resulting identity can be directly matched to the mass obtained from MALDI imaging. On-tissue (*in situ*) identifications are only possible for low mass proteins and peptides (<3,500 Da) [186]. Larger proteins cannot be identified by top-down on-tissue and have to be first extracted and isolated by gel or liquid chromatography steps. The isolation process of tissue extracts, however, is tedious and complicated.

Identifications involving digestion of proteins is called bottom-up identification. The bottom-up analysis of tissue extracts provides long lists of identities. However, they are difficult to match to the unknown masses from undigested MALDI imaging experiments. Successful on-tissue identifications have been achieved in analyzing FFPE or frozen tissue sections which underwent previous digestion process. This generated hundreds of tryptic peptides in a mass range (*m/z* 500-3,000) amenable for sequence

analysis directly from their location in the tissue [179, 187, 188]. However, with a digest the information about the full protein is lost (isoforms, possible modifications on the undetected fragments, etc.).

Taken together, there are examples of successful identifications, either with or without application of digest, but a standardized protocol is not available yet.

Advantages and limitations of MALDI imaging mass spectrometry

Despite the limitation of not providing directly the identity for each *m/z* value, MALDI imaging constitutes a powerful discovery tool for clinical research in the field of proteomics, lipidomics and pharmacokinetics, which has its strengths and limitations [98, 99, 133, 189].

- Advantages: analysis of smallest sample amounts (biopsies); histology-driven analysis;
  label-free; multiplexing; full protein analysis (PTMs); avoids time-consuming extraction, purification or separation steps, which have the potential for producing artifacts; application to FFPE/frozen tissue micro arrays; high throughput
- Limitations: no direct protein identification; potential ion suppression; restricted to low molecular weight (<30 kDa) and soluble proteins

4.1.3 Road map to clinical-relevant markers by MALDI imaging studies

As shown, MALDI imaging is a powerful proteomic screening tool that may constitute the first step for providing specific marker candidates. However, as MALDI imaging detects “only” masses, subsequent protein identification approaches have to provide the molecular identity of the mass of interest.

The knowledge of the molecular identity facilitates the validation of the significance of the candidate marker. A validation, especially in proteomics or transcriptomics studies, by a large number of independent patients is considered of great importance, as lots of previously proposed markers have shown not to be reproducible [64, 90, 190]. For example, a meta-analysis of the most prominent cancer studies using expression profiling showed that in five studies the original results could not be reproduced [191]. The fact that until 2004 in only 10% of microarray studies an independent validation has been performed may explain why only few markers have

so far reached the phase of clinical trials or even the integration into clinical practice [54, 190]. In this context and for an initial intra-study validation, Meyer *et al*. favor immunohistochemistry using tissue microarrays, as they allow a parallel analysis of multiple tissue specimens for statistical validation under marginal methodical variances [64].

In consequence, the validation of a marker candidate by immunohistochemistry on tissue microarrays of independent patient cohorts has been incorporated into most marker discovery workflows (Figure 4-7) [68]. To exclude subjective observer evaluation of staining, objective image evaluation may be performed by digital image analysis software.

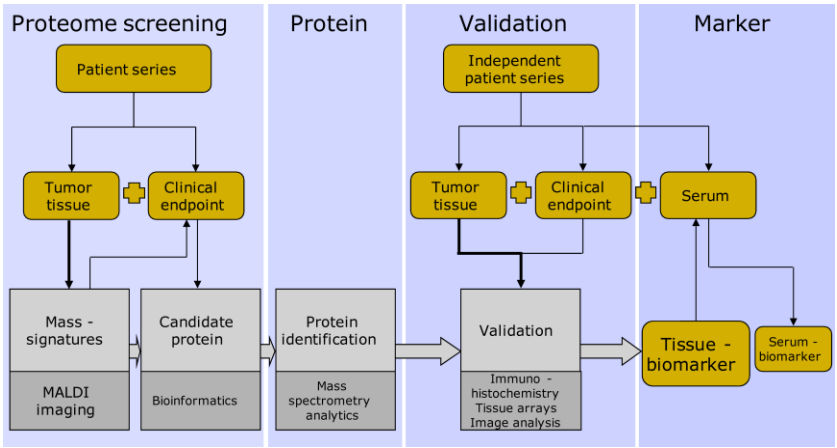

Figure 4-7 MALDI imaging mass spectrometry based biomarker identification workflow. As an unlabeled, multiplexing, morphology-driven approach, MALDI imaging is a powerful method for the discovery of protein signals as candidate biomarkers for a given clinical end point. After protein analytic identification of a candidate signal, the protein should be validated in an independent patient cohort by a different technique such as immunohistochemistry before being considered as a reliable tissue biomarker candidate. Taken from [68].

In addition, if a tissue marker has proven reliability in the validation cohort, it may be considered to check its applicability to serum. In contrast to direct serum studies, the depicted road map bypasses the sensitivity problem of traditional serum biomarker discovery, which is due to the dynamic range of the serum proteome, by delivering a target molecule from the possible origin of the disease [55].

4.2 Statistical methods and considerations in MALDI imaging studies

MALDI imaging analyses result in high-dimensional data sets consisting of several thousand of spatially resolved mass spectra, each of which contains hundreds or thousands of mass signals [192]. Such data sets are known to suffer the 'curse of dimensionality' [193].

As a consequence, advanced statistical data mining methods are required which take into account the nature of MALDI imaging data. Several of these techniques have been imported from the gene expression analysis community, which faces similar problems [68].

With regard to the presented thesis here, deeper explanations will be given on the methods applied in these studies. However, it is also intended to provide a general overview on the most important aspects of data mining and methods applied in MALDI imaging.

4.2.1 Marker discovery/feature selection

For studies with clinical questions, the first step in the MALDI imaging data analysis pipeline is to extract the mass spectrometric data from histological interesting regions with designated states (e.g. healthy, tumor, HER2 positive or poor survivor). After extraction of the corresponding spectra and subsequent spectra processing, the mass signals (features) of these spectra can be tested for correlation with given biological or clinical end points.

Statistical tests

These tests are performed by classical statistical tests like the Mann-Whitney *U* test, *t* test, Fisher test, Pearson's correlation, or the log rank test for survival analysis. However, due to the *curse of dimensionality*, there is a risk of identifying false-positive features, as the type I error (error for false-positive discovery) has to be multiplied by the number of features that are tested. For instance, by setting the significance level of type I error to α=0.05, and testing 100 features, there will be 5 potential type I errors, i.e. 5 signals that are expected to be significant by mistake [193]. This multiple-testing error can be corrected by p-value adjustment procedures like the ones from Bonferroni or Benjamini-Hochberg [194]. If not stated otherwise, reported p-values of

m/z species in the studies presented here were adjusted by Benjamini-Hochberg correction.

Other techniques to control for the false discovery rate have already been employed in the field of MALDI imaging like the permutation *t*-test [79] or the weighted flexible compound covariate method [70]. Similar to the permutation *t*-test, the widely used significance analysis of microarrays (SAM) uses repeated permutations of the data to determine if a feature is significantly related to a clinical endpoint [71].

Another critical issue is the study size. To improve statistical reliability in preclinical MALDI imaging research studies, a minimum number of 50–60 samples have been proposed [189]. In both studies conducted for this thesis, the number of involved sample surpasses this recommended minimum number: for the study on prognostic proteins 63 patient samples have been measured and the HER2 classification study involves 107 samples.

Other selection criteria

In terms of applicable biomarkers, high values for sensitivity and specificity are of importance. A high discriminatory power may be indicated by the significance of a statistical test. However, the mutual relationship between sensitivity and specificity is best represented graphically by a receiver operating characteristic (ROC) curve (Figure 4-8). The true positive rate is plotted versus the false positive rate for a varying cut-off. The resulting area under the curve (AUC) is an indication for the discriminatory power of the marker [41]. The AUC ranges from 0.5 for a total random classification to 1.00 for a perfect classification, where both sensitivity and specificity have values of 100%.

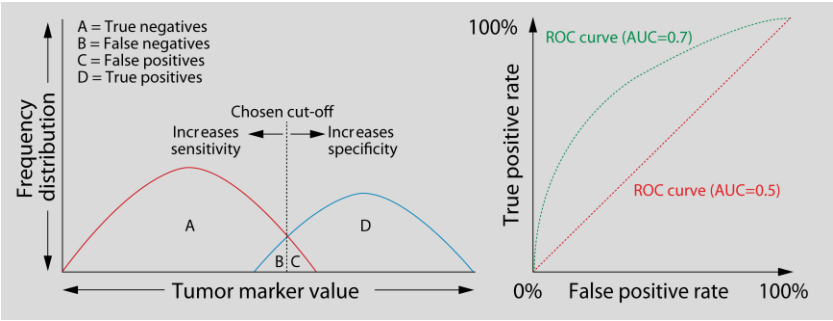

Figure 4-8 Receiver operating characteristic (ROC) curve. The ROC curve (right panel) is a graphical representation of the mutual relationship between sensitivity (true positive rate) and

specificity (1 - false positive rate) by varying a cut-off for the separation of two groups (red and blue, left panel). The discriminatory power may be represented by the area under the ROC curve (AUC), where the area 1 represents maximum discriminatory power and 0.5 is equal to a random classification (red dashed curve in the right graph). Taken from [41].

Other techniques alter the original representation of the variables by projection (principal components analysis) or compression using information theory [195]. The principal components analysis (PCA) is mostly used to reduce the number of variables to so called principal components while maintaining most of the information.

In my presented studies, SAM and ROC analyses have been used to identify relevant features in terms of prognostic significance and discriminatory power between HER2 positive and negative samples, respectively.

4.2.2 Classification algorithms

Classification algorithms are used to group objects according to their differences or similarities in a defined feature space. For MALDI imaging data sets, usual objects to classify may be single spectra of a tissue section or a representative spectrum taken from a region of a sample (e.g. tumor areas). The mentioned feature space can be based on all mass signals detected or on a signature of relevant mass signals which may had been determined previously by a feature selection process, as explained before.

Two types of classification algorithms can be distinguished: unsupervised or supervised. Unsupervised methods can be applied to the objects without prior knowledge, making it a discovery tool for identifying molecularly similar groups of objects, termed 'clustering'. In contrast, supervised methods rely on a previous training of the classification model by samples with known status (e.g. responder, poor survivor). Thus, depending on the combination of classification algorithm and objects to classify, different scientific questions can be addressed in MALDI imaging studies (Table 4-2).

Table 4-2 Types and application of classification algorithms in MALDI imaging

Classification of spectra …	*Statistical classification method*	
	Unsupervised	Supervised
Within one sample for …	Investigation of molecular composition within one sample (e.g. to study tumor heterogeneity) by clustering algorithms [88]	Spatially-resolved classification of tissue regions (e.g. HER2 status, potential metastatic cells) [76]
Between samples for …	*Ad hoc* clustering of samples/patients with known or unknown status into different groups (e.g. for discovery of cancer subtypes) [196]	Predictive classification of samples with unknown status after training of the classifier with samples of known status (e.g. responder, poor survivor) [72]

The most important aspects to consider when choosing a certain algorithm are the degree of parameterization of the method and its susceptibility to overfit i.e. not being able to reproduce the results in another sample set. Both are closely connected. As results are prone to vary with increased freedom of parameterization, reproducibility is assured by employing algorithms with a very low number of parameters.

In the following paragraphs, several of the most commonly employed classification methods are introduced; however, the focus will be on methods used in this thesis.

Hierarchical clustering (Unsupervised clustering)

Unsupervised algorithms group objects according to their distance in a given feature space which is defined in MALDI imaging by the selected *m/z* species. One of the most popular unsupervised methods is the hierarchical clustering. The peculiarity of hierarchical clustering is that it organizes the single objects and clusters according to their similarities in a tree-like structure called dendrogram (see Figure 1-8, B). Clusters, represented by nodes in the tree, are built by iteratively grouping single objects or clusters according to a defined distance metric until all objects are located in the same cluster (root of the tree).

The advantage of this procedure is that it does not require prior knowledge about the number of expected clusters as it finds a whole cluster hierarchy. Disadvantages are the memory consumption during calculation and the parameterization, which are the distance metric and linkage method.

However, this method has extensively been employed in gene-expression analyses where profiles have been used to discover new cancer subtypes or to predict survival [197, 198].

In MALDI imaging, this method has been used by Deininger *et al*. to assess molecular heterogeneities within morphological identical entities of gastric cancer tissue sections [88]. Another work by Yanagisawa *et al*., could distinguish subgroups of non-small-cell lung cancer with different disease outcome on basis of clustering MALDI profiles [69].

Other unsupervised algorithms

Similarly, there are also non-tree based clustering algorithms. Importantly, the number of expected clusters has to be defined in advance.

Some of them have been employed to perform spatial segmentation on MALDI imaging data sets [199]. Alexandrov *et al*., for example, used high dimensional discriminant clustering (HDDC) to group MALDI imaging spectra whereas the number of groups was defined beforehand according to the morphological entities observed in the sections [200]. Subsequent super-resolution segmentation was applied to artificially increase the resolution of the images for better interpretation [201].

Decision tree (Supervised classification)

Supervised methods, in contrast, make use of additional information that comes with the initial data to construct a classifier. This model may then be used to predict the unknown status of other data.

A very intuitive representation of a supervised algorithm is the decision tree. As the name says, decisions are organized in a tree where each node represents a decision according to a certain feature. For classification of a test object, it has to make its way from the root node to one of the leaves which represent the final assignment. An example is given as tree 1 from Figure 4-9. As depicted, the decisions of the tree define regions in an n-dimensional space where n is the number of involved features.

The construction of the tree is an iterative process which starts at the root node. At each step the optimal feature for division of the remaining objects is selected. The process stops at perfect separation of objects or in case no divisive feature is left.

Main advantage of this method is the easy interpretability of the tree by humans. That is why it is commonly used e.g. in medicine for diagnostic or treatment guidelines.

Disadvantage is its susceptibility for overfitting, i.e. the lack of generalization capability which is recognizable at the strict decision boundaries of tree 1 in Figure 4-9 which are localized very closely to the objects.

Random Forest

Random Forest can be described as a collection of decision trees with controlled variation (Figure 4-9). In contrast to single decision trees, the algorithm is robust to overfitting, while yielding high prediction accuracy [145, 202]. It is capable of dealing with a large number of input variables, and performance is robust with respect to parameterization [145].

Overfitting is avoided by introducing several random elements during the learning phase of the forest. These include random sample selection for construction of each new tree and random feature selection for samples splitting at each node. Thus, the major parameters for training are the numbers of trees and features randomly chosen at a node [145].

For classification of a test sample, each tree of the forest is evaluated individually. The class label with the highest number in votes is assigned to the test sample.

In MALDI imaging, Hanselmann *et al.* have provided evidence that the Random Forest classifier can be used for accurate, automated *in situ* annotation of tissues [145].

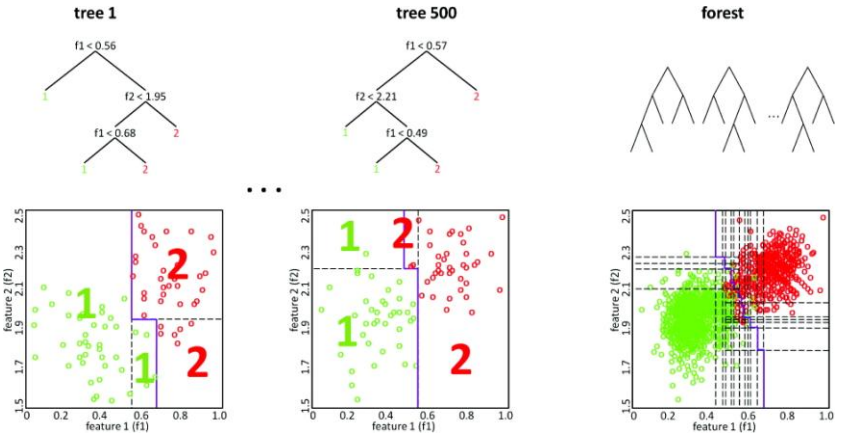

Figure 4-9 The Random Forest classification algorithm. A Random Forest classifier is a collection of decision trees where the single trees are constructed from bootstrap samples. Two trees of

the forest are shown in detail (left and center panels): at each node, the feature which allows for the best class separation is chosen (with respect to the subset of features selected for that node). The corresponding partitioning of the objects in the feature space is shown below with the decision boundary plotted in purple. On the very right, the decision boundary of the combined Random Forest is displayed which is based on the majority vote of the individual trees. Taken from [145].

Support Vector Machine

The Support Vector Machine (SVM) is a powerful classifier which has been extensively used in a variety of high-dimensional classification problems in biomedicine, amongst others also for proteomic data sets [142, 143, 146].

Learning of a SVM involves the finding of an optimal hyperplane in the feature space. The optimal hyperplane is defined as having the maximum distance from the objects of the different classes (Figure 4-10) [193]. The support vectors, which are perpendicular to the hyperplane help to find the optimal hyperplane, as they define the distance between the objects and the separating plane. This maximum margin method guarantees generalizability, and thus less overfitting [193]. Mathematical kernels are used to transform the data into a higher-dimensional feature space in order to facilitate separability by the plane.

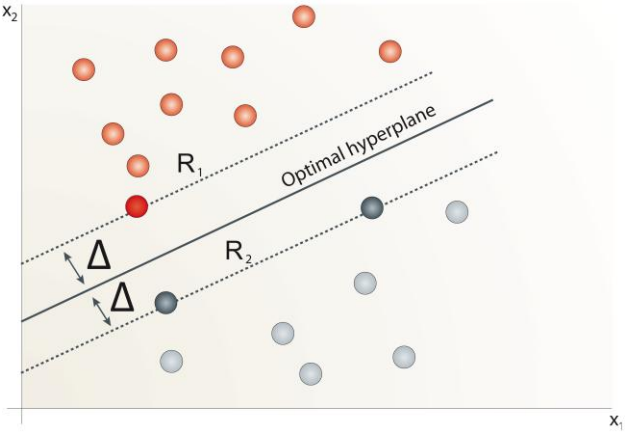

Figure 4-10 The Support Vector Machine (SVM) classification algorithm. The SVM is a supervised classification algorithm which is trained by finding the optimal separating hyperplane with the maximum distance from the nearest training objects. Here, the SVM finds an optimal hyperplane for separating the objects of R_1 (red circles) and R_2 (grey circles) with the

help of the support vectors (dashed lines). The hyperplane constitutes the decision boundary to classify an unknown pattern into one of the two regions. Taken from [193].

Classification of an unknown object is simple since the hyperplane serves as decision boundary [193]. Main disadvantage of a SVM-based classification is the extensive parameterization which includes kernel selection, kernel parameterization, and cost definition for hyperplane construction violations.

SVMs have been successfully employed in MALDI imaging studies to classify breast cancer samples or prostate carcinomas [53, 103].

4.2.3 Validation of marker and classifier performance

Particular care must be given to the validation of potential markers and classifiers based on signatures, as the *curse of dimensionality* may also result in a poor generalization capability (*overfitting)*. Overfitting can occur very often in discovery-based research where large numbers of potential features are used to discriminate a small number of samples [190]. As overfitting causes non-reproducible results in independent sample collections, the solution to test for overfitting is to assess reproducibility [190]. If supervised methods are employed, this may be done initially by cross-validation methods. The principle is to iteratively split the available samples into a model generation set and a test set. Each time the model is evaluated by the test set and the final classification accuracy is averaged across all steps. Reproducibility can also be confirmed when different classification algorithms were employed on the same problem while reaching the same results.

However, the application of the classifier or a single marker to an independent test set is considered the gold-standard to evaluate reproducibility [193]. Thus, in the here presented studies, an independent test set was used to validate the reproducibility of the results — where applicable. Otherwise a cross-validation was used to assess the classifier's accuracy.

5 References

1. Kumar V, Robbins SL (Eds.): Robbins basic pathology. 8th ed. Saunders Elsevier: Philadelphia, PA. 2007.
2. ACS (Eds.): Global Cancer Facts & Figures. 2nd ed. American Cancer Society: Atlanta 2011.
3. Ferlay J, Shin HR, Bray F, et al. Estimates of worldwide burden of cancer in 2008: GLOBOCAN 2008. Int J Cancer 2010;127:2893-917.
4. Kaatsch P, Spix C, Katalinic A, et al. (Eds.): Krebs in Deutschland : 2007/2008. 8th ed. Robert Koch-Institut und Gesellschaft der epidemiologischen Krebsregister in Deutschland e.V.: Berlin 2012:pp 19-20, 32-35.
5. Stoeckli M, Chaurand P, Hallahan DE, et al. Imaging mass spectrometry: a new technology for the analysis of protein expression in mammalian tissues. Nat Med 2001;7:493-6.
6. Kaspar S, Peukert M, Svatos A, et al. MALDI-imaging mass spectrometry - An emerging technique in plant biology. Proteomics 2011;11:1840-50.
7. Zimmerman TA, Rubakhin SS, Sweedler JV. MALDI mass spectrometry imaging of neuronal cell cultures. J Am Soc Mass Spectrom 2011;22:828-36.
8. Schoenian I, Spiteller M, Ghaste M, et al. Chemical basis of the synergism and antagonism in microbial communities in the nests of leaf-cutting ants. Proc Natl Acad Sci U S A 2011;108:1955-60.
9. Ronci M, Sharma S, Chataway T, et al. MALDI-MS-imaging of whole human lens capsule. J Proteome Res 2011;10:3522-9.
10. McDonnell LA, Corthals GL, Willems SM, et al. Peptide and protein imaging mass spectrometry in cancer research. J Proteomics 2010;73:1921-44.
11. Schwamborn K, Caprioli RM. Molecular imaging by mass spectrometry--looking beyond classical histology. Nat Rev Cancer 2010;10:639-46.
12. Hartgrink HH, Jansen EP, van Grieken NC, et al. Gastric cancer. Lancet 2009;374:477-90.
13. Bae JM, Lee EJ, Guyatt G. Citrus fruit intake and stomach cancer risk: a quantitative systematic review. Gastric Cancer 2008;11:23-32.
14. Tsugane S, Sasazuki S. Diet and the risk of gastric cancer: review of epidemiological evidence. Gastric Cancer 2007;10:75-83.
15. Bruns C (Eds.): Gastrointestinale Tumoren. 8th ed. Zuckschwerdt: München; Wien ; New York, NY 2010:pp 23-51.
16. Howlader N, Noone AM, Krapcho M, et al. (Eds.): SEER Cancer Statistics Review, 1975-2008. National Cancer Institute: Bethesda, MD, USA 2011.
17. Yalamarthi S, Witherspoon P, McCole D, et al. Missed diagnoses in patients with upper gastrointestinal cancers. Endoscopy 2004;36:874-9.

18. Martini F (Eds.): Fundamentals of anatomy and physiology. 3rd ed. Prentice Hall: Englewood Cliffs, NJ 1995:pp 895-899.
19. Marieb EN (Eds.): Essentials of human anatomy & physiology. 8th ed. Benjamin Cummings: San Francisco, CA. 2006.
20. Welsch U, Sobotta J (Eds.): Lehrbuch Histologie. 2nd ed. Elsevier, Urban & Fischer: München 2006:pp 362-369.
21. Mills JC, Shivdasani RA. Gastric epithelial stem cells. Gastroenterology 2011;140:412-24.
22. Bosman FT, Carneiro F, Hruban RH, et al. (Eds.): WHO classification of tumours of the digestive system. 4th ed. IARC Press: Lyon 2010:pp 48-58.
23. Hamilton SR, Aaltonen LA (Eds.): World Health Organization Classification of Tumours. Pathology and genetics of tumours of the digestive system. IARC Press: Lyon 2000:pp. 39-52
24. Lauren P. The Two Histological Main Types of Gastric Carcinoma: Diffuse and So-Called Intestinal-Type Carcinoma. An Attempt at a Histo-Clinical Classification. Acta Pathol Microbiol Scand 1965;64:31-49.
25. Yuasa Y. Control of gut differentiation and intestinal-type gastric carcinogenesis. Nat Rev Cancer 2003;3:592-600.
26. Tahara E. Genetic pathways of two types of gastric cancer. IARC Sci Publ 2004:327-49.
27. Correa P, Houghton J. Carcinogenesis of Helicobacter pylori. Gastroenterology 2007;133:659-72.
28. Silberg DG, Sullivan J, Kang E, et al. Cdx2 ectopic expression induces gastric intestinal metaplasia in transgenic mice. Gastroenterology 2002;122:689-96.
29. Lee JH, Abraham SC, Kim HS, et al. Inverse relationship between APC gene mutation in gastric adenomas and development of adenocarcinoma. Am J Pathol 2002;161:611-8.
30. Lee KH, Lee JS, Suh C, et al. Clinicopathologic significance of the K-ras gene codon 12 point mutation in stomach cancer. An analysis of 140 cases. Cancer 1995;75:2794-801.
31. Panani AD. Cytogenetic and molecular aspects of gastric cancer: clinical implications. Cancer Lett 2008;266:99-115.
32. Becker KF, Atkinson MJ, Reich U, et al. E-cadherin gene mutations provide clues to diffuse type gastric carcinomas. Cancer Res 1994;54:3845-52.
33. Bang YJ, Van Cutsem E, Feyereislova A, et al. Trastuzumab in combination with chemotherapy versus chemotherapy alone for treatment of HER2-positive advanced gastric or gastro-oesophageal junction cancer (ToGA): a phase 3, open-label, randomised controlled trial. Lancet 2010;376:687-97.
34. Garcia I, Vizoso F, Martin A, et al. Clinical significance of the epidermal growth factor receptor and HER2 receptor in resectable gastric cancer. Ann Surg Oncol 2003;10:234-41.

35. Sobin LH, Gospodarowicz MK, Wittekind C (Eds.): TNM classification of malignant tumours. 7th ed. Wiley-Blackwell: Chichester, West Sussex, UK ; Hoboken, NJ 2010:pp 73-77.
36. Jaffer AA, Gerdes H, Washington MK (Eds.): NCCN Clinical Practice Guidelines in Oncology: Gastric Cancer. 2.2011 ed. National Comprehensive Cancer Network 2011.
37. Gravalos C, Jimeno A. HER2 in gastric cancer: a new prognostic factor and a novel therapeutic target. Ann Oncol 2008;19:1523-9.
38. Boige V, Pignon J, Saint-Aubert B, et al. Final results of a randomized trial comparing preoperative 5-fluorouracil (F)/cisplatin (P) to surgery alone in adenocarcinoma of stomach and lower esophagus (ASLE): FNLCC ACCORD07-FFCD 9703 trial. Journal of Clinical Oncology 2007;25.
39. Cunningham D, Allum WH, Stenning SP, et al. Perioperative chemotherapy versus surgery alone for resectable gastroesophageal cancer. N Engl J Med 2006;355:11-20.
40. Macdonald JS, Smalley SR, Benedetti J, et al. Chemoradiotherapy after surgery compared with surgery alone for adenocarcinoma of the stomach or gastroesophageal junction. N Engl J Med 2001;345:725-30.
41. Kulasingam V, Diamandis EP. Strategies for discovering novel cancer biomarkers through utilization of emerging technologies. Nat Clin Pract Oncol 2008;5:588-99.
42. Moehler M, Mueller A, Hartmann JT, et al. An open-label, multicentre biomarker-oriented AIO phase II trial of sunitinib for patients with chemo-refractory advanced gastric cancer. Eur J Cancer 2011;47:1511-20.
43. Allgayer H, Babic R, Gruetzner KU, et al. c-erbB-2 is of independent prognostic relevance in gastric cancer and is associated with the expression of tumor-associated protease systems. J Clin Oncol 2000;18:2201-9.
44. Park DI, Yun JW, Park JH, et al. HER-2/neu amplification is an independent prognostic factor in gastric cancer. Dig Dis Sci 2006;51:1371-9.
45. Barros-Silva JD, Leitao D, Afonso L, et al. Association of ERBB2 gene status with histopathological parameters and disease-specific survival in gastric carcinoma patients. Br J Cancer 2009;100:487-93.
46. Petricoin EF, Zoon KC, Kohn EC, et al. Clinical proteomics: translating benchside promise into bedside reality. Nat Rev Drug Discov 2002;1:683-95.
47. POST-AUTHORISATION SUMMARY OF POSITIVE OPINION for HERCEPTIN. European Medicines Agency: London 2009. www.emea.europa.eu/pdfs/human/opinion/Herceptin_82246709en.pdf
48. Hofmann M, Stoss O, Shi D, et al. Assessment of a HER2 scoring system for gastric cancer: results from a validation study. Histopathology 2008;52:797-805.
49. Albarello L, Pecciarini L, Doglioni C. HER2 testing in gastric cancer. Adv Anat Pathol 2011;18:53-9.

50. Bartlett J, Mallon E, Cooke T. The clinical evaluation of HER-2 status: which test to use? J Pathol 2003;199:411-7.
51. Cayre A, Mishellany F, Lagarde N, et al. Comparison of different commercial kits for HER2 testing in breast cancer: looking for the accurate cutoff for amplification. Breast Cancer Res 2007;9:R64.
52. Sauter G, Lee J, Bartlett JM, et al. Guidelines for human epidermal growth factor receptor 2 testing: biologic and methodologic considerations. J Clin Oncol 2009;27:1323-33.
53. Rauser S, Marquardt C, Balluff B, et al. Classification of HER2 receptor status in breast cancer tissues by MALDI imaging mass spectrometry. J Proteome Res 2010;9:1854-63.
54. Ludwig JA, Weinstein JN. Biomarkers in cancer staging, prognosis and treatment selection. Nat Rev Cancer 2005;5:845-56.
55. Kulasingam V, Pavlou MP, Diamandis EP. Integrating high-throughput technologies in the quest for effective biomarkers for ovarian cancer. Nat Rev Cancer 2010;10:371-8.
56. Ebert MP, Korc M, Malfertheiner P, et al. Advances, challenges, and limitations in serum-proteome-based cancer diagnosis. J Proteome Res 2006;5:19-25.
57. Caprioli RM. Deciphering protein molecular signatures in cancer tissues to aid in diagnosis, prognosis, and therapy. Cancer Res 2005;65:10642-5.
58. Din S, Lennon AM, Arnott ID, et al. Technology insight: the application of proteomics in gastrointestinal disease. Nat Clin Pract Gastroenterol Hepatol 2007;4:372-85.
59. Gygi SP, Rochon Y, Franza BR, et al. Correlation between protein and mRNA abundance in yeast. Mol Cell Biol 1999;19:1720-30.
60. Mallick P, Kuster B. Proteomics: a pragmatic perspective. Nat Biotechnol 2010;28:695-709.
61. Anderson NL, Anderson NG. The human plasma proteome: history, character, and diagnostic prospects. Mol Cell Proteomics 2002;1:845-67.
62. Baggerly KA, Morris JS, Edmonson SR, et al. Signal in noise: evaluating reported reproducibility of serum proteomic tests for ovarian cancer. J Natl Cancer Inst 2005;97:307-9.
63. Mitchell P. Proteomics retrenches. Nat Biotechnol 2010;28:665-70.
64. Meyer HE, Stuhler K. High-performance proteomics as a tool in biomarker discovery. Proteomics 2007;7 Suppl 1:18-26.
65. Romeis B (Eds.): Romeis Mikroskopische Technik. 18th ed. Spektrum Akad. Verl.: Heidelberg 2010.
66. Van Eyk JE, Dunn MJ (Eds.): Clinical proteomics : from diagnosis to therapy. Wiley VCH: Weinheim 2008:p 552.
67. Han X, Aslanian A, Yates JR, 3rd. Mass spectrometry for proteomics. Curr Opin Chem Biol 2008;12:483-90.

68. Balluff B, Schone C, Hofler H, et al. MALDI imaging mass spectrometry for direct tissue analysis: technological advancements and recent applications. Histochem Cell Biol 2011;136:227-44.
69. Yanagisawa K, Shyr Y, Xu BJ, et al. Proteomic patterns of tumour subsets in non-small-cell lung cancer. Lancet 2003;362:433-9.
70. Schwartz SA, Weil RJ, Thompson RC, et al. Proteomic-based prognosis of brain tumor patients using direct-tissue matrix-assisted laser desorption ionization mass spectrometry. Cancer Res 2005;65:7674-81.
71. Bauer JA, Chakravarthy AB, Rosenbluth JM, et al. Identification of markers of taxane sensitivity using proteomic and genomic analyses of breast tumors from patients receiving neoadjuvant paclitaxel and radiation. Clin Cancer Res 2010;16:681-90.
72. Cazares LH, Troyer D, Mendrinos S, et al. Imaging mass spectrometry of a specific fragment of mitogen-activated protein kinase/extracellular signal-regulated kinase kinase kinase 2 discriminates cancer from uninvolved prostate tissue. Clin Cancer Res 2009;15:5541-51.
73. Hardesty WM, Kelley MC, Mi D, et al. Protein signatures for survival and recurrence in metastatic melanoma. J Proteomics 2011;74:1002-14.
74. Schwamborn K, Krieg RC, Jirak P, et al. Application of MALDI imaging for the diagnosis of classical Hodgkin lymphoma. J Cancer Res Clin Oncol 2010;136:1651-5.
75. Oppenheimer SR, Mi D, Sanders ME, et al. Molecular analysis of tumor margins by MALDI mass spectrometry in renal carcinoma. J Proteome Res 2010;9:2182-90.
76. Willems SM, van Remoortere A, van Zeijl R, et al. Imaging mass spectrometry of myxoid sarcomas identifies proteins and lipids specific to tumour type and grade, and reveals biochemical intratumour heterogeneity. J Pathol 2010;222:400-9.
77. Balluff B, Rauser S, Ebert MP, et al. Direct molecular tissue analysis by MALDI imaging mass spectrometry in the field of gastrointestinal disease. Gastroenterology 2012;accepted.
78. Elsner M, Rauser S, Maier S, et al. MALDI imaging mass spectrometry reveals COX7A2, TAGLN2 and S100-A10 as novel prognostic markers in barrett's adenocarcinoma. Journal of Proteomics 2012.
79. Kim HK, Reyzer ML, Choi IJ, et al. Gastric cancer-specific protein profile identified using endoscopic biopsy samples via MALDI mass spectrometry. J Proteome Res 2010;9:4123-30.
80. Balluff B, Rauser S, Meding S, et al. MALDI imaging identifies prognostic seven-protein signature of novel tissue markers in intestinal-type gastric cancer. Am J Pathol 2011;179:2720-9.

81. Le Faouder J, Laouirem S, Chapelle M, et al. Imaging mass spectrometry provides fingerprints for distinguishing hepatocellular carcinoma from cirrhosis. J Proteome Res 2011;10:3755-65.
82. Bowlus CL, Seeley EH, Roder J, et al. In situ mass spectrometry of autoimmune liver diseases. Cell Mol Immunol 2011;8:237-42.
83. Djidja MC, Claude E, Snel MF, et al. MALDI-ion mobility separation-mass spectrometry imaging of glucose-regulated protein 78 kDa (Grp78) in human formalin-fixed, paraffin-embedded pancreatic adenocarcinoma tissue sections. J Proteome Res 2009;8:4876-84.
84. M'Koma AE, Seeley EH, Washington MK, et al. Proteomic profiling of mucosal and submucosal colonic tissues yields protein signatures that differentiate the inflammatory colitides. Inflamm Bowel Dis 2011;17:875-83.
85. Meding S, Nitsche U, Balluff B, et al. Tumor Classification of Six Common Cancer Types Based on Proteomic Profiling by MALDI Imaging. J Proteome Res 2012;11:1996-2003.
86. Meding S, Balluff B, Elsner M, et al. Tissue Based Proteomics Reveals FXYD3, S100A11 and GSTM3 as Novel Markers for Regional Lymph Node Metastasis in Colon Cancer. J Pathol 2012.
87. Zheng L, Wang L, Ajani J, et al. Molecular basis of gastric cancer development and progression. Gastric Cancer 2004;7:61-77.
88. Deininger SO, Ebert MP, Futterer A, et al. MALDI imaging combined with hierarchical clustering as a new tool for the interpretation of complex human cancers. J Proteome Res 2008;7:5230-6.
89. Morita Y, Ikegami K, Goto-Inoue N, et al. Imaging mass spectrometry of gastric carcinoma in formalin-fixed paraffin-embedded tissue microarray. Cancer Sci 2010;101:267-73.
90. Ioannidis JP. A roadmap for successful applications of clinical proteomics. Proteomics Clin Appl 2011;5:241-7.
91. Jemal A, Siegel R, Ward E, et al. Cancer statistics, 2008. CA Cancer J Clin 2008;58:71-96.
92. Shi Y, Zhou Y. The role of surgery in the treatment of gastric cancer. J Surg Oncol 2010;101:687-92.
93. Allgayer H, Heiss MM, Schildberg FW. Prognostic factors in gastric cancer. Br J Surg 1997;84:1651-64.
94. Chen CN, Lin JJ, Chen JJ, et al. Gene expression profile predicts patient survival of gastric cancer after surgical resection. J Clin Oncol 2005;23:7286-95.
95. Leung SY, Yuen ST, Chu KM, et al. Expression profiling identifies chemokine (C-C motif) ligand 18 as an independent prognostic indicator in gastric cancer. Gastroenterology 2004;127:457-69.
96. Xu ZY, Chen JS, Shu YQ. Gene expression profile towards the prediction of patient survival of gastric cancer. Biomed Pharmacother 2010;64:133-9.

97. Wulfkuhle JD, Liotta LA, Petricoin EF. Proteomic applications for the early detection of cancer. Nat Rev Cancer 2003;3:267-75.
98. Walch A, Rauser S, Deininger SO, et al. MALDI imaging mass spectrometry for direct tissue analysis: a new frontier for molecular histology. Histochem Cell Biol 2008;130:421-34.
99. Chaurand P, Sanders ME, Jensen RA, et al. Proteomics in diagnostic pathology: profiling and imaging proteins directly in tissue sections. Am J Pathol 2004;165:1057-68.
100. Chaurand P, Schwartz SA, Caprioli RM. Profiling and imaging proteins in tissue sections by MS. Anal Chem 2004;76:87A-93A.
101. Cornett DS, Mobley JA, Dias EC, et al. A novel histology-directed strategy for MALDI-MS tissue profiling that improves throughput and cellular specificity in human breast cancer. Mol Cell Proteomics 2006;5:1975-83.
102. Lemaire R, Menguellet SA, Stauber J, et al. Specific MALDI imaging and profiling for biomarker hunting and validation: fragment of the 11S proteasome activator complex, Reg alpha fragment, is a new potential ovary cancer biomarker. J Proteome Res 2007;6:4127-34.
103. Schwamborn K, Krieg RC, Reska M, et al. Identifying prostate carcinoma by MALDI-Imaging. Int J Mol Med 2007;20:155-9.
104. Sobin LH, Wittekind C, International Union against Cancer. (Eds.): TNM classification of malignant tumours (German edition). 6th ed. Wiley-Liss: New York 2002:pp 59-62.
105. Tusher VG, Tibshirani R, Chu G. Significance analysis of microarrays applied to the ionizing radiation response. Proc Natl Acad Sci U S A 2001;98:5116-21.
106. Li X, Zhang Y, Zhang Y, et al. Survival prediction of gastric cancer by a seven-microRNA signature. Gut 2010;59:579-85.
107. Anderson L, Seilhamer J. A comparison of selected mRNA and protein abundances in human liver. Electrophoresis 1997;18:533-7.
108. Wilkins MR, Sanchez JC, Williams KL, et al. Current challenges and future applications for protein maps and post-translational vector maps in proteome projects. Electrophoresis 1996;17:830-8.
109. Melle C, Ernst G, Schimmel B, et al. Characterization of pepsinogen C as a potential biomarker for gastric cancer using a histo-proteomic approach. J Proteome Res 2005;4:1799-804.
110. Mohri Y, Mohri T, Wei W, et al. Identification of macrophage migration inhibitory factor and human neutrophil peptides 1-3 as potential biomarkers for gastric cancer. Br J Cancer 2009;101:295-302.
111. Albrethsen J, Bogebo R, Gammeltoft S, et al. Upregulated expression of human neutrophil peptides 1, 2 and 3 (HNP 1-3) in colon cancer serum and tumours: a biomarker study. BMC Cancer 2005;5:8.

112. Lanningham-Foster L, Green CL, Langkamp-Henken B, et al. Overexpression of CRIP in transgenic mice alters cytokine patterns and the immune response. Am J Physiol Endocrinol Metab 2002;282:E1197-203.
113. de Visser KE, Eichten A, Coussens LM. Paradoxical roles of the immune system during cancer development. Nat Rev Cancer 2006;6:24-37.
114. Hao J, Serohijos AW, Newton G, et al. Identification and rational redesign of peptide ligands to CRIP1, a novel biomarker for cancers. PLoS Comput Biol 2008;4:e1000138.
115. Jurata LW, Kenny DA, Gill GN. Nuclear LIM interactor, a rhombotin and LIM homeodomain interacting protein, is expressed early in neuronal development. Proc Natl Acad Sci U S A 1996;93:11693-8.
116. Khoo C, Blanchard RK, Sullivan VK, et al. Human cysteine-rich intestinal protein: cDNA cloning and expression of recombinant protein and identification in human peripheral blood mononuclear cells. Protein Expr Purif 1997;9:379-87.
117. Levenson CW, Shay NF, Lee-Ambrose LM, et al. Regulation of cysteine-rich intestinal protein by dexamethasone in the neonatal rat. Proc Natl Acad Sci U S A 1993;90:712-5.
118. Chen Y, Miller C, Mosher R, et al. Identification of cervical cancer markers by cDNA and tissue microarrays. Cancer Res 2003;63:1927-35.
119. Groene J, Mansmann U, Meister R, et al. Transcriptional census of 36 microdissected colorectal cancers yields a gene signature to distinguish UICC II and III. Int J Cancer 2006;119:1829-36.
120. Ma XJ, Salunga R, Tuggle JT, et al. Gene expression profiles of human breast cancer progression. Proc Natl Acad Sci U S A 2003;100:5974-9.
121. Terris B, Blaveri E, Crnogorac-Jurcevic T, et al. Characterization of gene expression profiles in intraductal papillary-mucinous tumors of the pancreas. Am J Pathol 2002;160:1745-54.
122. Wang Q, Williamson M, Bott S, et al. Hypomethylation of WNT5A, CRIP1 and S100P in prostate cancer. Oncogene 2007;26:6560-5.
123. Droin N, Hendra JB, Ducoroy P, et al. Human defensins as cancer biomarkers and antitumour molecules. J Proteomics 2009;72:918-27.
124. Hofman PM. Pathobiology of the neutrophil-intestinal epithelial cell interaction: role in carcinogenesis. World J Gastroenterol 2010;16:5790-800.
125. Azab B, Bhatt VR, Phookan J, et al. Usefulness of the neutrophil-to-lymphocyte ratio in predicting short- and long-term mortality in breast cancer patients. Ann Surg Oncol 2012;19:217-24.
126. Jensen HK, Donskov F, Marcussen N, et al. Presence of intratumoral neutrophils is an independent prognostic factor in localized renal cell carcinoma. J Clin Oncol 2009;27:4709-17.
127. Lesniak W, Slomnicki LP, Filipek A. S100A6 - new facts and features. Biochem Biophys Res Commun 2009;390:1087-92.

128. Nedjadi T, Kitteringham N, Campbell F, et al. S100A6 binds to annexin 2 in pancreatic cancer cells and promotes pancreatic cancer cell motility. Br J Cancer 2009;101:1145-54.
129. Slomnicki LP, Nawrot B, Lesniak W. S100A6 binds p53 and affects its activity. Int J Biochem Cell Biol 2009;41:784-90.
130. Komatsu K, Murata K, Kameyama M, et al. Expression of S100A6 and S100A4 in matched samples of human colorectal mucosa, primary colorectal adenocarcinomas and liver metastases. Oncology 2002;63:192-200.
131. Vimalachandran D, Greenhalf W, Thompson C, et al. High nuclear S100A6 (Calcyclin) is significantly associated with poor survival in pancreatic cancer patients. Cancer Res 2005;65:3218-25.
132. Wang XH, Zhang LH, Zhong XY, et al. S100A6 Overexpression Associates with Poor Prognosis and Is Epigenetically Up-Regulated in Gastric Cancer. Am J Pathol 2010;177:586-597.
133. Rauser S, Deininger SO, Suckau D, et al. Approaching MALDI molecular imaging for clinical proteomic research: current state and fields of application. Expert Rev Proteomics 2010;7:927-41.
134. Parkin DM, Bray F, Ferlay J, et al. Global cancer statistics, 2002. CA Cancer J Clin 2005;55:74-108.
135. Hede K. Gastric cancer: trastuzumab trial results spur search for other targets. J Natl Cancer Inst 2009;101:1306-7.
136. Herrmann K, Walch A, Balluff B, et al. Proteomic and metabolic prediction of response to therapy in gastrointestinal cancers. Nat Clin Pract Gastroenterol Hepatol 2009;6:170-83.
137. Caprioli RM, Farmer TB, Gile J. Molecular imaging of biological samples: localization of peptides and proteins using MALDI-TOF MS. Anal Chem 1997;69:4751-60.
138. Cornett DS, Reyzer ML, Chaurand P, et al. MALDI imaging mass spectrometry: molecular snapshots of biochemical systems. Nat Methods 2007;4:828-33.
139. Franck J, Arafah K, Elayed M, et al. MALDI imaging mass spectrometry: state of the art technology in clinical proteomics. Mol Cell Proteomics 2009;8:2023-33.
140. Reyzer ML, Caldwell RL, Dugger TC, et al. Early changes in protein expression detected by mass spectrometry predict tumor response to molecular therapeutics. Cancer Res 2004;64:9093-100.
141. Wolff AC, Hammond ME, Schwartz JN, et al. American Society of Clinical Oncology/College of American Pathologists guideline recommendations for human epidermal growth factor receptor 2 testing in breast cancer. J Clin Oncol 2007;25:118-45.

142. Adam BL, Qu Y, Davis JW, et al. Serum protein fingerprinting coupled with a pattern-matching algorithm distinguishes prostate cancer from benign prostate hyperplasia and healthy men. Cancer Res 2002;62:3609-14.
143. Agranoff D, Fernandez-Reyes D, Papadopoulos MC, et al. Identification of diagnostic markers for tuberculosis by proteomic fingerprinting of serum. Lancet 2006;368:1012-21.
144. Fusaro VA, Mani DR, Mesirov JP, et al. Prediction of high-responding peptides for targeted protein assays by mass spectrometry. Nat Biotechnol 2009;27:190-8.
145. Hanselmann M, Kothe U, Kirchner M, et al. Toward digital staining using imaging mass spectrometry and random forests. J Proteome Res 2009;8:3558-67.
146. Ma Y, Ding Z, Qian Y, et al. Predicting cancer drug response by proteomic profiling. Clin Cancer Res 2006;12:4583-9.
147. Noble WS. What is a support vector machine? Nat Biotechnol 2006;24:1565-7.
148. Drobatz KJ. Measures of accuracy and performance of diagnostic tests. J Vet Cardiol 2009;11 Suppl 1:S33-40.
149. Japkowicz N, Stephen S. The class imbalance problem: A systematic study. Intell Data Anal 2002;6:429-449.
150. Breiman L. Random Forests. Machine Learning 2001;45:5-32.
151. Kaptain S, Tan LK, Chen B. Her-2/neu and breast cancer. Diagn Mol Pathol 2001;10:139-52.
152. Shak S. Overview of the trastuzumab (Herceptin) anti-HER2 monoclonal antibody clinical program in HER2-overexpressing metastatic breast cancer. Herceptin Multinational Investigator Study Group. Semin Oncol 1999;26:71-7.
153. Slamon DJ, Leyland-Jones B, Shak S, et al. Use of chemotherapy plus a monoclonal antibody against HER2 for metastatic breast cancer that overexpresses HER2. N Engl J Med 2001;344:783-92.
154. Gong SJ, Jin CJ, Rha SY, et al. Growth inhibitory effects of trastuzumab and chemotherapeutic drugs in gastric cancer cell lines. Cancer Lett 2004;214:215-24.
155. Kim SY, Kim HP, Kim YJ, et al. Trastuzumab inhibits the growth of human gastric cancer cell lines with HER2 amplification synergistically with cisplatin. Int J Oncol 2008;32:89-95.
156. Shinohara H, Morita S, Kawai M, et al. Expression of HER2 in human gastric cancer cells directly correlates with antitumor activity of a recombinant disulfide-stabilized anti-HER2 immunotoxin. J Surg Res 2002;102:169-77.
157. Tanner M, Hollmen M, Junttila TT, et al. Amplification of HER-2 in gastric carcinoma: association with Topoisomerase IIalpha gene amplification,

intestinal type, poor prognosis and sensitivity to trastuzumab. Ann Oncol 2005;16:273-8.
158. Fujimoto-Ouchi K, Sekiguchi F, Yasuno H, et al. Antitumor activity of trastuzumab in combination with chemotherapy in human gastric cancer xenograft models. Cancer Chemother Pharmacol 2007;59:795-805.
159. Matsui Y, Inomata M, Tojigamori M, et al. Suppression of tumor growth in human gastric cancer with HER2 overexpression by an anti-HER2 antibody in a murine model. Int J Oncol 2005;27:681-5.
160. Diaz-Uriarte R, Alvarez de Andres S. Gene selection and classification of microarray data using random forest. BMC Bioinformatics 2006;7:3.
161. Gustafsson JO, Eddes JS, Meding S, et al. Internal calibrants allow high accuracy peptide matching between MALDI imaging MS and LC-MS/MS. J Proteomics 2012.
162. Schober Y, Schramm T, Spengler B, et al. Protein identification by accurate mass matrix-assisted laser desorption/ionization imaging of tryptic peptides. Rapid Commun Mass Spectrom 2011;25:2475-83.
163. Young NL, Dimaggio PA, Garcia BA. The significance, development and progress of high-throughput combinatorial histone code analysis. Cell Mol Life Sci 2010;67:3983-4000.
164. Esteller M. Cancer epigenomics: DNA methylomes and histone-modification maps. Nat Rev Genet 2007;8:286-98.
165. Mack GS. To selectivity and beyond. Nat Biotechnol 2010;28:1259-66.
166. Dekker TJ, Ter Borg S, Hooijer GK, et al. Determining sensitivity and specificity of HER2 testing in breast cancer using a tissue micro-array (TMA) approach. Breast Cancer Res 2012;14:R93.
167. Wu JM, Halushka MK, Argani P. Intratumoral heterogeneity of HER-2 gene amplification and protein overexpression in breast cancer. Hum Pathol 2010;41:914-7.
168. Gerlinger M, Rowan AJ, Horswell S, et al. Intratumor heterogeneity and branched evolution revealed by multiregion sequencing. N Engl J Med 2012;366:883-92.
169. Turner NC, Reis-Filho JS. Genetic heterogeneity and cancer drug resistance. Lancet Oncol 2012;13:e178-85.
170. Chaurand P, Cornett DS, Angel PM, et al. From whole-body sections down to cellular level, multiscale imaging of phospholipids by MALDI mass spectrometry. Mol Cell Proteomics 2011;10:O110 004259.
171. Rompp A, Guenther S, Takats Z, et al. Mass spectrometry imaging with high resolution in mass and space (HR(2) MSI) for reliable investigation of drug compound distributions on the cellular level. Anal Bioanal Chem 2011;401:65-73.
172. Clemis EJ, Smith DS, Camenzind AG, et al. Quantitation of Spatially-Localized Proteins in Tissue Samples using MALDI-MRM Imaging. Anal Chem 2012.

173. Lottspeich F (Eds.): Bioanalytik. 2nd ed. Elsevier, Spektrum Akad. Verl.: München 2006:pp 329-338.
174. Pol J, Strohalm M, Havlicek V, et al. Molecular mass spectrometry imaging in biomedical and life science research. Histochem Cell Biol 2010;134:423-43.
175. Gustafsson JO, Oehler MK, Ruszkiewicz A, et al. MALDI Imaging Mass Spectrometry (MALDI-IMS)-Application of Spatial Proteomics for Ovarian Cancer Classification and Diagnosis. Int J Mol Sci 2011;12:773-94.
176. Gross JH (Eds.): Mass spectrometry. 2nd ed. Springer: Berlin; Heidelberg 2011:p 125.
177. Suckau D, Resemann A, Schuerenberg M, et al. A novel MALDI LIFT-TOF/TOF mass spectrometer for proteomics. Anal Bioanal Chem 2003;376:952-65.
178. Watrous JD, Alexandrov T, Dorrestein PC. The evolving field of imaging mass spectrometry and its impact on future biological research. J Mass Spectrom 2011;46:209-22.
179. Groseclose MR, Massion PP, Chaurand P, et al. High-throughput proteomic analysis of formalin-fixed paraffin-embedded tissue microarrays using MALDI imaging mass spectrometry. Proteomics 2008;8:3715-24.
180. Gustafsson JO, Oehler MK, McColl SR, et al. Citric acid antigen retrieval (CAAR) for tryptic peptide imaging directly on archived formalin-fixed paraffin-embedded tissue. J Proteome Res 2010;9:4315-28.
181. Ronci M, Bonanno E, Colantoni A, et al. Protein unlocking procedures of formalin-fixed paraffin-embedded tissues: application to MALDI-TOF imaging MS investigations. Proteomics 2008;8:3702-14.
182. Stauber J, Lemaire R, Franck J, et al. MALDI imaging of formalin-fixed paraffin-embedded tissues: application to model animals of Parkinson disease for biomarker hunting. J Proteome Res 2008;7:969-78.
183. Jones EA, van Remoortere A, van Zeijl RJ, et al. Multiple statistical analysis techniques corroborate intratumor heterogeneity in imaging mass spectrometry datasets of myxofibrosarcoma. PLoS One 2011;6:e24913.
184. Lagarrigue M, Becker M, Lavigne R, et al. Revisiting rat spermatogenesis with MALDI imaging at 20-microm resolution. Mol Cell Proteomics 2011;10:M110 005991.
185. Amstalden van Hove ER, Smith DF, Heeren RM. A concise review of mass spectrometry imaging. J Chromatogr A 2010;1217:3946-54.
186. Minerva L, Clerens S, Baggerman G, et al. Direct profiling and identification of peptide expression differences in the pancreas of control and ob/ob mice by imaging mass spectrometry. Proteomics 2008;8:3763-74.
187. Djidja MC, Claude E, Snel MF, et al. Novel molecular tumour classification using MALDI-mass spectrometry imaging of tissue micro-array. Anal Bioanal Chem 2010;397:587-601.

188. Groseclose MR, Andersson M, Hardesty WM, et al. Identification of proteins directly from tissue: in situ tryptic digestions coupled with imaging mass spectrometry. J Mass Spectrom 2007;42:254-62.
189. Seeley EH, Caprioli RM. MALDI imaging mass spectrometry of human tissue: method challenges and clinical perspectives. Trends Biotechnol 2011;29:136-43.
190. Ransohoff DF. Rules of evidence for cancer molecular-marker discovery and validation. Nat Rev Cancer 2004;4:309-14.
191. Michiels S, Koscielny S, Hill C. Prediction of cancer outcome with microarrays: a multiple random validation strategy. Lancet 2005;365:488-92.
192. McDonnell LA, van Remoortere A, de Velde N, et al. Imaging mass spectrometry data reduction: automated feature identification and extraction. J Am Soc Mass Spectrom 2010;21:1969-78.
193. Clarke R, Ressom HW, Wang A, et al. The properties of high-dimensional data spaces: implications for exploring gene and protein expression data. Nat Rev Cancer 2008;8:37-49.
194. Benjamini Y, Hochberg Y. Controlling the False Discovery Rate: A Practical and Powerful Approach to Multiple Testing. Journal of the Royal Statistical Society. Series B (Methodological) 1995;57:289-300.
195. Saeys Y, Inza I, Larranaga P. A review of feature selection techniques in bioinformatics. Bioinformatics 2007;23:2507-17.
196. Nipp M, Elsner M, Balluff B, et al. S100-A10, thioredoxin, and S100-A6 as biomarkers of papillary thyroid carcinoma with lymph node metastasis identified by MALDI imaging. J Mol Med (Berl) 2012;90:163-74.
197. Perou CM, Sorlie T, Eisen MB, et al. Molecular portraits of human breast tumours. Nature 2000;406:747-52.
198. van de Vijver MJ, He YD, van't Veer LJ, et al. A gene-expression signature as a predictor of survival in breast cancer. N Engl J Med 2002;347:1999-2009.
199. Hanselmann M, Kirchner M, Renard BY, et al. Concise representation of mass spectrometry images by probabilistic latent semantic analysis. Anal Chem 2008;80:9649-58.
200. Alexandrov T, Becker M, Deininger SO, et al. Spatial segmentation of imaging mass spectrometry data with edge-preserving image denoising and clustering. J Proteome Res 2010;9:6535-46.
201. Alexandrov T, Meding S, Trede D, et al. Super-resolution segmentation of imaging mass spectrometry data: Solving the issue of low lateral resolution. J Proteomics 2011;75:237-45.
202. Barrett JH, Cairns DA. Application of the random forest classification method to peaks detected from mass spectrometric proteomic profiles of cancer patients and controls. Stat Appl Genet Mol Biol 2008;7:Article4.

6 Acknowledgements

First of all, I want to thank Horst Zitzelsberger, Axel Walch, and Matthias Ebert for giving me the opportunity to do my thesis in this exciting new field of proteomics on a topic with clinical relevance. They were not only excellent supervisors, but also motivators and promoters. I also want to give my appreciations to the Post-Docs Sandra Rauser and Elke Burgermeister for my daily guidance.

Equally important for me were my colleagues: Marc, Mareike, Cédrik, Stefan, Claudio, Uli, Stephan, Rebecca, Julia, Andreas, Annette, Katharina, Dietmar, Duarte, Susanne, Moritz, Barbara, Sonja, Martin, Yvonne, Daniela, Patrick, Claudia-Mareike, and Gerhard (please note that the order does not reflect the importance of the persons to me). You did not only enrich my time at work, but also besides work!

I also want to thank all my collaborators, especially Hakan Sarioglu from the Helmholtz Zentrum München, Michael Hanselmann from the University of Heidelberg, Axel Imhof and Teresa Barth from the Ludwigs-Maximilians-Universität München, Bernhard Küster from the Technische Universität München, Giuseppina Maccarrone from the Max-Planck Institute of Psychiatry, Theodore Alexandrov from the University of Bremen, and Sören-Oliver Deininger from Bruker Daltonik.

Finally, I want to give special thanks to the thesis office secretary Andrea Hinkelmann who took over a formally very difficult case, but nevertheless, supported me wholeheartedly during this long and stony process.

7 Publications

7.1 Publications in peer-reviewed journals

1. **Balluff B**, Rauser S, Ebert MP, Siveke J, Höfler H, Walch A. Direct molecular tissue analysis by MALDI imaging mass spectrometry in the field of gastrointestinal disease. **Gastroenterology. 2012** Sep;143(3):544-9.e1-2.

2. Meding S, **Balluff B**, Elsner M, Schöne C, Rauser S, Nitsche U, Maak M, Schäfer A, Hauck SM, Ueffing M, Langer R, Höfler H, Friess H, Rosenberg R, Walch A. Tissue Based Proteomics Reveals FXYD3, S100A11 and GSTM3 as Novel Markers for Regional Lymph Node Metastasis in Colon Cancer. **J Pathol. 2012** May 25;228(4):459-470.

3. Elsner M, Rauser S, Maier S, Schöne C, **Balluff B**, Meding S, Jung G, Nipp M, Sarioglu H, Maccarrone G, Aichler M, Feuchtinger A, Langer R, Jütting U, Feith M, Küster B, Ueffing M, Zitzelsberger H, Höfler H, Walch A. MALDI Imaging Mass Spectrometry reveals COX7A2, TAGLN2 and S100-A10 as novel Prognostic Markers in Barrett's Adenocarcinoma. **J Proteomics. 2012** Aug 3;75(15):4693-704.

4. Meding S, Nitsche U, **Balluff B**, Elsner M, Rauser S, Schöne C, Nipp M, Maak M, Feith M, Ebert M, Friess H, Langer R, Höfler H, Zitzelsberger H, Rosenberg R, Walch A. Tumor Classification of Six Common Cancer Types Based on Proteomic Profiling by MALDI Imaging. **J Proteome Res. 2012** Mar 2;11(3):1996-2003.

5. Ebert MP, Tänzer M, **Balluff B**, Burgermeister E, Kretzschmar AK, Hughes DJ, Tetzner R, Lofton-Day C, Rosenberg R, Reinacher-Schick AC, Schulmann K, Tannapfel A, Hofheinz R, Röcken C, Keller G, Langer R, Specht K, Porschen R, Stöhlmacher-Williams J, Schuster T, Ströbel P, Schmid RM. TFAP2E-DKK4 and chemoresistance in colorectal cancer. **N Engl J Med. 2012** Jan 5;366(1):44-53.

6. Baumhoer D, Elsner M, Smida J, Zillmer S, Rauser S, Schoene C, **Balluff B**, Bielack S, Jundt G, Walch A, Nathrath M. CRIP1 expression is correlated with a favorable outcome and less metastases in osteosarcoma patients. **Oncotarget. 2011** Dec;2(12):970-5.

7. Alexandrov T, Meding S, Trede D, Kobarg JH, **Balluff B**, Walch A, Thiele H, Maass P. Super-resolution segmentation of imaging mass spectrometry data: Solving the issue of low lateral resolution. **J Proteomics. 2011** Dec 10;75(1):237-45.

8. **Balluff B**, Rauser S, Meding S, Elsner M, Schöne C, Feuchtinger A, Schuhmacher C, Novotny A, Jütting U, Maccarrone G, Sarioglu H, Ueffing M, Braselmann H, Zitzelsberger H, Schmid RM, Höfler H, Ebert MP, Walch A. MALDI imaging identifies prognostic seven-protein signature of novel tissue markers in intestinal-type gastric cancer. **Am J Pathol. 2011** Dec;179(6):2720-9.

9. Nipp M, Elsner M, **Balluff B**, Meding S, Sarioglu H, Ueffing M, Rauser S, Unger K, Höfler H, Walch A, Zitzelsberger H. S100-A10, thioredoxin, and S100-A6 as biomarkers of papillary thyroid carcinoma with lymph node metastasis identified by MALDI Imaging. **J Mol Med (Berl). 2011** Sep 22.

10. **Balluff B**, Schöne C, Höfler H, Walch A. MALDI imaging mass spectrometry for direct tissue analysis: technological advancements and recent applications. **Histochem Cell Biol. 2011** Sep;136(3):227-44.

11. **Balluff B**, Elsner M, Kowarsch A, Rauser S, Meding S, Schuhmacher C, Feith M, Herrmann K, Röcken C, Schmid RM, Höfler H, Walch A, Ebert MP. Classification of HER2/neu status in gastric cancer using a breast-cancer derived proteome classifier. **J Proteome Res. 2010** Dec 3;9(12):6317-22.

12. **Balluff B**, Rauser S, Marquardt C, Deininger SO, Albers C, Belau E, Hartmer R, Suckau D, Specht K, Ebert MP, Schmitt M, Aubele M, Höfler H, Walch A. Classification of HER2 receptor status in breast cancer tissues by MALDI imaging mass spectrometry. **J Proteome Res. 2010** Apr 5;9(4):1854-63.

13. Tänzer M, **Balluff B**, Distler J, Hale K, Leodolter A, Röcken C, Molnar B, Schmid R, Lofton-Day C, Schuster T, Ebert MP. Performance of epigenetic markers SEPT9 and ALX4 in plasma for detection of colorectal precancerous lesions. **PLoS One. 2010** Feb 4;5(2):e9061

14. Herrmann K, Walch A, **Balluff B**, Tänzer M, Höfler H, Krause BJ, Schwaiger M,Friess H, Schmid RM, Ebert MP. Proteomic and metabolic prediction of response to therapy in gastrointestinal cancers. **Nat Clin Pract Gastroenterol Hepatol. 2009** Mar;6(3):170-83. Review.

7.2 Presentations

7.2.1 Oral presentations

1. Balluff B. Application of MALDI imaging in clinical proteomics research of gastric cancer. **Canadian National Proteomics Network - Annual Symposium**. April 23, 2012, Toronto, Canada
2. Balluff B and Maier S. How to study proteins? **EScoP (European School of Pathology) –Molecular Biology for Pathologists**. March 22, 2012, Pisa, Italy
3. Balluff B. MALDI imaging mass spectrometry in pre-clinical cancer research. **Mass Spectrometry @ Manchester Symposium**. December 8, 2011, Manchester, United Kingdom
4. Balluff B. MALDI imaging mass spectrometry in gastric cancer. **7th Symposium of the Society for Histochemistry**. October 13, 2011, Munich, Germany
5. Balluff B et al. MALDI Imaging zur Identifizierung prognostischer Gewebsmarker im intestinalen Magenkarzinom. **Jahrestagung der Deutschen Gesellschaft für Pathologie**. June 16, 2011, Leipzig, Germany
6. Balluff B et al. Proteome based response prediction in gastrointestinal cancers. **Stem Cell – Tumor – Proteome**. February 6, 2010, Hamburg, Germany
7. Balluff B. Biomarker discovery by Imaging Mass Spectrometry. **German Polish Life Science Meeting**. March 26, 2009, Kracow, Poland
8. Balluff B, et al. Rapid binning and taxonomic profiling of metagenomes. **BAGECO 9**. June 24, 2007, Wernigerode, Germany

7.2.2 Poster presentations

1. Balluff B et al. Classification of HER2/neu status in gastric cancer using a breast-cancer derived proteome classifier / MALDI imaging identifies

prognostic seven-protein signature of novel tissue markers in gastric cancer. **7th Symposium of the Society for Histochemistry**. October 13, 2011, Munich, Germany

2. Balluff B et al. MALDI imaging identifies prognostic seven-protein signature of novel tissue markers in gastric cancer. **Proteomic Forum**. April 4, 2011, Berlin, Germany

3. Balluff B et al. Proteombasierte Klassifikation des HER2/neu-Status im Magenkarzinom mittels Mammakarzinom-spezifischer Klassifikatoren. **Jahrestagung der Deutschen Gesellschaft für Verdauungs- und Stoffwechselkrankheiten**. September 16, 2010, Stuttgart, Germany

4. Balluff B et al. Classification of HER2 Receptor Status in Breast Cancer Tissues by Imaging Mass Spectrometry. **CancerOmics**. May 6, 2010, Erice, Italy

7.3 Book chapters

1. Tänzer M, **Balluff B**, Walch A, Ebert M. “Epigenetik und Proteomik des Magenkarzinoms.” *Biologie und zielgerichtete Therapie des Magenkarzinoms*. Priv.-Doz. Dr. Florian Lordick (Hrsg.), 2010. UNI-MED Verlag, Bremen, Germany. ISBN 978-3-8374-2168-2